The morphology and growth behavior of human gingival fibroblasts on three different titanium alloy surfaces

Liya Zhao

2016

Aus der Poliklinik für Zahnerhaltung und Parodontologie der
Ludwig-Maximilians-Universität München

Direktor: Prof. Dr. med. dent. Reinhard Hickel

The morphology and growth behavior of human gingival fibroblasts on three different titanium alloy surfaces

Dissertation
zum Erwerb des Doktorgrades der Zahnmedizin
an der Medizinischen Fakultät der
Ludwig-Maximilians-Universität zu München

vorgelegt von

Liya Zhao

aus

Hubei, China

2016

Mit Genehmigung der Medizinischen Fakultät
der Universität München

Berichterstatter:	Prof. Dr. Karl-Heinz Kunzelmann
Mitberichterstatter:	Priv. Doz. Dr. Dr. Wenke Smolka
Mitbetreuung durch den promovierten Mitarbeiter:	---
Dekan:	Prof. Dr. med. dent. Reinhard Hickel
Tag der mündlichen Prüfung:	22.07.2016

For my parents and my husband

Contents

List of Figures

LMU LUDWIG-MAXIMILIANS-UNIVERSITÄT MÜNCHEN

Dean's Office
Medical Faculty

Affidavit

Zhao Liya

Surname, first name

Goethe Strasse 72

Street

80336, Munich

Zip code, town

Germany

Country

I hereby declare, that the submitted thesis entitled

The morphology and growth behavior of human gingival fibroblasts on three different titanium alloy surfaces

is my own work. I have only used the sources indicated and have not made unauthorised use of services of a third party. Where the work of others has been quoted or reproduced, the source is always given.

I further declare that the submitted thesis or parts thereof have not been presented as part of an examination degree to any other university.

Place, date

Signature doctoral candidate

Summary

Research on dental implants over the last decades mainly concentrated on the osseointegration between bone-to-implant interface; however, studies on the assessment of soft tissue incorporation around dental implant are still limited. As innovative materials were developed, each new alternative demands the assessment of its biocompatibility and performance on both bone and soft tissue integration onto dental implant surfaces. The understanding of cell-substrate interactions is of high importance for the development of biocompatible implants, it paves the way for in vivo studies into device functionality, it is important to study how Ti surfaces with different microstructures affect the behaviour of spreading and attached cells. However, the future of the cells on the materials cannot be presumed with the evaluation after short-time seeding, the method that allows long-term study of an cell-to-material interface is closer to the in vivo situation. The goal of this project is to evaluate the influence of different topographies and roughness of titanium specimens on human gingival fibroblast's morphology, adhesion, cellular proliferation with SEM and CLSM and to evaluate by FACS the expression of proteins involved in cell/surfaces adhesion. In this study, the initial attachment and subsequent growth behaviour up to 30 days of human fibroblasts on three different commercial Ti substrates were investigated and compared with confocal microscopic imaging, it could be shown that the extent of fibroblast's spreading at various points of time differed on the implant surfaces tested, the cells responded to Osseotite surfaces in a manner similar to or even better than their behavior on Nanotite surfaces. The cells cultured on Osseotite and Nanotite surfaces are cuboidal in shape and have the dendritic branching pattern characteristic. In contrast, the cells on the Machined surfaces appear more flattened. Alamar Blue assay demonstrated the gingival fibroblasts grown on Osseotite and Nanotite surfaces showed a notable higher proliferation compared to the Machined

surfaces after two weeks of incubation; however, there is no considerable difference on cell proliferation between these two groups. The flow cytometry data analysis suggested that the cells grown on the Osseotite implant material produce a better initial attachment with a higher $\alpha 5$ and $\beta 1$ integrins expression than on machined and Nanotite materials. After 24 days of cell incubation, immunofluorescence labelling analysis showed that more extended actin stress fibers and higher vinculin expression were on Osseotite compared to Nanotite samples. Vinculin expression localized mainly within central areas of the cell grown on the Machined and the Osseotite surfaces; distinct focal contacts localizations were evident at the cell edges on the Nanotite surface. At day 30, high vinculin expression and a dense network of actin stress fibers on the human gingival fibroblasts were observed on all tested substrates; a similar F-actin distribution was found on Osseotite and Nanotite surfaces.

The present in vitro study for long-term cellular responses on three different titanium surfaces demonstrated that topographic structures can influence the morphology, proliferation and adhesion of human gingival fibroblasts. With the limitation of our study, there is not enough evidence to show that the Nanotite implants is more benificial to the growth behavior of human gingival fibroblasts, compared with Osseotite surfaces; especially at the early stage of incubation. our findings may contribute to a better understanding of the processes involved in the soft tissue integration surrounding dental implants and hopefully give information for the development of innovative implant materials.

Zusammenfassung

Forschung über Zahnimplantate konzentriert in den letzten Jahrzehnten vor allem auf die Osseointegration zwischen Knochen-Implantat-Schnittstelle; sind jedoch Studien zur Beurteilung der Weichgewebe Einbau rund Zahnimplantat noch begrenzt. Als innovative Materialien entwickelt wurden, verlangt jede neue Alternative der Beurteilung ihrer Biokompatibilität und Leistung sowohl auf Knochen- als auch Weichgewebeintegration auf Implantatoberflächen. Das Verständnis der Zell-Substrat-Wechselwirkungen ist für die Entwicklung biokompatibler Implantate großer Bedeutung, den Weg für eine in vivo-Studie in Gerätefunktionalität ebnet es, ist es wichtig zu untersuchen, wie Ti Oberflächen mit unterschiedlichen Mikrostrukturen beeinflussen das Verhalten der Verbreitung und anhaftenden Zellen. Jedoch kann die Zukunft der Zellen auf den Materialien, die nicht mit der Bewertung nach dem kurzzeitigen Aussäen der Methode, die Langzeit-Studie einer Zelle-zu-Material-Grenzfläche näher an der in vivo Situation kann angenommen werden. Das Ziel dieses Projektes ist es, zu bewerten den Einfluss von unterschiedlichen Topographien und Rauheit der Titanproben auf die menschliche gingivale Fibroblasten-Morphologie, Adhäsion, Zellproliferation mit SEM und CLSM und FACS bewerten die Expression von Proteinen in der Zelle beteiligt / Flächen Haftung.

In dieser Studie wurden die anfängliche Befestigung und das anschließende Wachstum Verhalten bis zu 30 Tage von menschlichen Fibroblasten auf drei verschiedenen kommerziellen Ti Substrate untersucht und mit konfokalen mikroskopischen Abbildungs, konnte gezeigt werden, dass das Ausmaß der Fibroblasten der Ausbreitung zu verschiedenen Zeitpunkten unterschieden sich auf Implantatoberflächen getestet, reagierten die Zellen an Oberflächen in einer Weise, die ähnlich oder sogar besser als ihr Verhalten auf Nanotite Oberflächen Osseotite. Die Zellen auf Osseotite und Nanotite Flächen kultiviert werden

quaderförmige Form auf und haben die dendritischen Verzweigungsmuster charakteristisch. Im Gegensatz dazu sind die Zellen auf den bearbeiteten Oberflächen erscheinen abgeflacht. Alamar-Blau-Assay zeigten die gingivale Fibroblasten auf Osseotite und Nanotite Oberflächen gewachsen zeigten einen bemerkenswerten Anstieg der Proliferationsgegenüber den bearbeiteten Oberflächen nach zwei Wochen der Inkubation; jedoch gibt es keinen wesentlichen Unterschied auf die Zellproliferation zwischen diesen beiden Gruppen. Die Durchflusszytometrie Datenanalyse vorgeschlagen, dass die Zellen auf der Osseotite Implantatmaterial gewachsen erzeugen eine bessere anfängliche Befestigungs mit höherer $\alpha 5$ und $\beta 1$ Integrin-Expression als an bearbeiteten und Nanotite Materialien. Nach 24 Tagen des Zell Inkubation Immunfluoreszenzmarkierungs Analyse zeigte, dass ausgedehntere Aktin-Stressfasern und höhere Vinculin Ausdruck waren Osseotite Vergleich zu Nanotite Proben. Vinculin Expression lokalisiert hauptsächlich im zentralen Bereiche der Zelle an dem bearbeiteten und Osseotite Oberflächen gewachsen; deutliche fokale Kontakte Lokalisierungen waren an den Zellrändern auf der Nanotite Oberfläche deutlich. Am Tag 30 wurden hohe Vinculin Ausdruck und ein dichtes Netz von Aktin-Stressfasern über die menschlichen gingivalen Fibroblasten auf allen getesteten Substraten beobachtet; eine ähnliche F-Actin-Verteilung wurde auf Osseotite und Nanotite Oberflächen gefunden.

Die vorliegende in vitro-Studie zur Langzeit-Zellantworten auf drei verschiedenen Titanoberflächen zeigte, daß topographische Strukturen die Morphologie, Proliferation und Adhäsion humaner Gingivafibroblasten beeinflussen können. Mit der Einschränkung, der Studie gab es nicht genügend Beweise zeigen, dass die Implantate Nanotite ist benificial auf das Wachstumsverhalten menschlicher Gingivafibroblasten, verglichen mit Osseotite Oberflächen; vor allem in der Frühphase der Inkubation. Unsere Ergebnisse können zu einem besseren Verständnis der Prozesse in der Weichgewebeintegration rund um Zahnimplantate Beteiligten beitragen und hoffentlich geben Informationen für die Entwicklung von innovativen Implantatmaterialien.

Abbreviations

AB:	Alamar Blue
ATCC:	American Type Culture Collection
CaP:	Calcium phosphate
CLSM:	Confocal Laser Scanning Microscope
NADH:	Nicotinamide adenine dinucleotide
DCD:	Discrete Crystalline Deposition
DMEM:	Dulbecco's Modied Eagle's Medium
DMSO:	Dimethylsulfoxid
DPBS:	Dulbecco's Phosphate Buffered Saline
ECM:	Extracellular matrix
EDTA:	Ethylene diaminetetraacetic acid
FACS:	Fluorescence Activated Cell Sorting
FADH:	Flavin adenine dinucleotide
FAK:	Focal Adhesion Kinase
FBS:	Fetal bovine serum

FEG:	Field emission gun
FFT:	Fast Fourier Transform
FMNH:	Flavin mononucleotide
HGF:	Human gingival fibroblasts
HMDS:	Hexamethyldisilazane
mRNA:	Messenger RNA
NADPH:	Nicotinamide adenine dinucleotide phosphate
Ra:	Roughness average
RT-PCR:	Reverse transcription-polymerase chain reaction
SEM:	Scanning Electron Microscope
VASP:	Vasodilator-stimulated phosphoprotein

Chapter 1

Introduction

Since the well-accepted concept of "osseointegration" introduced by Brånemark *et al.* (1969) in the late 1960's, titanium and its alloys have been extensively used for endosseous dental implants because of their excellent biocompatibility and superior mechanical properties.

Basic and clinical research on dental implants in the last two decades have mainly concentrated on the bone-to-implant interface, while studies on the assessment of soft tissue incorporation around dental implant are still limited. This is largely because the direct bone contact with an implant was thought to be a key factor which contributes to the success of implant integration. However, in dental implant therapy, the long-term support for a prosthesis is determined, in part, by the profile and biologic seal formed by the soft tissue around the implant as it helps to stabilize and maintain the peri-implant tissues during the healing phase following surgical implant placement.

Research advances in modern dental implantology have led to the development of various approaches which aim to fabricate improved implant surfaces. The behavior and attachment of cells on the implant surface determine the success of the implant. The topography and texture of the titanium surface can in turn influence the behavior of cells and genetic expression (i.e. cytoskeleton) in the cells. Therefore, it is important to investigate how the titanium surfaces with different structures may impact the morphology and attachment of human gingival fibroblasts, which will be meaningful and significant

for cell-nanostructure relationship studies and novel dental implant surface design.

1.1 Soft tissues around implants

Similar to natural teeth, the soft tissue around the implant includes oral epithelium, the junctional epithelium and the underlying fibrous connective tissue. However, there are significant differences between them: it was reported that the epithelium and connective tissues around the implant present a poorer quality of attachment than that of natural teeth (Berglundh *et al.* 1991). In vitro and in vivo animal and human studies manifested the formation of attachment structures at the implant-epithelium interface (Abrahamsson *et al.* 1996, Gould *et al.* 1984, McKinney *et al.* 1985). The peri-implant epithelium forms internal basal lamina and hemidesmosomes, provides epithelial attachment similar to that in the natural teeth, which enable them to attach onto the implant surface. However, this attachment structure is limited to the apical region of peri-implant epithelium Atsuta *et al.* (2005). While the connective tissues around a dental implant were believed mostly to be oriented parallel to the implant surface, with no perpendicular insertion to the implant (Bauman *et al.* 1993).

In dental implant therapy, a satisfying outcome depends on both bone and soft tissue integration into the implant. The implant should not only anchor in the neighboring bone but also be in direct contact with gingival epithelium and connective tissue.

Titanium and its alloys are widely used in dental implant treatment as the replacement of natural tooth, because they offer good biocompatibility and showed high long-term success rates. During the surgical procedure, the screw-like implant, is placed into the jaw bone. After a period of a few months for ridge healing, a strong bond is formed between the bone and titanium surface, then the dental prosthesis can be connected to

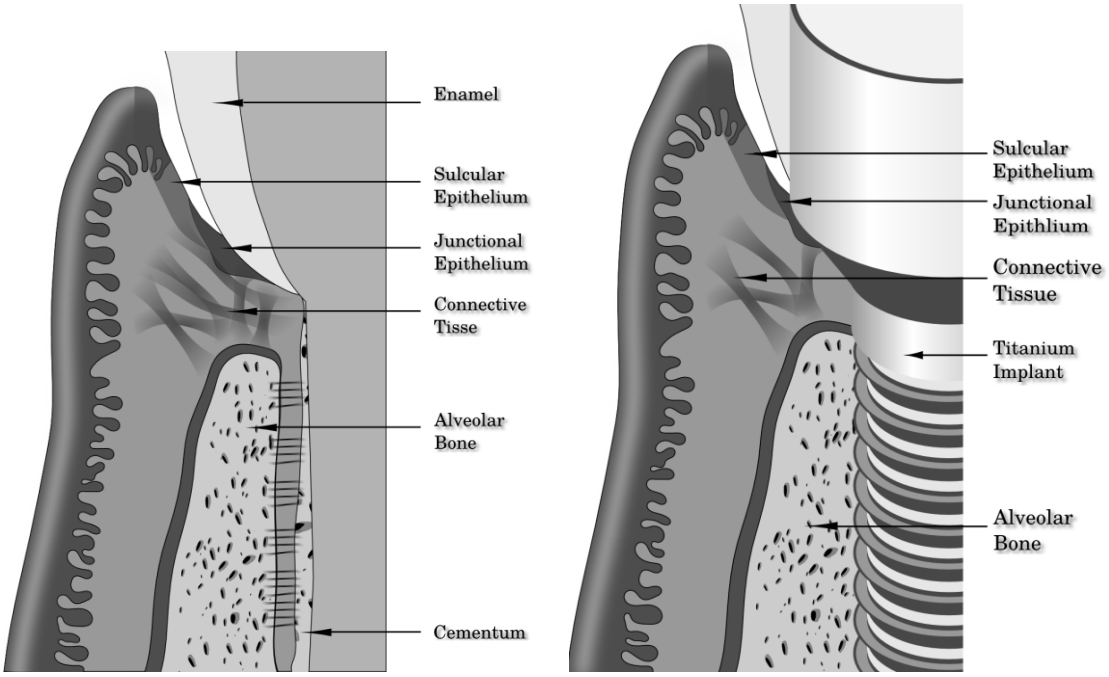

1.1-a) Tooth-soft tissue interface

1.1-b) Implant-soft tissue interface

Image modified from Rose L.F et al. (2004)

Figure 1.1: Difference between tooth- and implant-soft tissue interfaces

the abutment. The recent basic criteria for evaluating the success of dental implants are immobility, absence of peri-implant radiolucency, adequate width of the attached gingiva and absence of infection (Karthik *et al.* 2013). Although success rates exceeding 90% were often reported in dental implant treatment over the last few years, there are still some risk factors associated with implant failure. For example, the formation of fibrous encapsulation is such a risk. Fibrous encapsulation is in fact a scar formation of fibrous connective tissue, it may cause the subsequent peri-implant bone loss and lead to isolation of the implant from surrounding tissue. Fibrous encapsulation has been found to correlate with the characteristics of the implant material. Other commonly occurring peri-implant diseases are the inflammatory reactions which take place in the tissue surrounding the implant, i.e. peri-implantitis or mucositis. It was well documented in the literature that the bacterial colonization is a main cause in the process of peri-implant disease. As advances have been made in implant materials and techniques, bulk of innovative materials were designed to enhance the interaction between implants and the surrounding environment. These materials have an effect on cellular behavior including cell proliferation, cell attachment and protein synthesis. An ideal implant material would facilitate cell growth on its surface, thereby helping to integrate both bone and soft tissue into the implant.

1.1.1 Anatomy and histology of the soft tissue around implant

After dental implant insertion, the soft tissue around a dental implant is formed during the stage of wound healing. Several studies in animals and in humans have investigated the morphologic characteristics of surrounding tissues of implant. In an experimental study in beagle dogs (Berglundh *et al.* 1991), Berglundh and his colleagues compared the common features in the peri-implant soft tissue with those of the gingival around teeth. This study was performed on 5 beagle dogs by installing two-stage

implants. After three months of implant placement, abutment connection was carried out. After another 2 months of healing, daily plaque control was kept for 8 weeks. At the end of the plaque control programme, clinical examinations were performed to verify the health conditions of surrounding tissues around implant. The histometric and morphometric examinations revealed that the epithelium attached the tooth or titanium surface in a similar way. Both the peri-implant mucosa and gingiva consisted of a well-keratinized oral epithelium connected with a 2 mm long junctional epithelium and a 1 mm high underlying connective tissue. The most striking observation is the collagen fiber orientation. Around the implant, collagen fibers were parallel with the abutment surface. Histological examinations of peri-implant tissues from this study indicated that under the practice of plaque removal, peri-implant mucosa had formed a comparable protective soft tissue barrier with the gingiva around the teeth, both of them have a potential to prevent bacterial infiltration and thus infection, too. Furthermore, in another beagle dogs study, the soft tissue structures around titanium implant were found to have similar dimensions and composition following 1-stage and 2-stage implant installations Abrahamsson *et al.* (1996), Buser *et al.* (1992) observed the healing pattern of soft tissue around the non-submerged unloaded titanium implants in beagle dogs. The authors showed similar soft tissue structures between three different implant surfaces, especially in terms of the length of direct connective tissue contact to the implant. It was also found that the integrated connective tissue is poor in blood vessels but rich in fibroblasts. This result was later reinforced by Berglundh *et al.* (1994), they confirmed the supracrestal connective tissue lateral to the implant was almost free of vascular supply. In an experimental study performed by Moon *et al.* (1999), the zone of peri-implant connective tissue was further divided into two units: the central unit close to the implant surface is characterized by its absence of blood vessels but an abundance of fibroblasts, the lateral unit which is continuous with the central one comprised of relatively fewer fibroblasts, but more collagen fibres and blood vessels. This outcome suggested that the fibroblasts rich layer plays a

part in maintaining the biological seal around a dental implant.

1.2 Influence of surface topography on soft tissue integration

It is generally accepted that the surface topography is crucial for long term success of dental implants. The effects of surface topography on implant performance including hard and soft tissue integration have been intensively investigated. In order to reduce the wound healing time and enhance the host tissue adaption to implant biomaterials, significant efforts have been made to optimize the titanium surfaces. Modifications of the implant surface topography can be achieved through a number of techniques: mechanical polishing, blasting with particles of various diameters, chemical etching, plasma spray, ion-sputtering coating, anodization, hydroxyapatite coating and various methods of coating (A Gupta, M Dhanraj, G Sivagami. 2008). The scale features obtained from these treatments can range from nanometers (below the cell-size) to milimetres (tissue size) (Rompen *et al.* 2006).

In a beagle dog model, Abrahamsson *et al.* (2002) studied the composition of the soft tissue barrier to titanium abutments prepared with either a turned (smooth) or acid-etched (rough) surface. In this study, implants made of c.p titanium were inserted in the right edentulous mandibular premolar region in five beagle dogs. After three months, two types of abutments with different roughness were connected. At the end of a 6-month period, biopsies were obtained, decalcified and prepared for light and electron microscopy. The results showed that the epithelial and connective tissue components are similar on the two titanium surfaces. The connective tissue attachment at both types of abutment was composed of about 30–33% fibroblasts and 63–66% collagen. Zitzmann *et al.* (2002)

studied the reactions of the peri-implant mucosa to plaque accumulation on implant abutments designed with either a rough or a smooth surface. They found that the plaque accumulation was not influenced by the roughness of titanium abutments. Furthermore, in a baboon trial, Watzak *et al.* (2006) compared the peri-implant soft tissue dimension and bone level with different surface modifications after 1.5 years functional loading and plaque formation. A histomorphometric observation of three types of titanium implants indicated that there was no significant difference in terms of sulcus depth, the dimension of the junctional epithelium and the connective tissue contact. Recently, Schwarz *et al.* (2013) performed a randomized controlled clinical multicentre study. Titanium implants with different surface roughness and hydrophilicity were placed in the posterior mandibular and maxilla of 30 patients. After eight weeks, the histological analysis of peri-implant soft tissue demonstrated that a modMA (modified hydrophilic) surface has a high potential to enhance soft tissue adhesion at the transmucosal site of implants. In a minipig study, Liñares *et al.* (2013) compared the soft tissue integration to three modified implant surfaces. It was concluded that the surface modification did not affect the peri-implant soft tissue dimensions.

However, some studies have showed that roughened implant surfaces might be favorable to soft tissue adhesion around implants. The soft tissue attachment around calcium phosphate coated and uncoated implants was evaluated in beagle dogs (Bao Hong Zhao *et al.* 2007). After a 3-month healing period, less gingival recession was found in the tested group. Moreover, collagen fibers of the connective tissue around calcium phosphate coated implants were found aligned mostly in oblique directions. It can be speculated that calcium phosphate coating can promote the soft tissue regeneration and prevent gingival recession. But the exact reason for this result is not quite clear, because the calcium phosphate coated surface may be assumed to have chemical effects but not enough roughness to promote collagen fiber orientation. In a study in humans, Glauser *et al.* (2005) detected the effect of surface topography modifications on peri-implant bar-

rier around one-piece mini-implants. In this study, five patients received the one-piece implant treatment with either an TiO2 layer oxidized, an acid-etched or a machined surface. Abutment connection was carried out after 8-week healing time. The implants and surrounding tissue were harvested and processed for histological examination. The authors found similar peri-implant soft tissue structures in humans with that in animals; furthermore, less epithelial downgrowth and longer connective tissue were found around oxidized and acid-etched implants than machined ones.

1.3 Cells frequently investigated in implant surface research

When dental implants are introduced into host bone, the biocompatibility of the materials depends not only on surface properties but also on the growth behavior of the cells on the material surface. The quality of early cell-material interaction will influence the cell's capacity to proliferate and differentiate. A successful dental implant therapy depends on three parts: osseointegration, epithelial seal and connective tissue attachment. Long-term stability of osseointegrated implants relies on the adhesion and growth of osteoblastic cells at tissue/implant interface (Palumbo 2011). A good sealing between the peri-implant epithelium and implant surface can avoid the epithelial downgrowth, prevent bacterial colonization, improve the barrier function of the implant. Promoting the epithelial cell adhesion on the implant surface is critical to form the epithelial attachment and maintain epithelial soft tissue seal. The interaction of connective tissue and fibroblasts with the implant surface plays an essential role in establishing a stable peri-implant supporting structure as well. The connective tissue around dental implants is characterized by collagen fibers aligned parallel to the vertical axis of the implant body (Bao Hong Zhao *et al.* 2007). Since the gingival fibroblasts have the function of producing

collagen, glycoproteins and extracellular matrix, their initial attachment and response to implant surface may decide the outcome of implant treatment. Thus, these three types of cells: osteoblasts, epithelial cells and gingival fibroblasts are the most investigated objects in designing biofunctional dental materials. Early stage cell reaction of the three different cell types such as adhesion, morphology and proliferation to the titanium surfaces can vary according to surface topography.

1.3.1 Cell culture studies for investigating implant-soft tissue interface

In order to develop highly controlled dental implants for better biological interaction, cell culture models have been developed to investigate the cell behavior on surfaces with different properties. Smooth, plasma-sprayed and hydroxyapatite-coated titanium implant materials were coated with either laminin, fibronectin or bovine serum albumin and used to test the gingival fibroblasts and epithelial cells attachment (Dean *et al.* 1995). The fibronectin coating surface showed the capacity of enhancing the gingival fibroblasts binding by two to three folds, while laminin coating resulted in three to four times the promotion of epithelial cell attachment. In another study, Köunönen *et al.* (1992) compared the adhesion, orientation and proliferation of human gingival fibroblasts on electropolished, etched and sandblasted titanium surfaces. The findings have shown that smooth titanium surfaces supported attachment and growth of gingival fibroblasts thus are suitable for soft tissue integration. Similar results were concluded from a study performed by Eisenbarth *et al.* (1996). Recently, Liugi Guida and his coworkers evaluated the influence of the modification of the surface topography at nano-scale level on gingival fibroblasts response Guida *et al.* (2013). Primary human gingival fibroblasts were cultured on oxidized or turned surfaces, cell morphology, adhesion, proliferation and collagen synthesis were analyzed. It was found that an oxidized nanostructured titanium surface offers

better growth behavior of gingival fibroblasts. Another finding in support of this data was concerning that the fibroblasts (NIH/3T3 murine fibroblasts) reactions were boosted on an odized-hydrothermally treated titanium with nano-scale level structure (Miura & Takebe 2012). Nevertheless, there are some studies have shown lower fibroblasts adhesion and proliferation on nano-scale surfaces than smooth surfaces (Cohen *et al.* 2007, Miller *et al.* 2005). There is a lack of correspondence in relation to optimal nanostructured titanium surfaces. Hence, it was assumed that nanometric titanium surface can control cell behavior and protein adsorption, and in turn determine the success of dental implants .

1.4 Cell attachment on substrates

The cell attachment on a substrate is directly involved with cell morphology, proliferation, migration and even determines its survival. It is widely understood that surface characteristics play an important role in cell-material interaction and surrounding tissue establishment. The process how cells adhere to each other or to a substrate (cell adhesion) is mediated by a complex mechanism. The sites of cell adhesion to the underlying surface are focal adhesions. Focal adhesions are multi-protein structures which contain integrins and act as a mechanical linkage between intracellular actin bundles and extracellular matrix via membrane-bound receptors (Abercrombie & Dunn 1975). It was reported that focal adhesions are large adhesion contacts which lie at the ends of actin stress fibers in cells (Petit & Thiery 2000). Focal adhesions are key regulators of cell behavior and have important functions in cell growth: they can transmit the external force signals to the adhesion sites and make the cells grow tightly on the materials. Many molecules involved in mediating signal transduction in response to force stimuli such as Src, FAK, Rho have been found at focal adhesions (Wozniak *et al.* 2004). The activation and clustering of integrins is a crucial event in cell adhesion formation. Through it, more cytoplasmic

proteins such like vinculin, talin and paxillin, are recruited to the adhesion site (Liu *et al.* 2010). The actin skeleton forms stress fibers, which are associated with actin and myosin filament, are contractible and responsible for the cell movement. These clustered integrins and bulk of cytoplasmic proteins are vital outside-inside signalling ports and help the cells bind to other cells and to keep the basic function (Liu et al., 2010b). Based on these facts, it is significant to observe the cell adhesion on dental implant surfaces with different chemical and physical properties, since after the placement of implants, the cells have to adapt a new environment and attach, grow on them.

1.4.1 Important proteins involved in cell adhesion

Integrin

Integrins are a large family of transmembrane proteins which act as major receptors for cell adhesion and link the extracellular matrix to the cell. Integrins are very important cell surface receptors in maintaining the cell survival and growth, because the signaling mediated from integrin/ECM interactions are also integrated with cellular response to growth factor signaling to regulate cellular functions including cell adhesion, cell migration, cell proliferation and other processes (Ojaniemi *et al.* 1997). All integrins are composed of two different noncovalently associated transmembrane glycoproteins, called a large α and a small β subunit. Each subunit of integrin $\alpha\beta$ heterodimers contains a extracellular domain, a transmembrane domain and a cytoplasmic tail. The integrin cytoplasmic tail domain binds with the actin skeleton, that inhibits clustering of subunits decrease cell adhesion, whereas transmembrane subunits that induce clustering enhance adhesion and FAK phosphorylation. This phenomenon suggests that the integrin function requires clustering and avidity change (Wozniak *et al.* 2004).

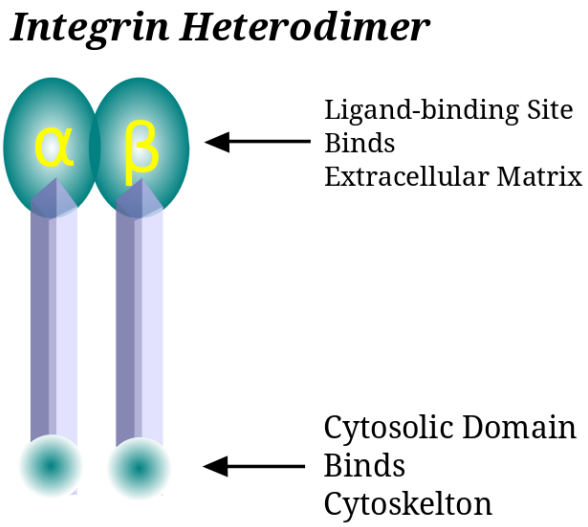

Image modified from Pivodova *et al.* (2011).

Figure 1.2: The integrin structure

Hormia *et al.* (1990) investigated the integrin expression in human gingiva through the method of immunostaining. The results showed that gingival connective tissue expresses specifically the fibronectin receptor $\alpha5\beta1$, which is the key characteristic that make it different from skin. Moreover, gingival epithelium has been shown to express a wide variety of integrins, including integrin subunits $\alpha2\beta1$, $\alpha3\beta1$, $\alpha6\beta1$ and $\alpha6\beta4$. The $\beta1$ integrin subunit was expressed in an overall cell-membrane localization in basal epithelial cells. In another study, Oates *et al.* (2005) examined the expression of integrin for gingival fibroblasts grew on titanium surfaces and the effect of surface roughness on integrin expression and cell morphology. Briefly, human gingival fibroblasts were cultured on three different surfaces: smooth, rough titanium surfaces and plastic surfaces for control group. The mRNA levels of integrin subunit for every group of cells were assessed by reverse transcription-polymerase chain reaction (RT-PCR). The expression of the integrin subunits was assessed at the protein level using flow cytometry and immunofluorescence analysis. Cell morphology was detected using SEM. The results demonstrated that the integrin subunits in human gingival fibroblasts expressed on both smooth and rough titanium surfaces, the roughness of titanium surface may alter the cell shape but have little effect on integrin expression. The cell morphology are quite different with the variation of surface roughness.

Vinculin

Vinculin is a 1066 amino acids cytoskeletal protein that has a molecular weight of 117 kDa, it is composed of a head and a tail domains (Veronika I. Zarnitsyna & Zhu 2011). Vinculin is also a important protein which localized on the cytoplasmic side and associated with cell adhesions and cell-cell junctions. Although it was shown that vinculin does not bind integrins directly, it is thought to play a dynamic role in focal adhesion assembly by indirectly connecting talin and α-actinin to the actin cytoskeleton

and recruiting additional proteins such as paxillin and vinexin (Ziegler *et al.* 2006).

The function of vinculin is highly regulated by interactions between proteins especially through conformation changes (Golji & Mofrad 2013). In this study, the authors utilized different molecular dynamics simulations to investigate the interaction of vinculin and actin. The results demonstrated that under different level of stress, vinculin would change its conformation and bind different sites on actin. An experimental study conducted by Wen *et al.* (2009) indicated that vinculin can establish a linkage between the adhesion plaques and the cytoskeleton by synthesizing bundled actin filaments or by remodeling existing filaments. The importance of vinculin on regulating focal adhesion formation and turnover was emphasized in a study performed by Humphries *et al.* (2007). They demonstrated that vinculin is a major linker protein associated with focal adhesions and the actin network. It can drive the formation and growth of cell-matrix adhesions by interacting with talin, this interaction occurs in the domain of vinculin head and leads to a cluster of activated integrins. While the tail of vinculin regulates the transmission of mechanical signal. A few publications showed that vinculin links not only to the actin cytoskeleton directly, but also interacts with the proteins that have the competent to regulate the actin, which including VASP (Reinhard *et al.* 1992), Arp 2/3 (Mullins *et al.* 1998) and vinexin (Kioka 1999). Gallant *et al.* (2005) have also proved that vinculin contributes around 30% of the 200-nN adhesive force in cell adhesion strengthening. Based on these studies, it was shown that vinculin is crucial to the cell-matrix adhesion regulation.

1.5 Aims of this study

The long-term successful performance of dental implant depends on both the bone stability and peri-implant mucosa integration. Recently, increasing attentions have been

addressed to the implant abutment interfaces and the transmucosal region of dental implant as dental implants require to form a soft tissue barrier to minimize the correlative complications. The mechanical and biological compatibility derived from surface design is important in maintaining a health and collagen rich connective tissue with minimal bacterial penetration. In order to improve the patients' satisfactions and increase the predictability of implant therapy, significant efforts have been made in the area of implant biomaterials development. These technologies have evolved from simple modification of the oxide surface to nano-scale modification technologies that involve the formation of a uniform and consistent surface that leads to altered cellular response.

The dual-acid-etched together with a proprietary treatment called Discrete Crystalline Deposition (DCD^{TM}) to deposit nanometer scale calcium phosphate hydroxide implementation to titanium surfaces has been reported in earlier studies (Ostman *et al.* 2010)and shown to promote bone integration. The present study sought to examine whether this nanotopographic structures on titanium surfaces could affect human gingival fibroblasts' behavior and enhance cell adhesion. The aim of this work was the detailed examination of the interaction between titanium surface and the biological objects, i.e. the adherent cells. The focus lies in nanostructured (Nanotite) surfaces, as on the one hand the modified titanium surfaces have been proven as particularly suitable for observation of cell shape and adhesion; on the other hand, a few studies have already demonstrated that cells grow on the surfaces with certain roughness adhere better than on smooth ones.

Individual tasks in the work were (a) to study surface modification properties of three different titanium disks, (b) to compare the morphology and proliferation of gingival fibroblasts on tested titanium surfaces and (c) to investigate the expression of integrin and distribution of the adhesion proteins of actin and vinculin in gingival fibroblasts closely. The method of fluorescence labeling and confocal laser scanning microscope were especially used in this part of work.

In this work, the following questions will be answered:

1. What are the differences of cell shape between experimental groups?
2. How was the gingival fibroblasts focal adhesion protein expression distribution on these three surfaces?
3. Can the surface treatment by depositing nanometer scale calcium phosphate hydroxide crystals enhance the cell interaction to titanium surface?

Chapter 2

Materials and Methods

2.1 Titanium alloy disks

The titanium substrates for the cell growth studies are commercially titanium disks of dental implant quality, which are sterilized and packaged individually (10 mm in diameter and 1.5 mm in thickness) were fabricated and kindly provided by BIOMET 3i (3i Implant Innovations, Palm Beach, FL, USA). The diameters of the disks were designed for clinicial studies and to ensure that the disks would match the diameter of 48-well plates. The disks were manufactured from Ti-6Al-4V-ELI alloy (Ti- Alloy) (grade II). Three types of disks were used for this study and each sample was textured on its both sides:

- Ti Alloy-Machined. This surface was prepared by machining (turning) process.

- Ti Alloy-Osseotite. This surface was obtained by dual thermal acid etching (DAE) procedure with hot hydrochloric and sulphuric acids H_2SO_4/HCl

- Ti Alloy-Nanotite. This surface was treated with a proprietary treatment called Discrete Crystalline Depositions (DCD^{TM}) to deposit nanometer-scale calcium phosphate (CaP) particles (20-80 nm nominal size) by sol gel application over the dual acid-etched Osseotite surface to obtain the resulting nanometer scale rough surface called NanoTite.

2.2 Surface characterization of the titanium samples

2.2.1 SEM Imaging

The surface topography of each titanium surface was characterized using a scanning electron microscope (SEM). Titanium surfaces were examined using a field emission scanning electron microscope (ZEISS Supra 55vp; Zeiss,) with the secondary electron detector (accelerating voltage 10keV, working distance approximately 4 mm). Prior to imaging, the titanium disks were sputter coated with 30 nm thickness film of gold palladium alloy in a vacuum evaporator (SC7620 Mini Sputter Coater; Quorum Technologies, Kent, UK) to ensure high reflectivity of the substrate surface. The magnifications selected were 1000, 5000, 10,000 and 20,000 and the micrographs were recorded at randomly chosen areas on the titanium surfaces.Three disks were tested for this assessment, each group contained one disk.

2.2.2 CLSM Imaging

Images of the surfaces were acquired using a laser scanning confocal microscope (CLSM). The titanium alloy disks were examined with a Leica TCS SP2 (Leica Microsystem, Mannheim, Germany). Serial optical sections were collected by 20 up to 30 horizontal images throughout the samples, with a 633 nm laser, using a z-step of 0.5 mm and a 10x objective, a 50x objective.Three disks were tested for this assessment, each group contained one disk.

To calculate the profile roughness values of the three testing surfaces, CLSM images were imported into the distribution of ImageJ program Fiji (Schindelin *et al.* 2012). To make the image stacks in a format suitable for roughness analysis, the ImageJ plugin “Stack

Sorter" (http://www.optinav.com/Stack-Sorter.htm) was installed into the plugins folder to sort the slices of a stack. Furthermore, the plugin "Extended Depth of Field" (Aguet *et al.* 2008) was used to generate a height profile image of the surface. Median filter and FFT filter were used to filter the original height map image, another plugin "SurfCharJ" (Chinga *et al.* 2007) was then used to calculate the Ra value based on the filtered image.

2.3 Cell Culture

Human gingival fibroblasts were purchased from American Type Culture Collection (ATCC, LGC Standard). The fibroblast cell line was originally derived from a gingival biopsy of a 28-year-old Caucasian man. The vial containing the HGF with total cells 7.9x10^5/ml was frozen with cryoprotectant medium consistsing of ATCC-formulated complete growth medium, supplemented with 5% (v/v) DMSO, and was stored in liquid nitrogen vapor phase. To perform the cell culture procedures, the cryovial was removed from the liquid nitrogen container and immediately placed on dry ice, thawed by continuously agitation in a water bath (37°C) according to the manufacturer's protocol. To remove permeable cryo-protective agents, the vial contents were transferred to a centrifuge tube containing 9.0 ml complete growth medium and spun at 1000rpm for 5 minutes. Subsequently, the cell pellet was resuspended and transferred into a 75 cm^2 tissue culture flask containing 10 ml of complete growth medium and antibiotics (10,000 U/ml penicillin, 10 mg/ml streptomycin, GIBCO, Invitrogen, Karlsruhe). To make the complete growth medium, a final concentration of 10 % fetal bovine serum (FBS, Gibco, Invitrogen) was added to ATCC-formulated Dulbecco's Modied Eagle's Medium (DMEM) which was modified to contain 4 mM L-glutamine, 4500 mg/L glucose, 1 mM sodium pyruvate, and 1500 mg/L sodium bicarbonate. Cells were incubated in a humidified 95 % air/5 % CO2 incubator, at 37°C for later subculturing. On the following day, adherence and

viability of cells were observed under the inverted microscope. Old culture medium was discarded and fresh culture medium was added. Thereafter the medium was changed every three days. When cells reached approximately 70 percent of confluence, they were washed with DPBS, (DPBS, GIBCO Invitrogen, Karlsruhe), and treated with $2ml$ 0.25% (w/v) Trypsin-EDTA (ethylene diaminetetraacetic acid), (2.5g/L of Trypsin, 0.38g/L of EDTA·4Na, Invitrogen) for 3-5 minutes until the cell layer was dispersed, adding growth medium to stop the trypsin action. Once the cells were fully detached from the flask surface, the suspension was transferred to a $15ml$ Falcon tube. Suspensions were centrifuged for 5 mins at 1000 rpm in a centrifuge (Sorvall. Langenselbold). Supernatant was then aspirated, carefully avoiding the cell pellet. Pellets were resuspended in 3 ml cell culture medium and were then transferred into new tissue culture asks in a typical ratio of 1:3. 9 ml cell culture medium was added to each of 3 x T75 cm^2 flasks before the cell suspension was added, 1 ml to each. Cells were used for experiments between the 3rd and 6th culture passage. Cells were seeded onto the titanium disks in 48-well cell culture multiwell plates (Greiner bio-one).

Cell counting using a counting chamber

The cell counting measurement was made using a Neubauer Hemocytometer. The Hemocytometer was rinsed with water, and then ethonal (70%) and wiped clean with kimwipes. Equal volumes of 0.4% trypan blue solution and well mixed cell suspension were mixed thoroughly and allowed to stand for 5 minutes. Trypan blue is a vital dye which can enter dead cells and stain them blue, while viable cells don't take up trypan blue, remain unstained. The chamber of the hemocytometer was filled with the well suspended mixture of cells by capillary action. The total number of cells in the four 1 mm outer squares (Figure 2.1) was counted under a standard microscopy and averaged. Each counting chamber of the hemocytometer is etched in a total surface area of 9 mm^2

and is divided into nine 1.0 mm squares. A cover slip is supported over the chambers therefore the volume of each square is 0.0001 ml (length x width x height; i.e. 1 mm x 1 mm x 0.1 mm). Since 1 cm^3 is equivalent to 1 ml, the viable cell concentration per ml will be the average count per square x dilution factor x 10^4 .

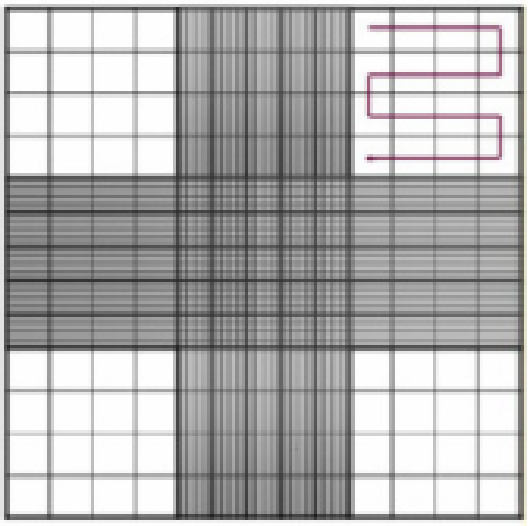

The full grid on a hemocytometer contains nine squares, each of which is 1 mm square. The central counting area of the hemocytometer contains 25 large squares and each large square has 16 smaller squares. Viable Cells /ml = Average viable cell count per square x Dilution Factor x 104.

Figure 2.1: The full grid on a hemocytometer

Cryopreservation of cells

In order to store the cultured cells at early passage for future studies, it is important to maintain them frozen in liquid nitrogen. The confluent gingival fibroblasts were trypsinzed for 3-5 minutes, culture medium was added into tissue culture flask to stop the enzyme treatment. Cell suspension was transferred into 15ml Falcon tube and centrifuged at 1000rpm (Sorvall. Langenselbold) for 5 min. Cell pellet were then resuspended in cold

freezing media (10% DMSO, 90% FCS). Cell suspension (1 ml) was placed in a cryogenic tube, labeled and stored first for 30 min at 4°C , then for 2 h at -20°C , and finally overnight at -80°C . On next day, cells were placed in a liquid nitrogen container.

2.4 Cell visualization assessment by CLSM

2.4.1 Confocal Laser Scanning Microscopy

The Confocal Laser Scanning Microscopy (CLSM) has the advantage of gaining optical images with a high resolution and it is widely used in biological research. The CLSM Leica TCS SP2 (Leica Microsystem, Mannheim, Germany) confocal system is equipped with three independent laser, allowing excitation of a broad range of spectra with the wavelength from 488nm to 633nm, including a blue Ar-laser with a wavelength of 488nm and 514nm, a green Helium/Neon (He/Ne) laser with a wavelength of 543nm and 594nm and a Red He/Ne laser with a wavelength of 633nm. A dye or fluorochrome that is excited by one of these wavelengths can be detected with fluoresence or reflection mode.

Calcein-AM

Calcein-AM (Molecular Probes Invitrogen, product information MAN0001771) is a cell permeant dye that can be used to determine cell viability and morphology. The aceto-methoxy derivate of calcein (Fig 2.2 calcein) can be transported through the cellular membrane into live cells, once inside the cells, intracellular esterases remove the acetomethoxy group and the molecule exhibits strong green fluorescence. As dead cells lack active esterases, only living cells are labeled. Calcein is optimally excited at 488 nm and has a peak emission of 515 nm.

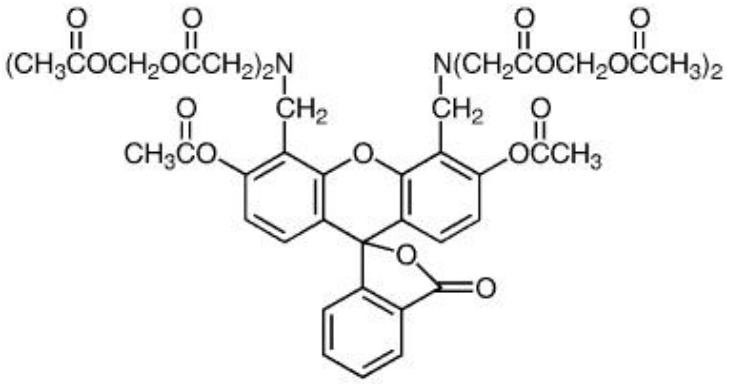

Figure 2.2: The chemical structure of calcein

To evaluate the morphology of the cells, human gingival fibroblasts were seeded onto 3 different titanium disks at a cell density of $0.5x10^4$cells/disk in 48-well cell culture mutiwell plates, cell suspension was applied carefully on each sample and the cells were allowed to attach for 2 h to the underlying substrate, then 1 ml of culture medium was also added. Calcein-AM (1 mg solid) was resuspended in $1000ml$ DMSO to make a 1 mM stock solution, from which $12ml$ was drawn and mixed into 6ml growth medium to make a final working concentration of 2 μM/L. Prior to CLSM analysis, the cells were incubated in 2 μM/L Calcein-AM at 37°C for 60 min and rinsed with DPBS for 3 times, were then transferred to a petri dish filled with 5-7ml growth medium. Images were obtained utilizing an Leica CLSM software, The objective lenses used were: x10 with 0.3 NA, x40 with 0.8 NA water immersion lens. A 488 nm Argon laser line was used for excitation of Calcein-AM with an 515 nm emission filter. A 633 nm laser line was used in order to visualize the underlying titanium surfaces.The cell morphology on 3 different Titanium surfaces were investigated after 1, 3, 7, 11, 18, 24 and 30 days of incubation. At each time point, each group contained three disks, 63 disks overall were tested for this assessment.

2.5 Cell morphology assessment by SEM

Gingival fibroblast morphology and interaction with 3 titanium surfaces were assessed by scanning electron microscope (SEM). The cells were seeded onto 3 different titanium disks at a cell density of $0.5x10^4$ cells/well in 48-well cell culture mutiwell plates. Culture medium was changed every 3-4 days for the duration of experiment. The cells and disks were removed from culture at 3, 11 and 18 days of incubation to study cell-materials interactions under SEM.At each time point, each group contained three disks, 27 disks overall were tested for this assessment.

There are six major steps to prepare a biological SEM specimen: primary fixation, washing, secondary fixation, rinsing, dehydration, drying. The main goal of fixation is to keep the structure of the specimen with minimal change from its living state, so it can resist the effects of subsequent preparing procedures and the exposure to the electron beam. The primary fixative is Karnovsky‘s fixative (2.5 % glutaraldehyde and 2 % of paraformaldehyde, in 0.1 M phosphate buffer pH 7.4), which is most widely used fixative for electron microscope. Formaldehyde and glutaraldehyde are cross-linking agents fixatives, which act by creating covalent chemical bonds between proteins in tissue (Bozzola 2001),herefore, are very effective fixatives for proteins and nucleic acids. After primary fixation, the specimen were washed in the same buffer as used in the primary fixation process. Dehydration is the process of removing water from cells. The water is generally replaced with ethanol or acetone. Usually 25 % ethanol is the first solvent in the dehydration procedure, followed by 50 %, 70 %, 95 % and 100 % ethanol. Cell morphology of the in vitro culture was visualized with a scanning electron microscope (SEM).

At the end of each culture period, the medium was removed from the wells, cells on titanium disks were rinsed with 0.1 M phosphate buffered saline (PBS). Samples were subsequently fixed with 2 % paraformaldehyde (Polysciences, Eppelheim, Germany)/2.5

% glutaraldehyde (Sigma-Aldrich, Munich, Germany) in 0.1M sodium cacodylate buffer overnight at 4°C . Following three rinses in 0.1 M cacodylate buffer, the fixed sample was then again rinsed three times in 0.1 M cacodylate and dehydrated through an ethanol series (25 %, 50 %, 70 %, 95 % and 100 % three times). Finally hexamethyldisilazane (HMDS) was used for complete dehydration of the samples. Samples were immersed in HMDS in glass vials. After a soak time of 30 minutes, the HMDS was removed, the cover of specimens was left over night which allows to evaporate HMDS in a fume hood. Dried samples were then mounted on aluminum stubs, cells on the disks were observed by a scanning electron microscopy (Quanta 200 FEG, FEI Company, Eindhoven, Netherland). Images were recorded at 150x, 400x and 800x magnification.

2.6 Cell proliferation using Alamar Blue assay

Alamar Blue (AB) is a water-soluble redox dye which has been used for quantifying in vitro viability and proliferation of various mammalian cells (Fields & Lancaster 1993). Due to its stability and safety, it allows for continuous real time and repeated monitoring of cell proliferation. The assay is based on the ability of viable, metabolically active cells to reduce resazurin to resorufin (Vega-Avila & Pugsley 2011). When added to cell cultures, the oxidized form of the AB enters the cytosol and is converted to the reduced form by mitochondrial enzyme activity by accepting electrons from NADPH, FADH, FMNH, NADH as well as from numerous cytochromes (Al-Nasiry et al., 2007). The reduction related to cell growth causes the AB to be converted from the oxidized (non-fluorescent) blue form to the reduced (fluorescent) red form. This color change can be monitored by absorbance (λ ex=570 nm and λ em=630 nm).

Briefly, cells were seeded onto titanium disks at 5,000 cells per well with 1 ml growth medium in 48-well cell culture multiwell plates (Becton Dickinson, , Germany). Cell

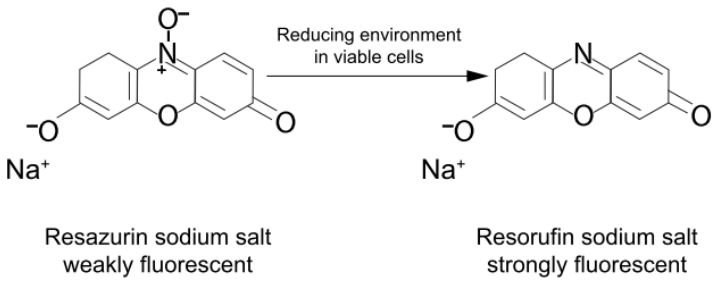

Alamar Blue assay is based on the ability of viable, metabolically active cells to reduce resazurin to resorufin.

Figure 2.3: Alamar Blue assay

proliferation was tested at 3, 7 and 14 days after incubation. At each specific culture time point, the growth medium was discarded and washed with PBS twice. Each well was filled with 0.5 ml AlamarBlue (Invitrogen, Life Technologies, Darmstadt, Germany)/fresh culture medium at a ratio of 1 : 9 and incubated at 37°C for 4 hours. As a negative control, AB was added to the medium without cells. 300μl of the solution from each well was transferred to a clear bottomed 96-well tissue culture plate (100μl/well). The absorbance of test and control wells was measured with a standard spectrophotometer (Thermo Scientific Multiskan GO) at a wavelength of 570 nm and 630 nm. The results were obtained from three separate experiments.At each time point, each group contained six disks, 18 disks were tested for this assessment. The remaining AB/culture medium solution in 48-well cell culture plates was discarded and fresh culture medium was added for the continuous cell growth. The number of viable cells correlates with the magnitude of dye reduction and is expressed as percentage of AB reduction Ahmed *et al.* (1994), Goegan *et al.* (1995). The calculation of the percentage reduction of AB (%AB reduction) is as follows according to the manufacturer's protocol:

$$\%ABreduction = \frac{(O_2 \times A_1) - (O_1 \times A_2)}{(R_1 \times N_2)} \times 100\% \tag{2.1}$$

In the formula, O_1 and O_2 are constants representing molar extinction coefficient (E) of oxidized AlamarBlue (Blue) at 570 nm and 630 nm, respectively ; R_1 and R_2 are E of reduced AlamarBlue at 570 nm and 630 nm; A_1 and A_2 represent the absorbance of test wells at 570 and 630 nm; N_1 and N_2 represent the absorbance of the negative control well (medium plus AlamarBlue but no cells) at 570 nm and 630nm.

2.7 Fluorescence Activated Cell Sorting (FACS) analysis

Flow cytometry or FACS is a technology that simultaneously measures and then analyzes multiple physical characteristics of single particles, usually cells, as they flow in a fluid stream through a beam of light. It measures a particle's or cell's: relative size, granularity or internal complexity and relative fluorescence intensity (BD Biosciences, Manual Part Number: 11-11032-01).

The cell surface expression of integrins subunit $\alpha5\beta1$ on human gingival fibroblasts grown on the titanium surfaces was estimated by direct immunofluorescence using flow cytometric techniques.

Briefly, human gingival fibroblasts were placed on titanium surfaces at a density of 5,000/well and cultured up to 14 days and harvested by treatment with trypsin/PBS for 5 minutes at room temperature. After the cells had been detached from the disks, 2 ml of serum-free medium was added and the cells were pelleted. The cells were resuspended in PBS. Sedimented cells were incubated with 20μl of monoclonal anti-integrin antibodies against $\beta1$(CD29), $\alpha5$(CD49e) (all from BD Biosciences) or for control with mouse IgG (BD Biosciences) for 30 min at room temperature while being protected from light. The cells were washed again 3 times with PBS and resuspended in 300μl of the

washing buffer. Finally, the surface expression of $\alpha 5\beta 1$ was measured on a FACS Calibur (Becton Dickinson, Heidelberg, Germany) with CELLQUEST software (BD Bioscience). Nonspecific IgGs of the same isotype were used as a negative control. Results were reported as relative fluorescence intensity, as compared to the negative control. Each group contained six disks, 18 disks were tested for this assessment. At least 10,000 cells were analyzed for each group.

2.8 Immunocytochemistry

Immunofluorescence is a method used to localize specific proteins in cells by using fluorescent-labeled monoclonal antibodies which bind to the epitope of antigens specifically. Therefore it allows the visualization of the target cellular protein with a fluorescence microscope.

There are two main types of immunofluorescence techniques: direct immunofluorescence staining uses a single direct antibody labeled with a fluorophore; indirect immunofloures-cence uses an unlabelled primary antibody which binds to an antigen, and a dye-labeled secondary antibody targets the FC end of the primary antibody. Multiple secondary antibodies bind to a single primary antibody make the signal amplified compare to direct immunofluorescence.

Multiple immunofluorescence staining can be achieved by using different fluorescent dyes to label two or more antigens in cells simultaneously. This method in combination with CLSM is a powerful strategy if exitation and emmision bandwidth of spectra of the fluorophores do not interfere with each other.

For immunofluorescent labeling of the actin cytoskeleton and the focal adhesion protein vinculin, the 3 different titanium disks were placed into 48-well Falcon culture plates

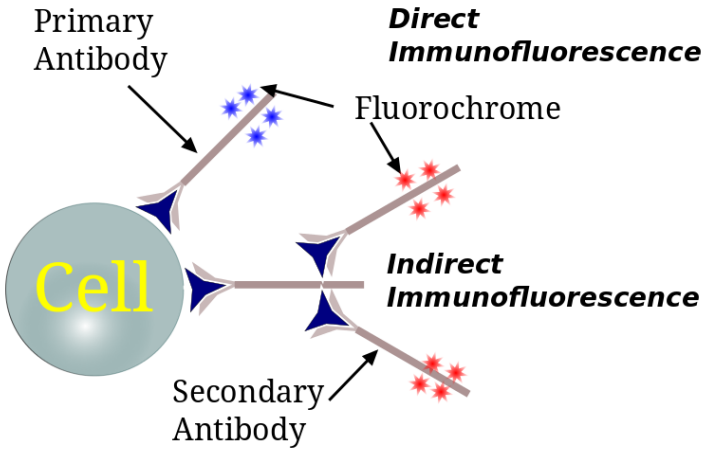

modified according to (Sawant, Kshar et al. 2014).

Figure 2.4: The principle of immunofluorescence

(Becton Dickinson, Heidelberg, Germany) and carefully covered with the gingival fibroblasts at the cell density of $0.5x10^4$ cells/well. The cells were allowed to settle for 2 h in the incubator at 37°C , after which 1 ml of complete medium was added. The cells were incubated for 24 and 30 days.

These cells were subjected to fluorescence staining for vinculin and actin filaments. All antibodies and blocking solutions were purchased from Invitrogen. After the indicated time periods, the cells were washed once with 37°C Phenol Red-free DMEM (with FCS) and fixed using pre-warmed formaldehyde (4% in Phenol Red-free DMEM, + L-glutamine, no FCS). The fixed cells were washed three times (5 min each) with PBS and incubated with 0.1% Triton® X-100 (Sigma-Aldrich, Munich, Germany) in PBS for 30 min at RT to permeabilize the cells. Then the cells were treated with the blocking buffer (3% Bovine serum albumin, BSA, in PBS) for 30 min at RT. Subsequent to the blocking procedure the cells were incubated with the primary antibody (anti-vinculin, 1:100 in 3% BSA in PBS) for 1h at RT. To remove the primary antibody, cells were washed three times with PBS for 5 min at RT and incubated with the secondary antibody Alexa Fluor

546 donkey anti-mouse IgG (1:200 in 3% BSA in PBS) for 1.5 h at RT. For a nuclear counterstaining, the cells then were washed three times with PBS for 5 min at RT and incubated with 10 μM TO-PRO®-3 solution (Invitrogen) (300μl/well) for 40min at RT. For labeling F–actin in adherent cells grown on titanium disks, 5μl MFP 488 phalloidin methanolic stock solution (MoBiTec GmbH, Germany) was diluted in 200μl 3% BSA in PBS for each disk to be stained after further washing steps with PBS. The cells then were incubated with phalloidin solution (200μl/well) for 20 min at RT. Phalloidin, a toxin from the toadstool "Death Cap" (Amanita phalloides) that binds actin (Lengsfeld *et al.* 1974), and it is conjugated with fluorescence dye MFP 488. Following this, the stained cells were observed and images of the stained cells were obtained using a confocal laser scanning microscopy Leica TCS SP2(Leica Microsystem, Mannheim, Germany).

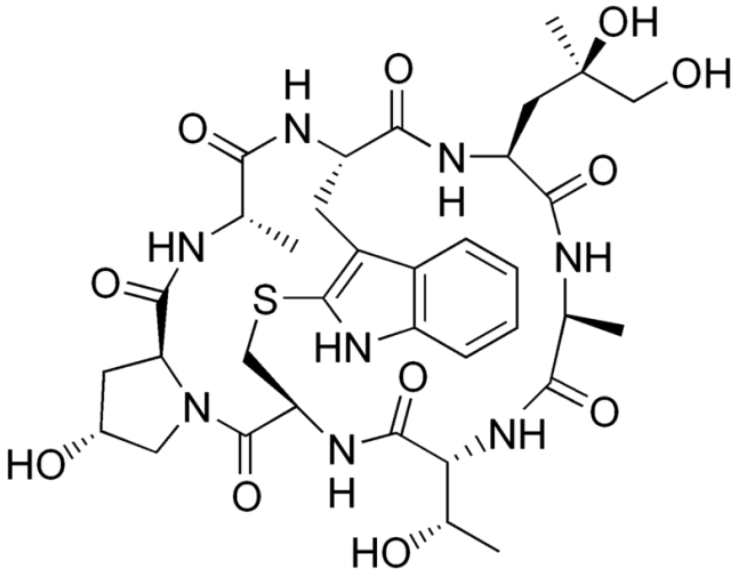

Phalloidin contains an unusual thioether bridge between a cysteine and tryptophan residue that forms an inner ring structure, it binds to actin filaments much more tightly than to actin monomers, leading to a decrease in the rate constant for the dissociation of actin subunits from filament ends, which essentially stabilizes actin filaments through the prevention of filament depolymerization (Cooper 1987).

Figure 2.5: Chemical structure of phalloidin

2.8.1 Confocal imaging

The fluorescent labeling of the actin cytoskeleton, the focal adhesion protein vinculin and the nuclear was examined using a Leica TCS SP2 confocal system. It was equipped with an argon laser (specific wavelengths at 488 nm) to excite MFP 488 phalloidin green dyes, one helium neon laser (543 nm) to excite Alexa Fluor 546 red dyes and also there is a third helium neon laser fluorescence channel at 633 nm excitation for nucleus staining to excite TO-PRO®-3. The system including a Leica TCS SP2 microscope equipped with filters for the detection of related dyes. The images were obtained with a zoom factor of 1.0 and a field resolution of 1024×1024 pixels using the CLSM software (Leica). The pinhole value which represents the thickness of the optical slide through the cell was always kept constant for all confocal channels during detection of the identical cell.

Chapter 3

Results

3.1 Surfaces Characterization

SEM and CLSM evaluation revealed marked topographic differences among Machined, Osseotite and Nanotite surfaces.

3.1.1 SEM Imaging

Figure 3.1-3.4 show representative scanning electron micrographs of Machined, Osseotite and Nanotite surfaces. Obvious difference in the fine structure was found among the three Ti surfaces at low and high magnification of microscopic level.

At low magnification (1000 x), the surface of Machined Ti disks is homogeneous and smoothest among the three experimental groups, it exhibited parallel grooves resulting from the machining process; the Osseotite surface exhibited many micropits and it was rougher in comparison with the Nanotite titanium surface.

At higher magnification (5000 x), the topographical features of the machined surfaces are similar, there are a few irregularities, which possibly due to mechanical processing resulted in the plastic deformation; a greater number of micropits structures were shown on Osseotite surface, which forms the appearance of open pores and are the typical

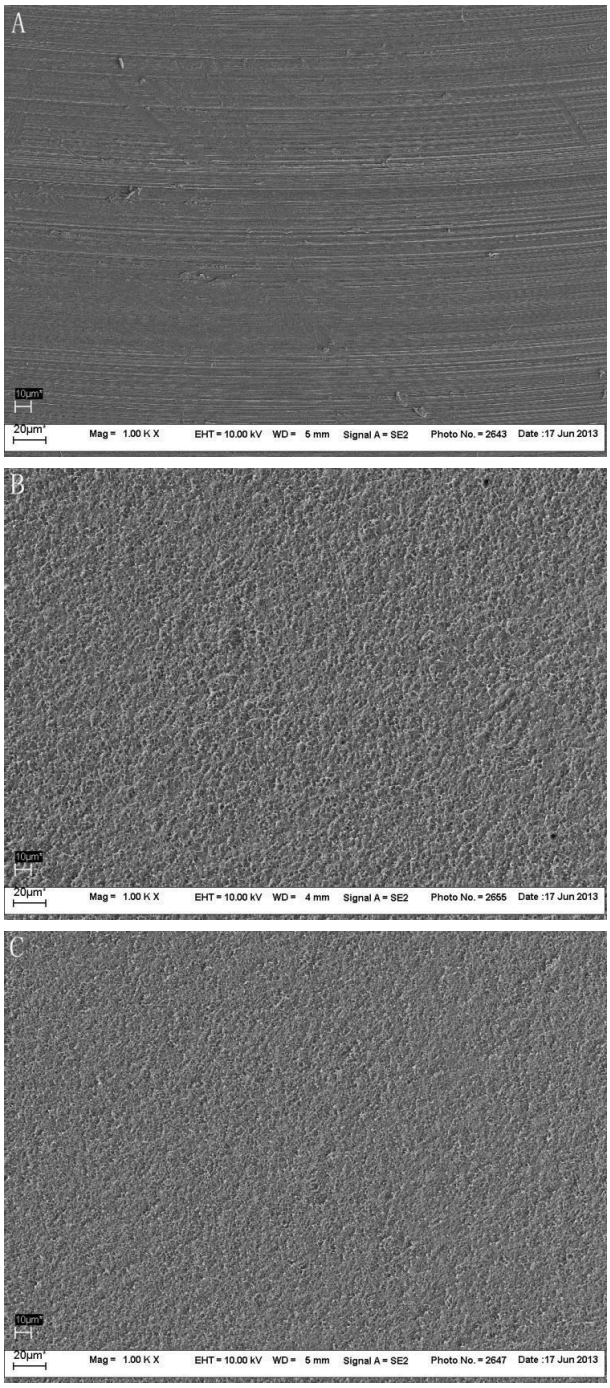

3.1-a) Machined Ti surface

3.1-b) Osseotite Ti surface

3.1-c) Nanotite Ti surface

Figure 3.1: Representative SEM images of Machined (A), Osseotite (B) and Nanotite (C) Ti surfaces. (magnification 1000, FE-SEM Supra 55vp, Carl Zeiss)

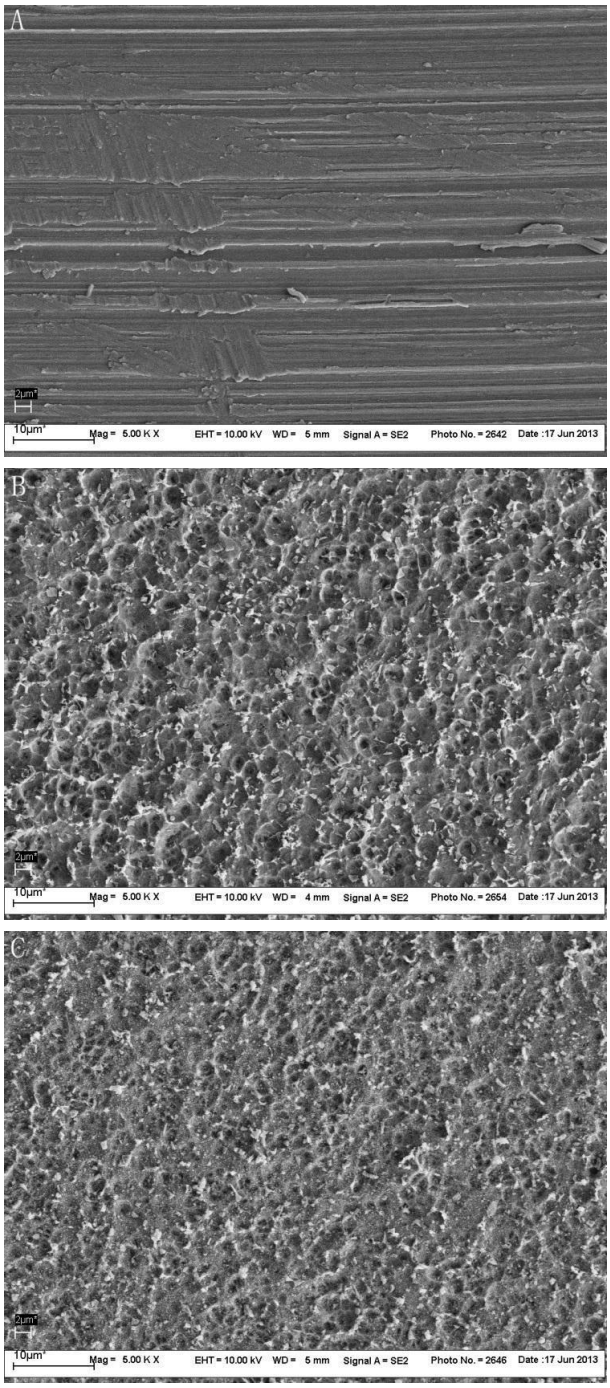

3.2-a) Machined Ti surface

3.2-b) Osseotite Ti surface

3.2-c) Nanotite Ti surface

Figure 3.2: Representative SEM images of Machined (A), Osseotite (B) and Nanotite (C) Ti surfaces. (magnification 5000, FE-SEM Supra 55vp, Carl Zeiss)

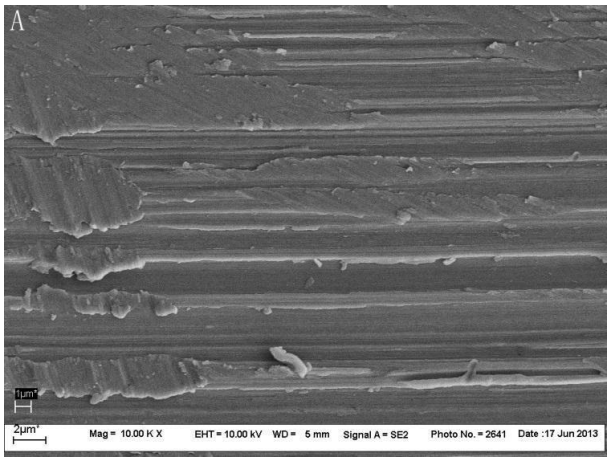

3.3-a) Machined Ti surface

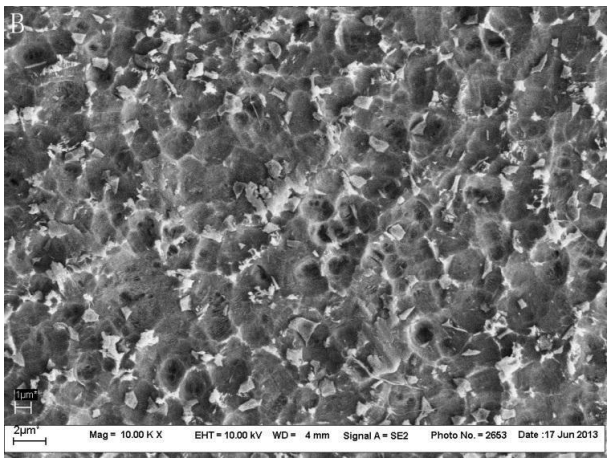

3.3-b) Osseotite Ti surface

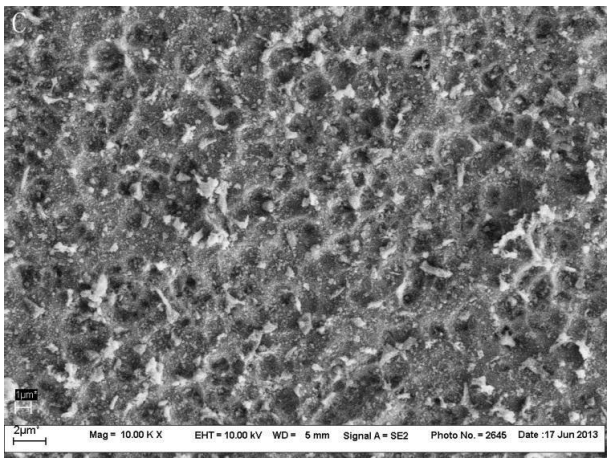

3.3-c) Nanotite Ti surface

Figure 3.3: Representative SEM images of Machined (A), Osseotite (B) and Nanotite (C) Ti surfaces. (magnification 10000, FE-SEM Supra 55vp, Carl Zeiss)

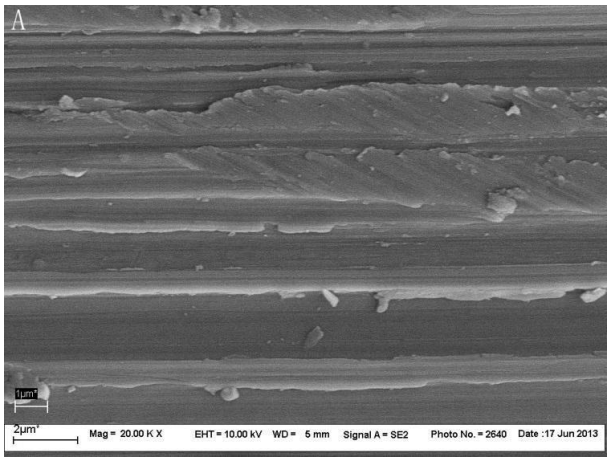

3.4-a) Machined Ti surface

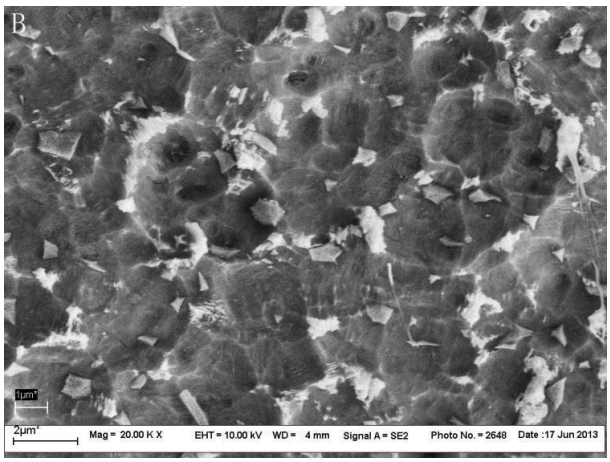

3.4-b) Osseotite Ti surface

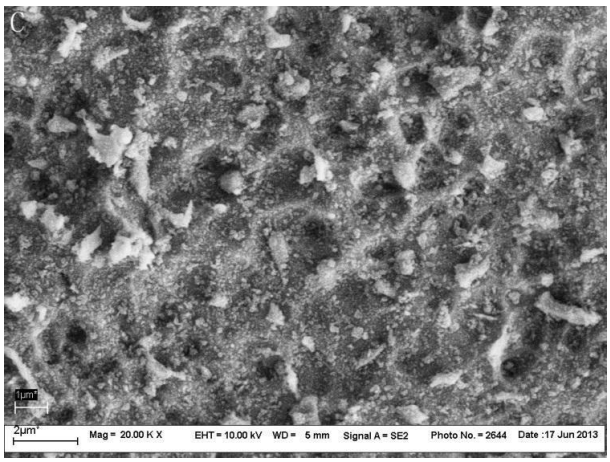

3.4-c) Nanotite Ti surface

Figure 3.4: Representative SEM images of Machined (A), Osseotite (B) and Nanotite (C) Ti surfaces. (magnification 20000, FE-SEM Supra 55vp, Carl Zeiss)

features produced by immersing the titanium surfaces in a mixture of concentrated HCl and H_2SO_4; the Nanotite surface showed similar underlayer structures with Osseotite surface, while even distributed fine particles are deposited densely onto the roughened surface.

At high magnifications (10000 x and 20000 x), the parallel grooves and the structure of the plastic deformed layer are obvious on the Machined surface; The Osseotite group uses an dual acid-etching process to produce irregular pits throughout the surface, it is mainly characterized by prominent peaks and valleys, some of them with well-defined contours; there are some micro particles covered on the surface, which may be caused by the participation of acid treatment. The Nanotite surface adds a thin layer of calcium phosphate crystals between 20-100 nm in length over the Osseotite surface, (Nanotite implant brochure BioMET 3i) showed nano scale particles covered on the surface, the roughness was reduced compared to Osseotite.

CLSM Imaging

The results of CLSM observation are shown in Figure 3.5 and 3.6; the machined surface reveals a regular planar surface, with parallel grooves caused by the machining process. The Osseotite disk shows an increase in the surface roughness compared to Nanotite disk.

After image processing and filtering by FFT, which are shown in Figure 3.7 and 3.8, the roughness values for Machined, Osseotite and Nanotite surfaces were calculated and are shown as follows: 11.614; 13.649; 12.530. Therefore, the roughness of three surfaces increased as follow: Machined < Nanotite < Osseotite.

To determine the average surface roughness (Ra) of three experimental dental implant surfaces from CLSM images, ImageJ programm was used for image processing. Since the

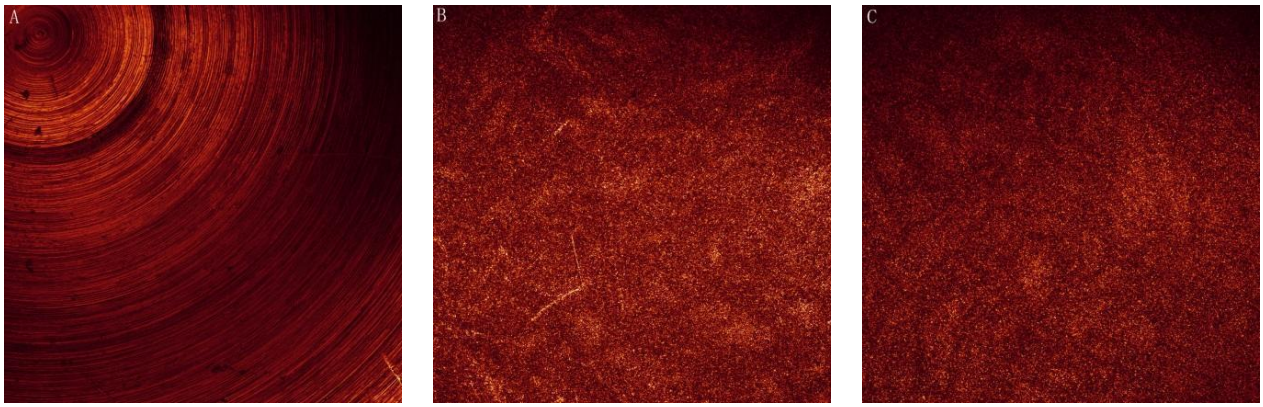

3.5-a) Machined Ti surface 3.5-b) Osseotite Ti surface 3.5-c) Nanotite Ti surface

Figure 3.5: Representative CLSM images of Machined (A), Osseotite (B) and Nanotite (C) Ti surfaces. (magnification 10X,)

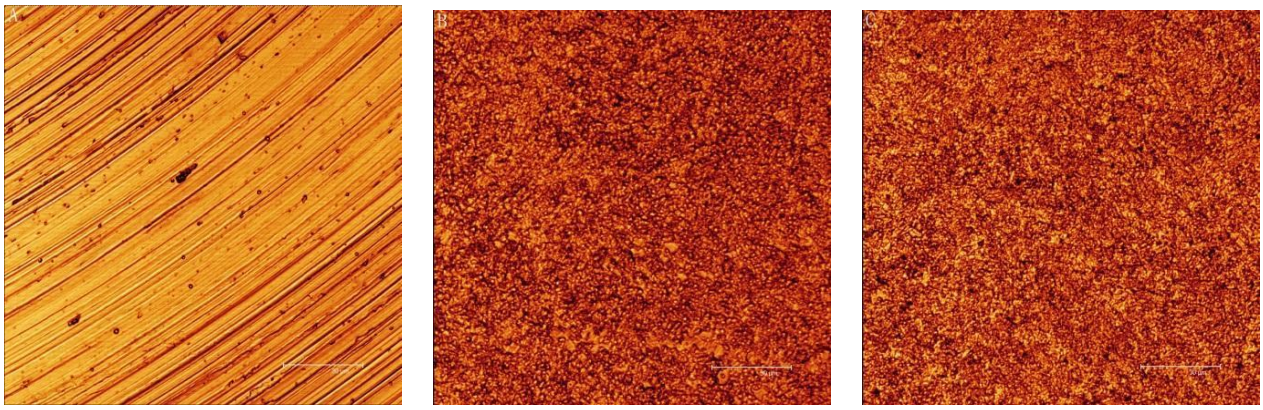

3.6-a) Machined Ti surface 3.6-b) Osseotite Ti surface 3.6-c) Nanotite Ti surface

Figure 3.6: Representative CLSM images of Machined (A), Osseotite (B) and Nanotite (C) Ti surfaces. (magnification 50X,)

3.7-a) Machined Ti surface

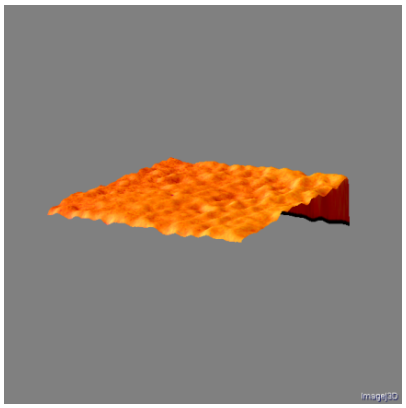

3.7-b) Osseotite Ti surface

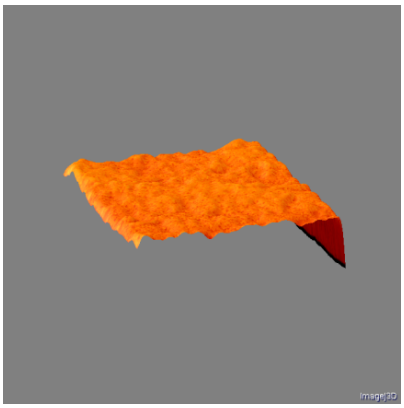

3.7-c) Nanotite Ti surface

The height map images of Machined (a), Osseotite (b) and Nanotite (c) Ti surfaces; a significant difference in the surface roughness was found between Osseotite surface and Nanotite surface.

Figure 3.7: The heightmap images of titanium surfaces

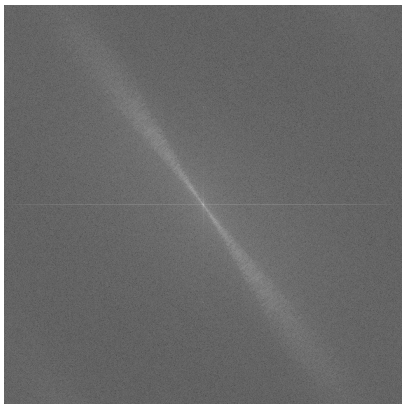

3.8-a) Machined Ti surface

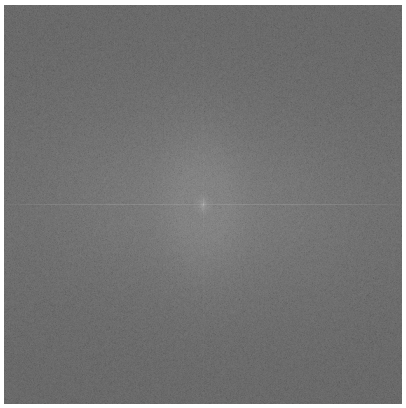

3.8-b) Osseotite Ti surface

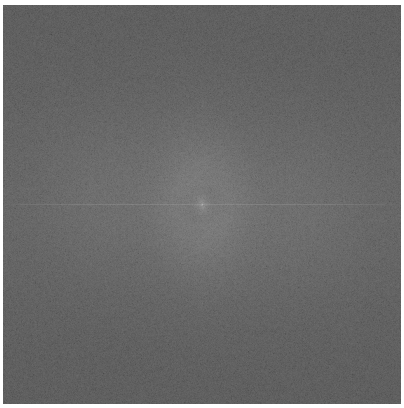

3.8-c) Nanotite Ti surface

The Fast Fourier Transform images of Machined (a), Osseotite (b) and Nanotite (c) Ti surfaces; visible proofs for the patterns of grooves were found on the FFT image of Machined surface since low frequency components values are close to the centre, while the high-frequency components are far from the centre. The FFT images of Osseotite and Nanotite titanium surfaces showed no visible surface patterns because the original images contain no patterns.

Figure 3.8: The Fast Fourier Transform images of titanium surfaces

Machined implant surface is polished mechanically, characterized by regular scratches mostly oriented along the machining direction, it has to be separated into roughness and waviness components. Moreover, two filters were used to filter the resulted heightmap images. Median filter was selected to reduce some noise on the image, it was considered better than mean filter or rolling ball. A FFT filter is used to separate the Machined surface and to show the different components of the surface. The Fourier transform of an image is symmetric to the centre, the centre of the FFT displays the image uniform component. From the FFT image of Machined surface, we can observe that low-frequency components (roughness) values, which are close to the centre, while the high-frequency components (waviness) are far from the centre. From the FFT images of Osseotite and Nanotite surface, we can only see the low-frequency components (roughness) values since they are even.The heightmap images of roughness (left) and waviness (right) component of Machined surface were shown in Figure 3.9. Thereafter the roughness values for Machined surface was calculated from the roughness component image.

After image processing and filtering by FFT, the average surface roughness (Ra) values for Machined, Osseotite and Nanotite surfaces were calculated and shown as follows: 1.16 μm; 1.36 μm; 1.25 μm. Therefore, the roughness of the three different surfaces increased as follow: Machined <Nanotite <Osseotite.

3.1.2 Confocal examination of cell morphology

The observations of cell morphology on 3 different Titanium surfaces after 1, 3, 7, 11, 18, 24 and 30 days of incubation are shown in Figure 3.10-3.23 . Cells stained with fluorescein Calcein-AM were photographed with CLSM, the recordings were performed with 10-fold and 40-fold magnification at a excitation wavelength of 488 nm. The imaging of the titanium samples was obtained by reflection of the 633 nm laser line. The selected

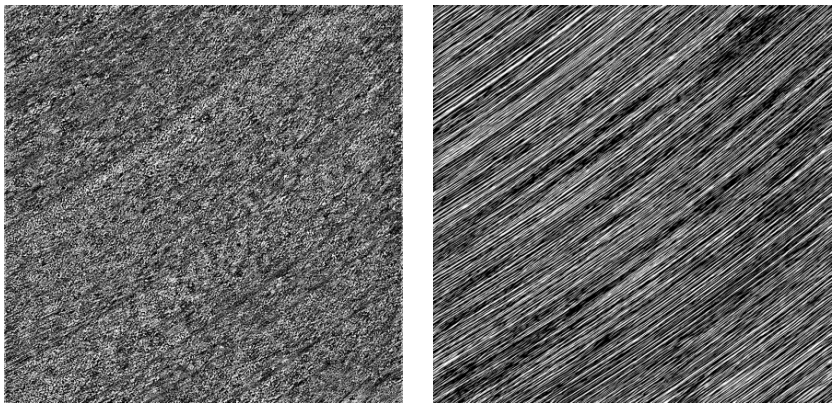

3.9-a) Roughness 3.9-b) Waviness

Figure 3.9: The heightmap images of roughness and waviness component of the Machined surface

images are representative of the all investigated surfaces. Fields were selected randomly; the only criterion for cell selection was that the cell was not in contact with other cells.

The CLSM pictures showed that: at day 1, the cells on machied surface were long and start to contact with neighbouring cells; they grew along the the circular pattern of grooves on the disks; on the Osseotite surfaces, the shape of fibroblasts were irregular, a few filopodias were produced at the cell edges and towards the neighbouring cells; on the Nanotite surfaces, the shapes of cells are round or dendritic, they looked relative isolated. As the culture period increased, the size, number of the cells as well as the number of filopodias are growing over time. From day 1 to day 7, the fibroblasts on the Nanotite surfaces were shorter and fewer than the cells on Osseitite surfaces; from day 11, this difference was not obvious. At day 18, most cells showed a elongated morphology on all surfaces; although some cells remained round on the surface of Nanotite whilst the cells on Osseitite were more spread and flat. This trend was kept at day 24. At day 30, human gingival fibroblasts formed a single monolayer of cells on Machined surfaces; it was additionally found that after a culture period of 30 days the cells on Osseotite surfaces

were more spread and formed a higher surface coverage than on Nanotite surfaces.

3.2 SEM imaging of cell morphology

A scanning electron microscope (Quanta 200 FEG SEM) using back scattered electrons, 2KV of voltage was used to acquire images of cells grown on three different titanium disks at 3, 11 and 18 days.

SEM observations showed that cells were able to adhere to all three different surfaces at the time points tested. At day 3, it is obvious that more cells were observed on Machined and Osseotite surfaces compared to Nanotite surfaces. Cells with greater extent of spreading and more filopodias were detected on Machined discs. After eleven days of culture, cell density was higher on all the groups. The cells attaching to the Machined surfaces elongated along the turning patters and produce prominent filopodias. The fibroblasts on Osseotite and Nanotite were unevenly distributed; most of the cells on both surfaces showed spindle, round or longer shapes, they are still relative isolated. By 18 days of incubation, the cells on Machined surfaces were on the process of becoming confluent, they spread quite well and covered a big area of the surface. In case of the cells cultured on Osseotite and Nanotite surfaces, in generally, they appeared larger, more spread out and formed cell-cell contacts; the cells showed a similar shape.

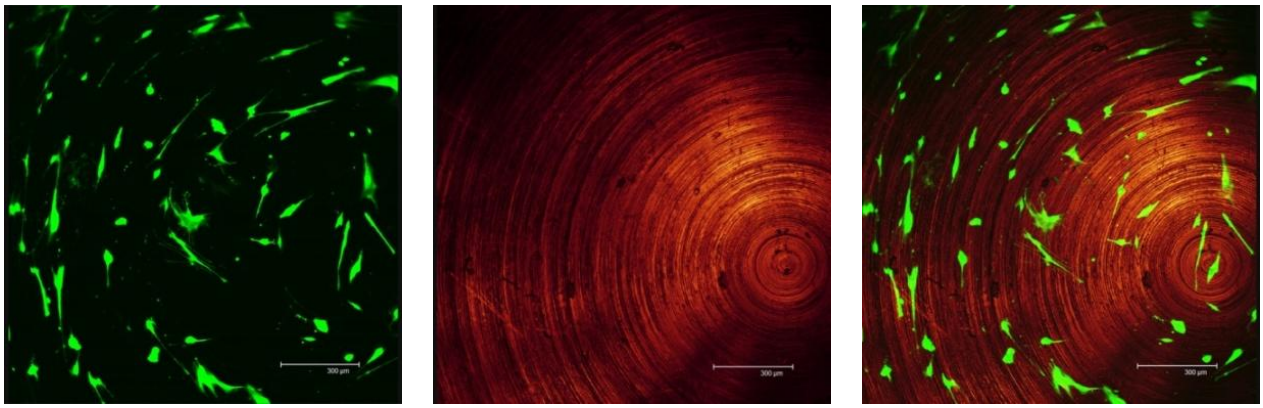

3.10-a) Mathines Ti surface

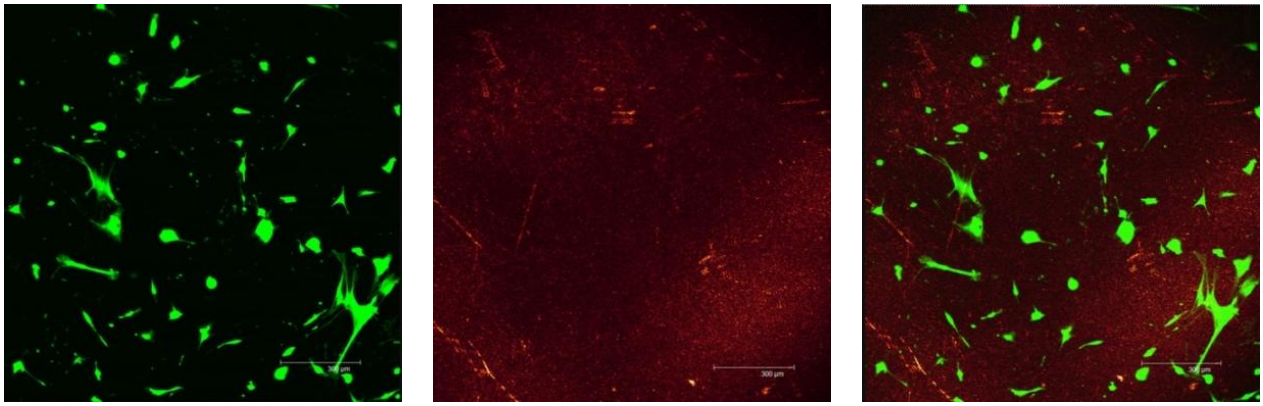

3.10-b) Osseotite Ti surface

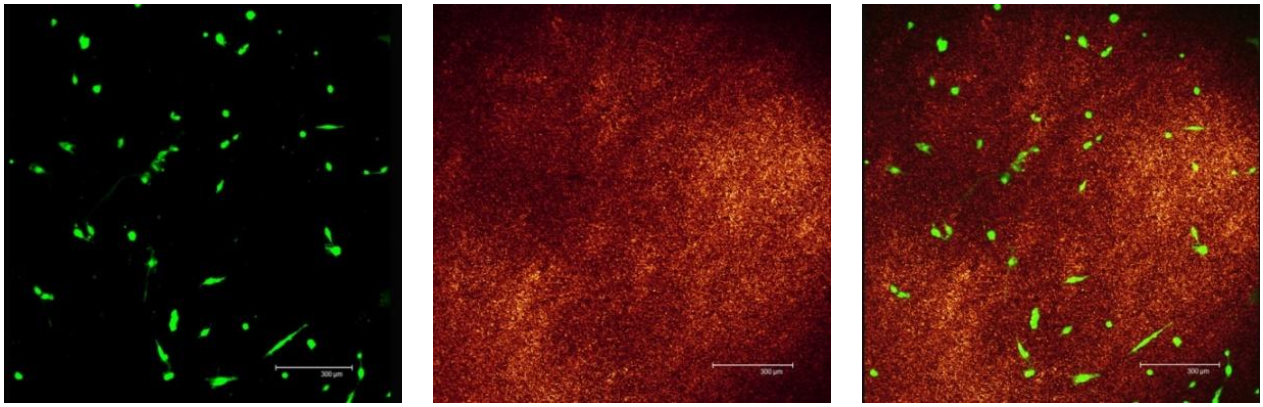

3.10-c) Nanotite Ti surface

Cell morphology of human gingival fibroblasts on Maschined (A), Osseotite (B) and Nanotite (C) titanium surfaces after 1-day incubation period. (magnification 10X,) The scale bar corresponds to a length of 300 μm.

Figure 3.10: Cell morphology of gingival fibroblasts after one day incubation A

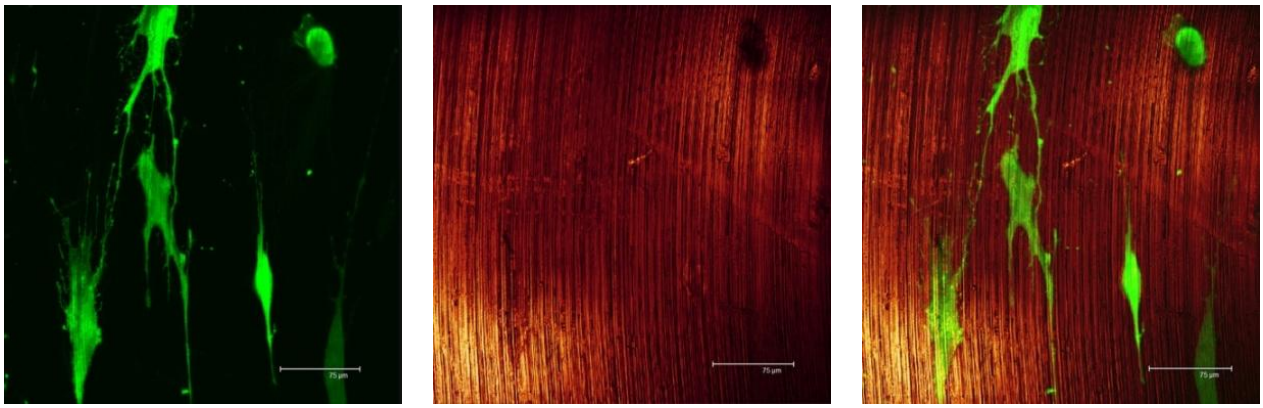

3.11-a) Mathines Ti surface

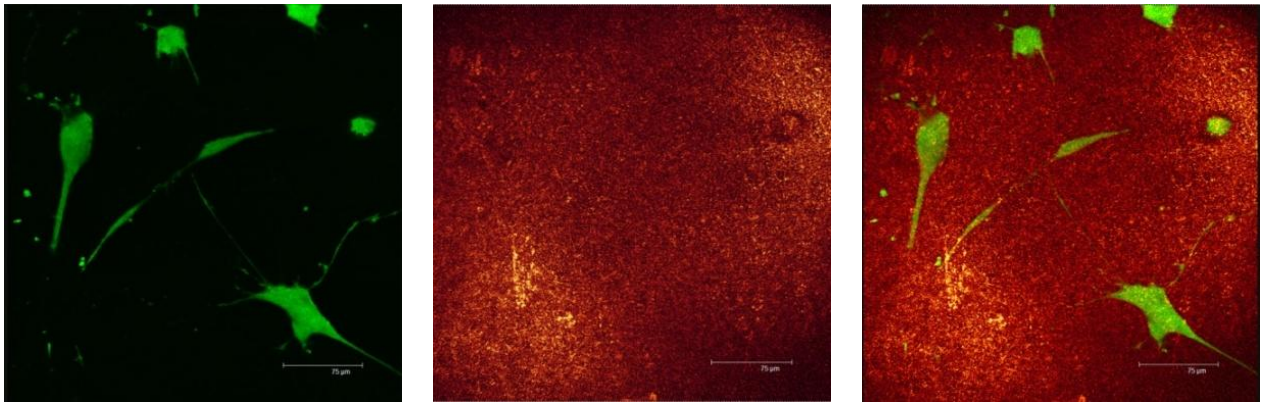

3.11-b) Osseotite Ti surface

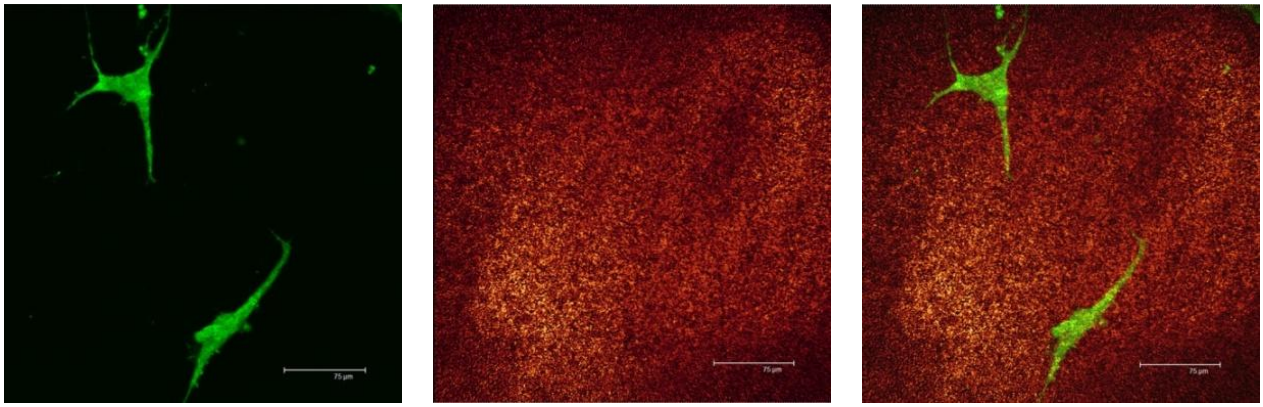

3.11-c) Nanotite Ti surface

Cell morphology of human gingival fibroblasts on Maschined (A), Osseotite (B) and Nanotite (C) titanium surfaces after 1-day incubation period. (magnification 40X,) The scale bar corresponds to a length of 300 μm.

Figure 3.11: Cell morphology of gingival fibroblasts after one day incubation B

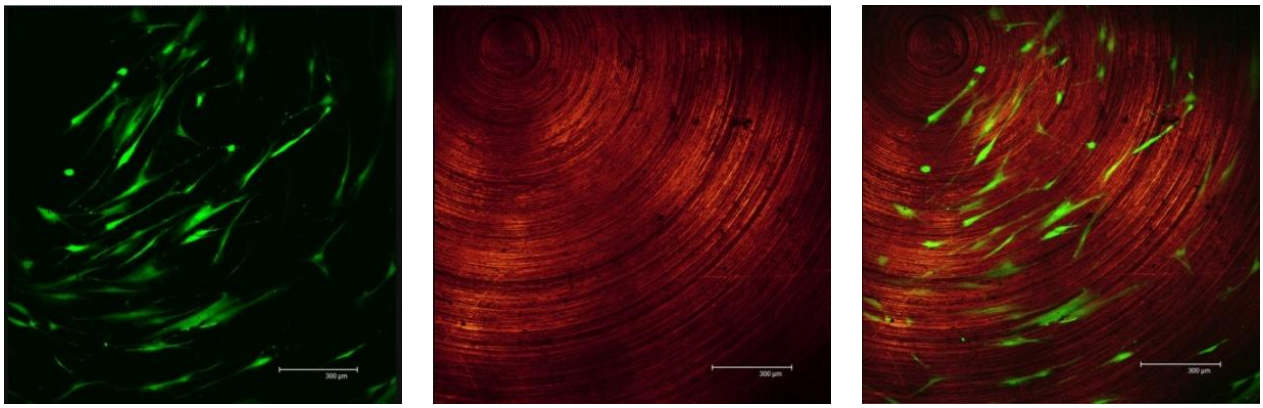

3.12-a) Mathines Ti surface

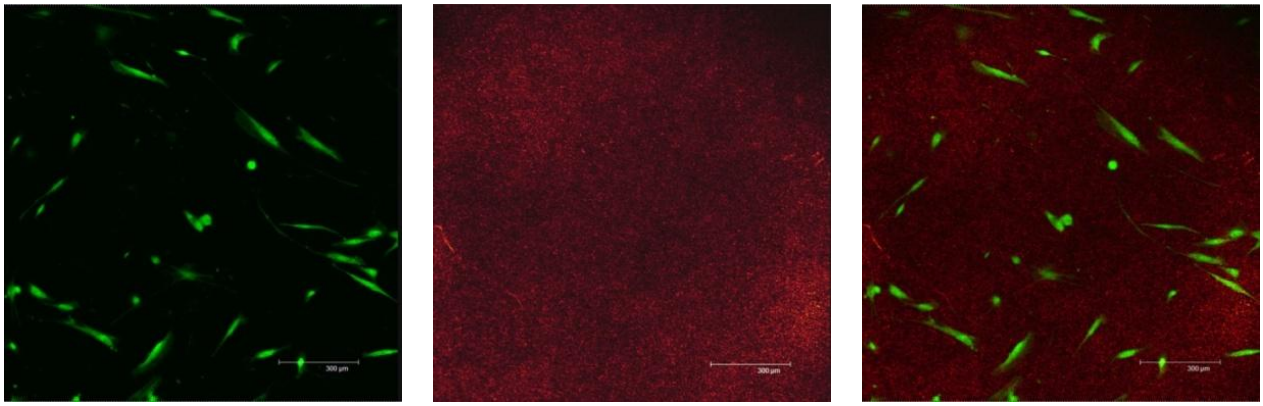

3.12-b) Osseotite Ti surface

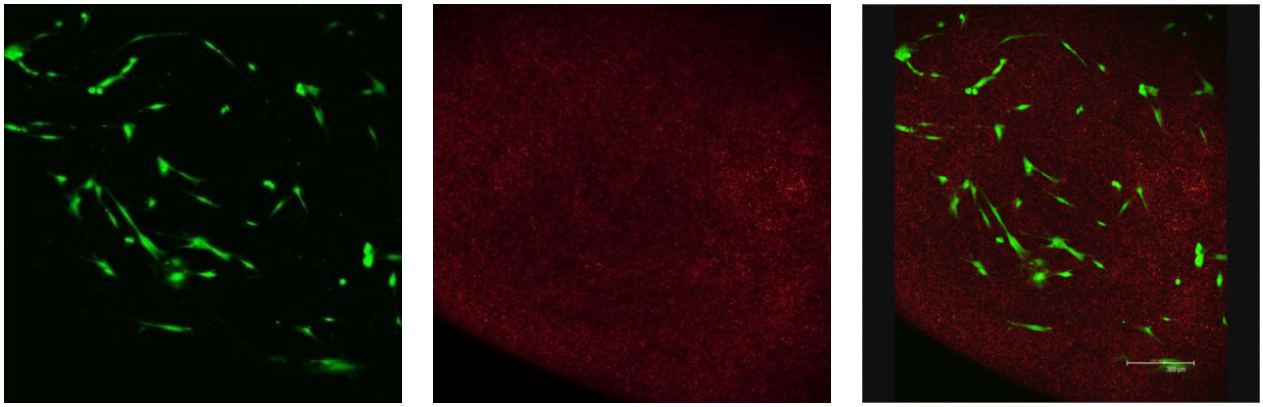

3.12-c) Nanotite Ti surface

Cell morphology of human gingival fibroblasts on Maschined (A), Osseotite (B) and Nanotite (C) titanium surfaces after 3-day incubation period. (magnification 10X,) The scale bar corresponds to a length of 300 μm.

Figure 3.12: Cell morphology of gingival fibroblasts after three days incubation A

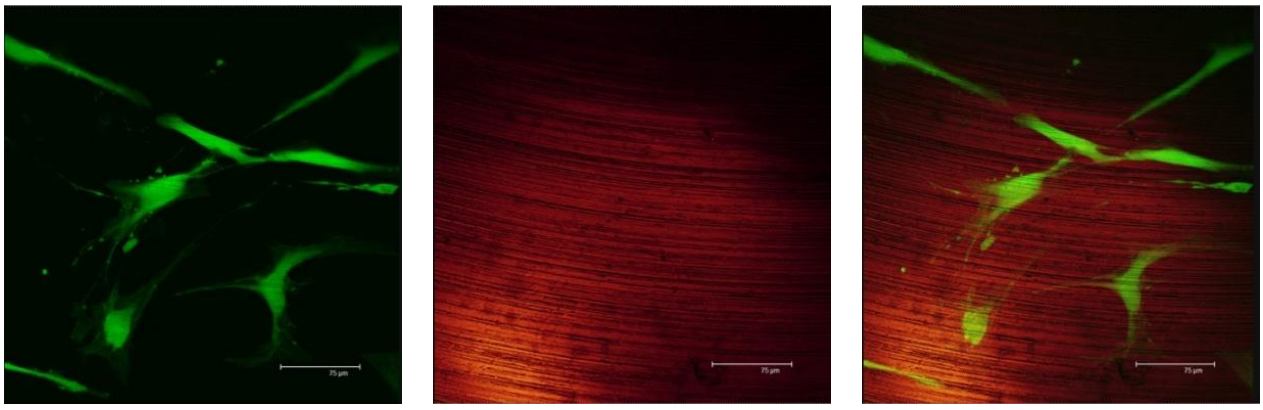

3.13-a) Mathines Ti surface

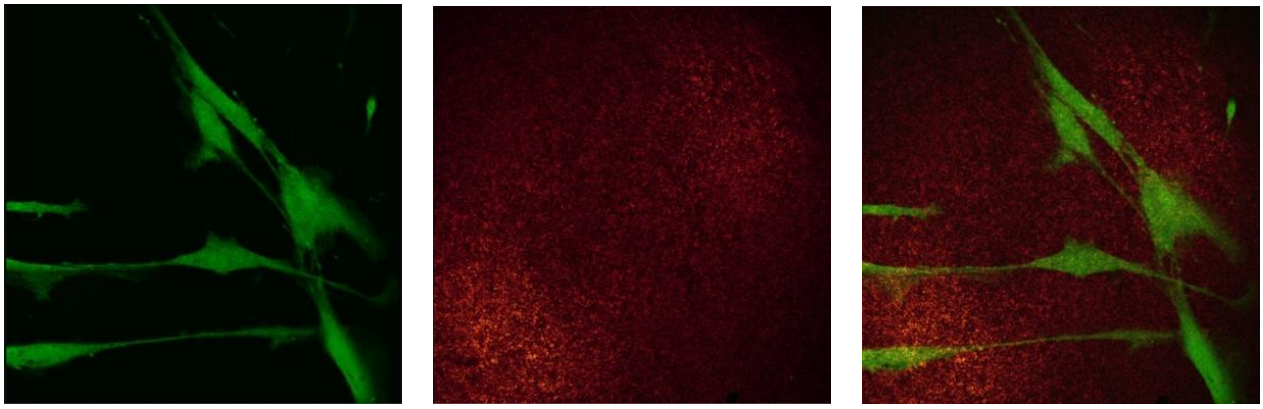

3.13-b) Osseotite Ti surface

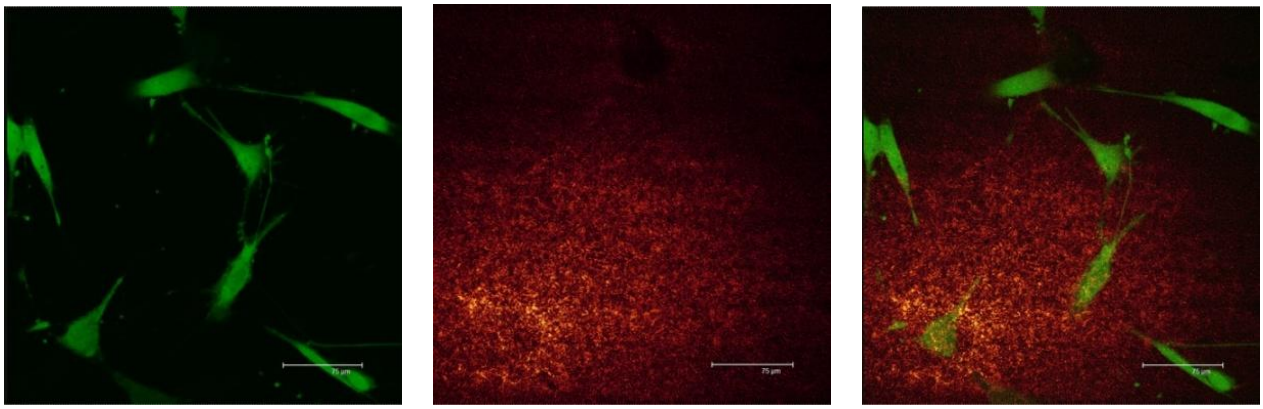

3.13-c) Nanotite Ti surface

Cell morphology of human gingival fibroblasts on Maschined (A), Osseotite (B) and Nanotite (C) titanium surfaces after 3-day incubation period. (magnification 40X,) The scale bar corresponds to a length of 300 μm.

Figure 3.13: Cell morphology of gingival fibroblasts after three days incubation B

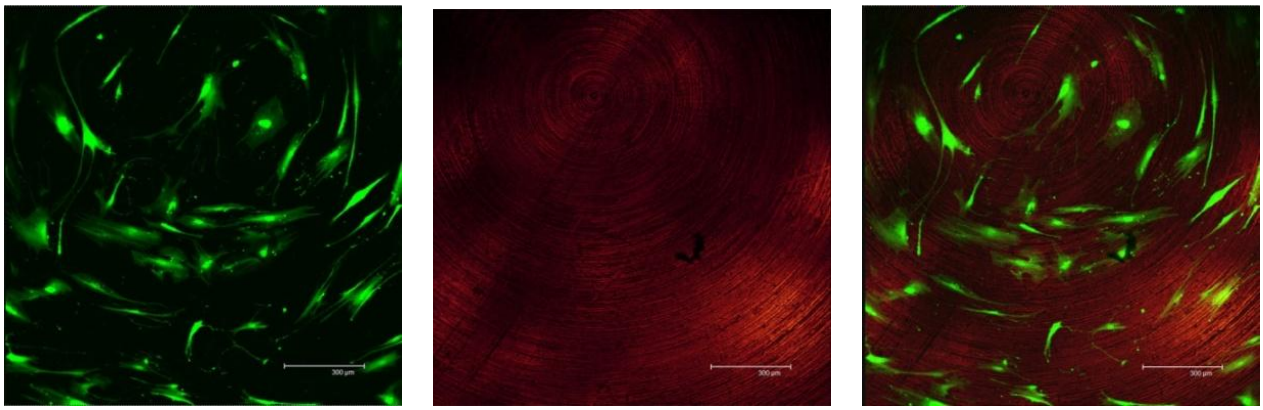

3.14-a) Mathines Ti surface

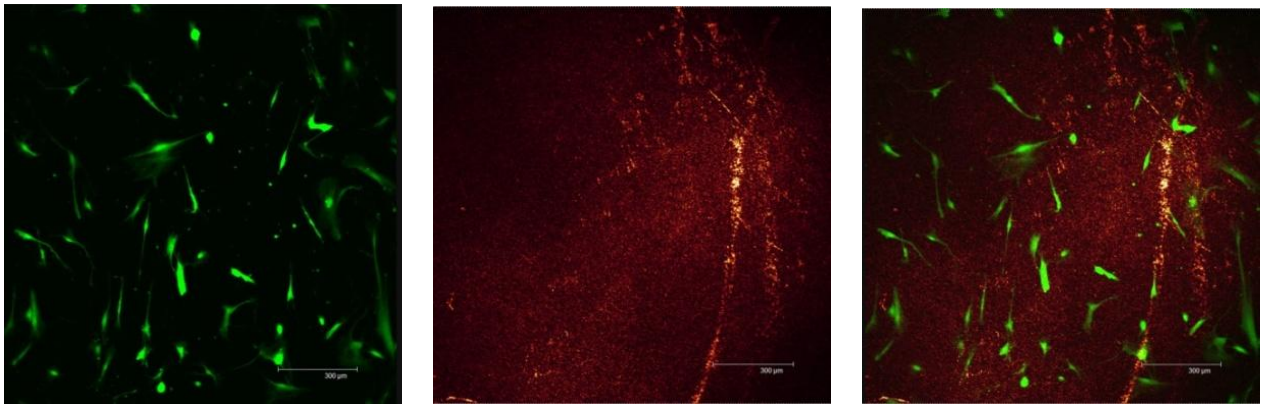

3.14-b) Osseotite Ti surface

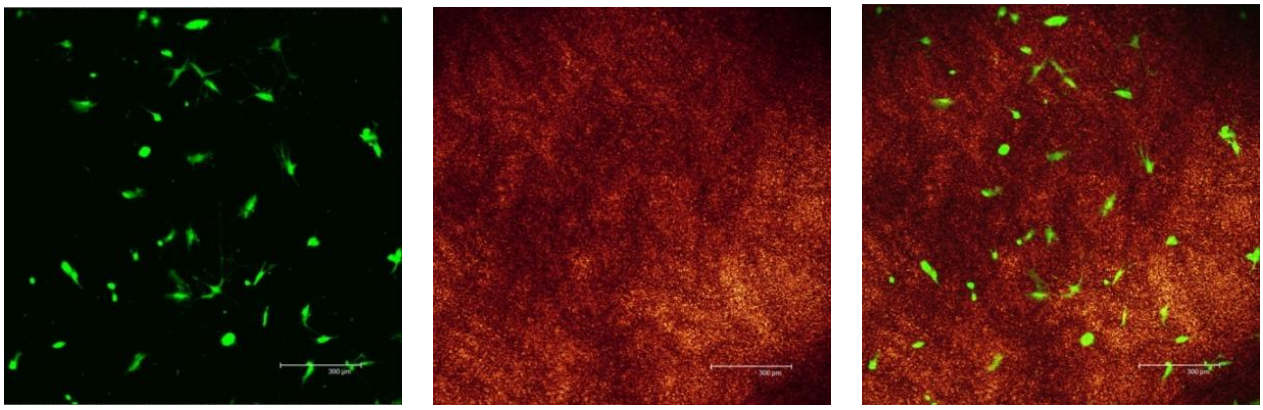

3.14-c) Nanotite Ti surface

Cell morphology of human gingival fibroblasts on Maschined (A), Osseotite (B) and Nanotite (C) titanium surfaces after 7-day incubation period. (magnification 10X,) The scale bar corresponds to a length of 300 μm.

Figure 3.14: Cell morphology of gingival fibroblasts after seven days incubation A

3.15-a) Mathines Ti surface

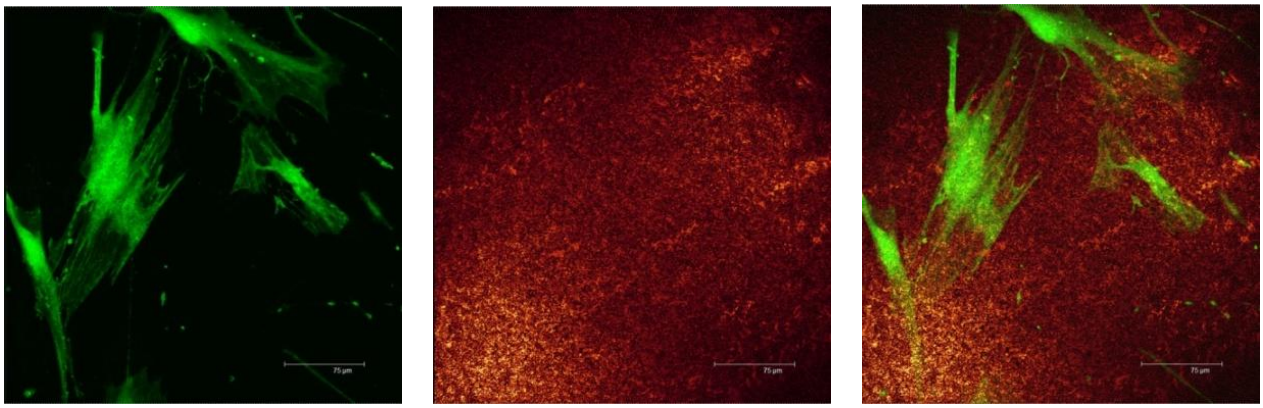

3.15-b) Osseotite Ti surface

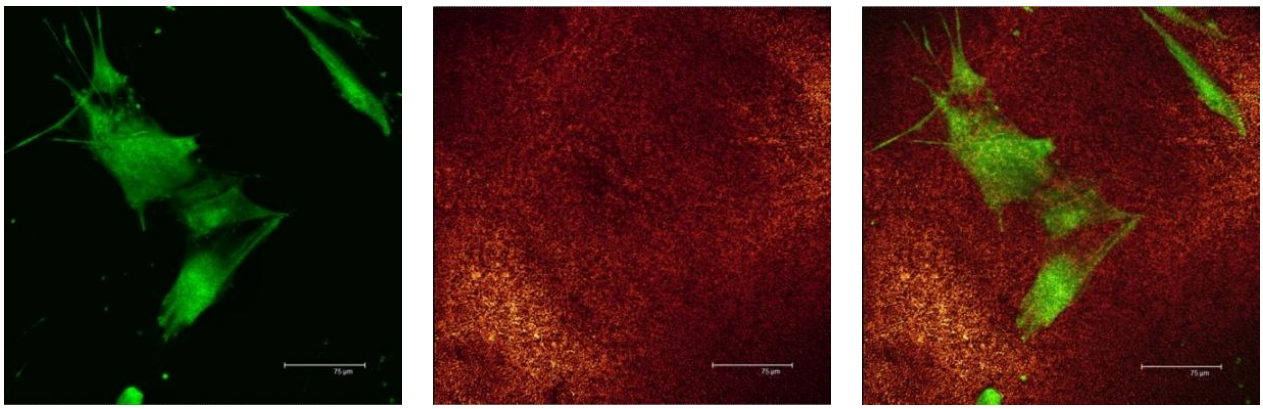

3.15-c) Nanotite Ti surface

Cell morphology of human gingival fibroblasts on Maschined (A), Osseotite (B) and Nanotite (C) titanium surfaces after 7-day incubation period. (magnification 40X,) The scale bar corresponds to a length of 300 μm.

Figure 3.15: Cell morphology of gingival fibroblasts after seven days incubation B

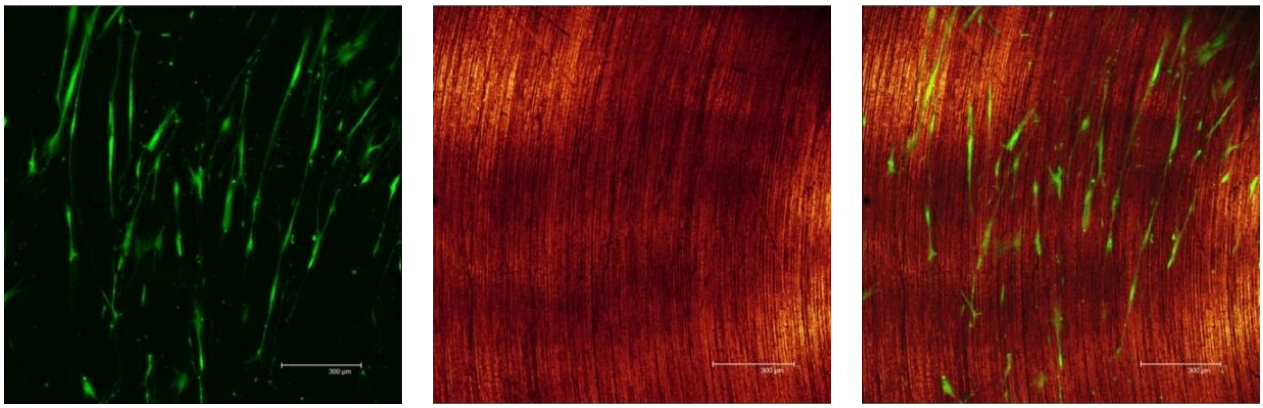

3.16-a) Mathines Ti surface

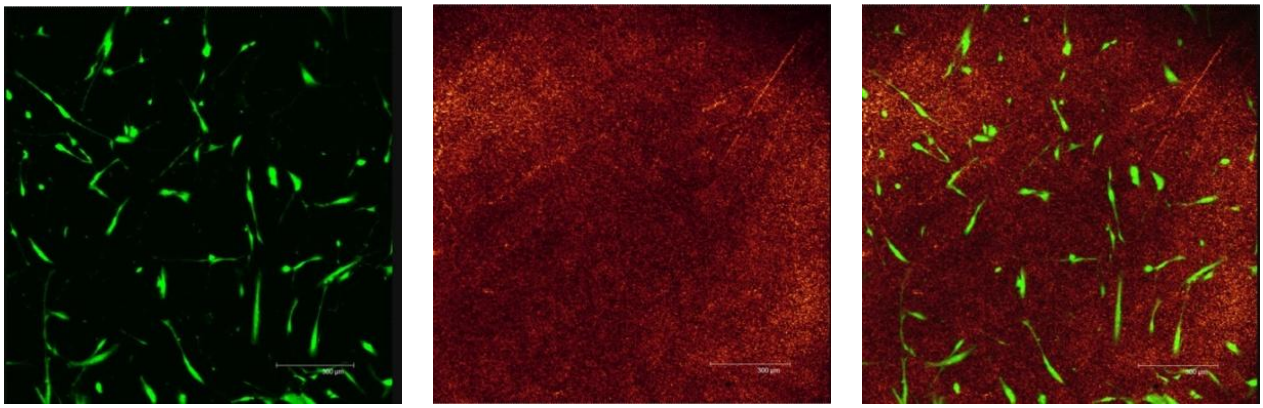

3.16-b) Osseotite Ti surface

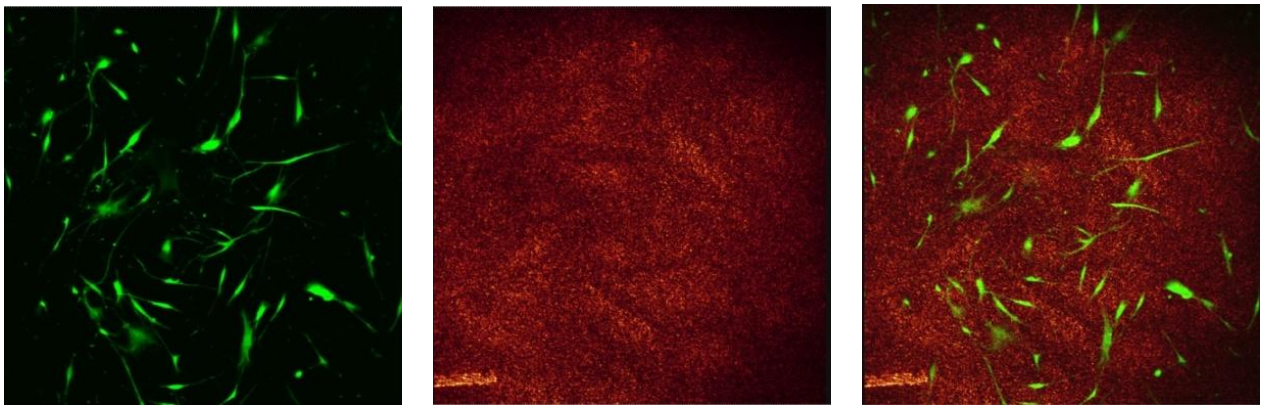

3.16-c) Nanotite Ti surface

Cell morphology of human gingival fibroblasts on Maschined (A), Osseotite (B) and Nanotite (C) titanium surfaces after 11-day incubation period. (magnification 10X,) The scale bar corresponds to a length of 300 μm.

Figure 3.16: Cell morphology of gingival fibroblasts after 11 days incubation A

3.17-a) Mathines Ti surface

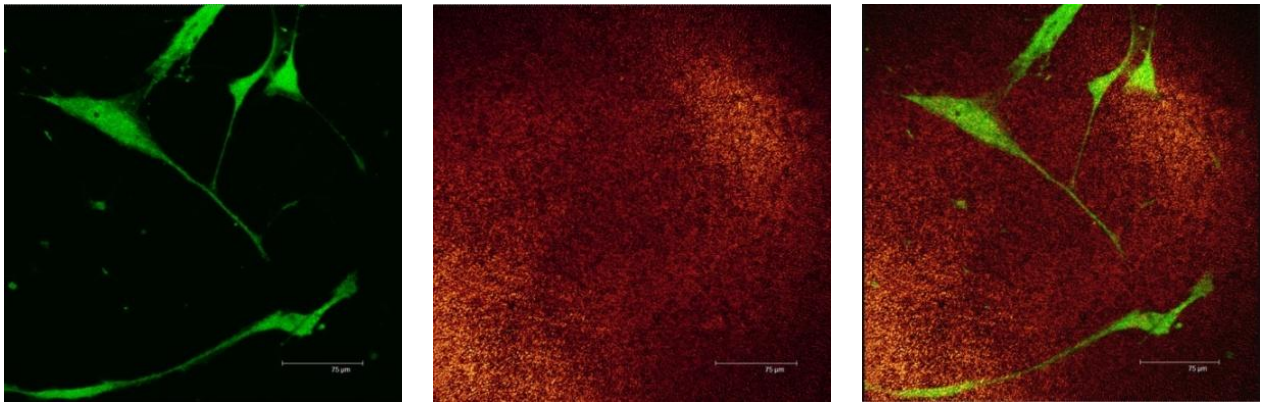

3.17-b) Osseotite Ti surface

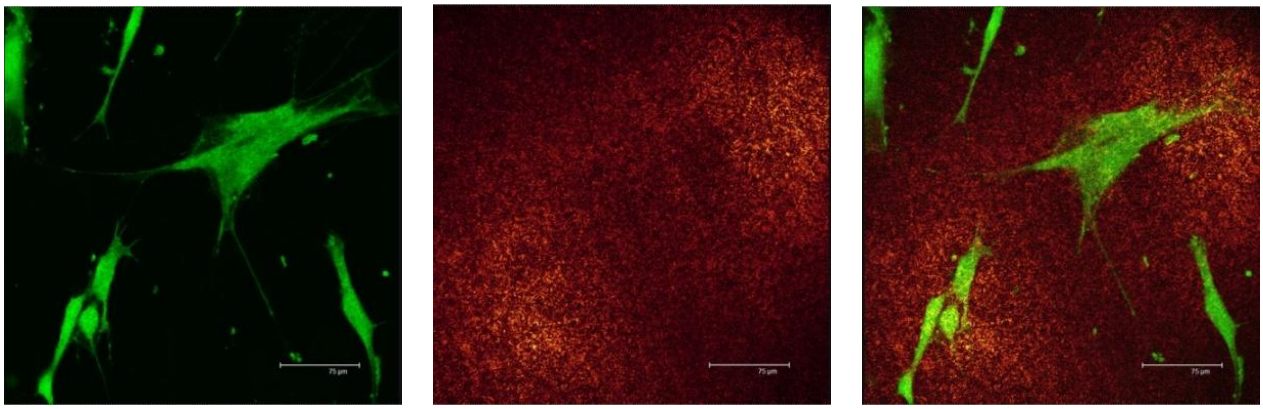

3.17-c) Nanotite Ti surface

Cell morphology of human gingival fibroblasts on Maschined (A), Osseotite (B) and Nanotite (C) titanium surfaces after 11-day incubation period. (magnification 40X,) The scale bar corresponds to a length of 300 μm.

Figure 3.17: Cell morphology of gingival fibroblasts after 11 days incubation B

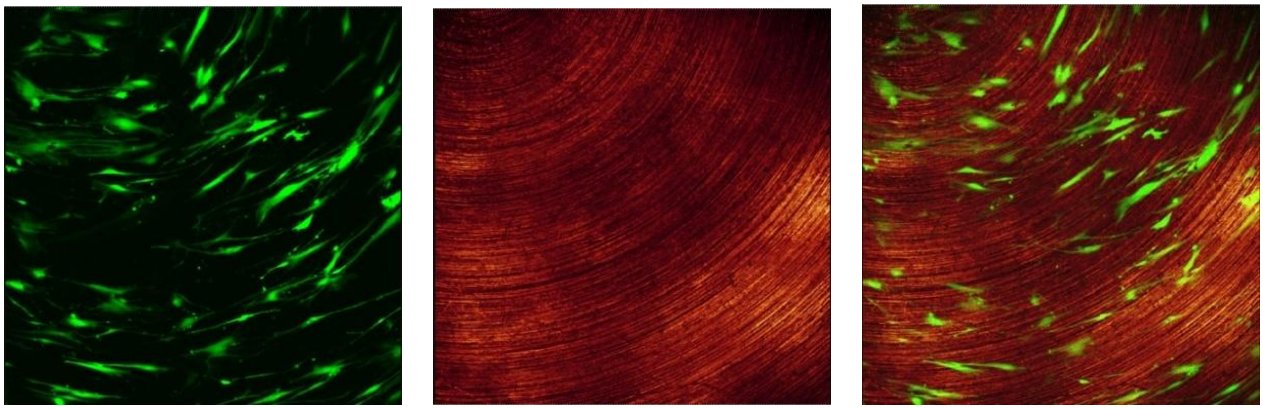

3.18-a) Mathines Ti surface

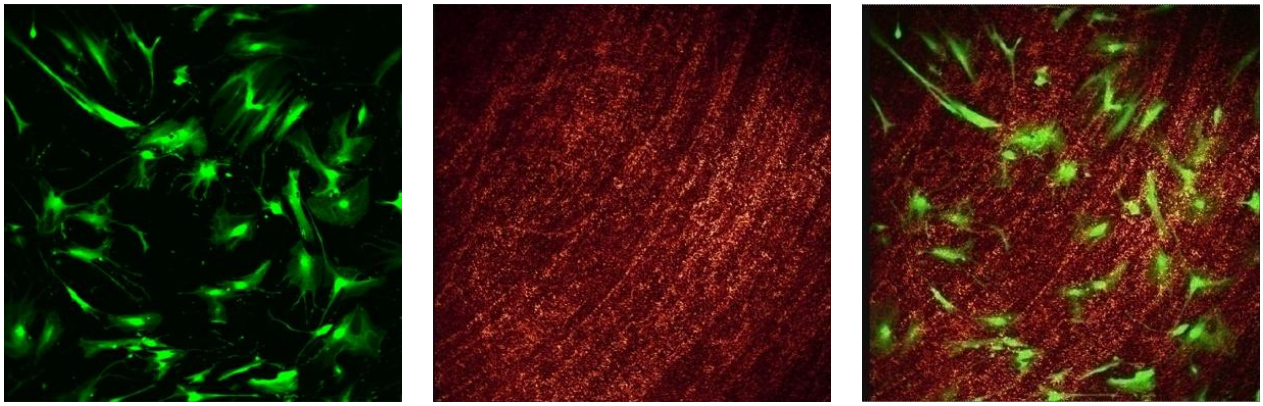

3.18-b) Osseotite Ti surface

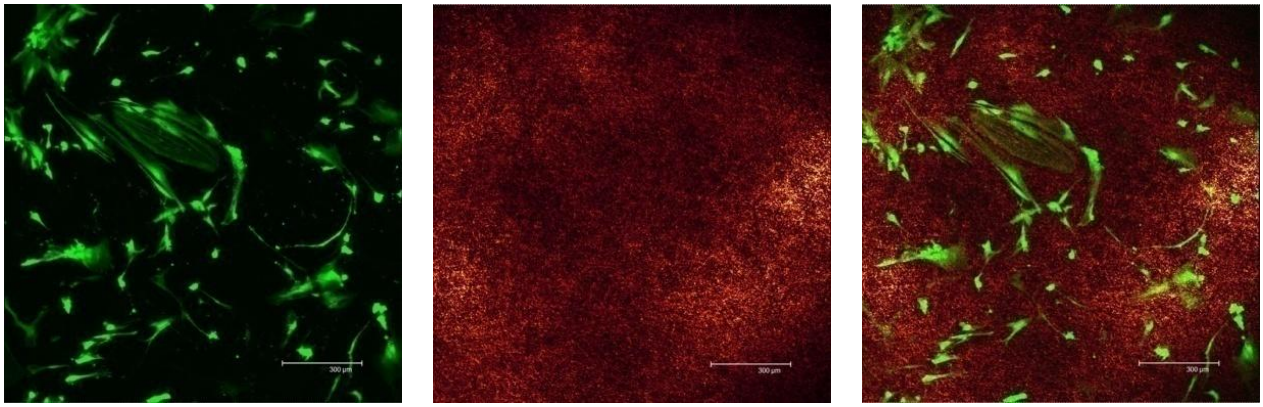

3.18-c) Nanotite Ti surface

Cell morphology of human gingival fibroblasts on Maschined (A), Osseotite (B) and Nanotite (C) titanium surfaces after 18-day incubation period. (magnification 10X,) The scale bar corresponds to a length of 300 μm.

Figure 3.18: Cell morphology of gingival fibroblasts after 18 days incubation A

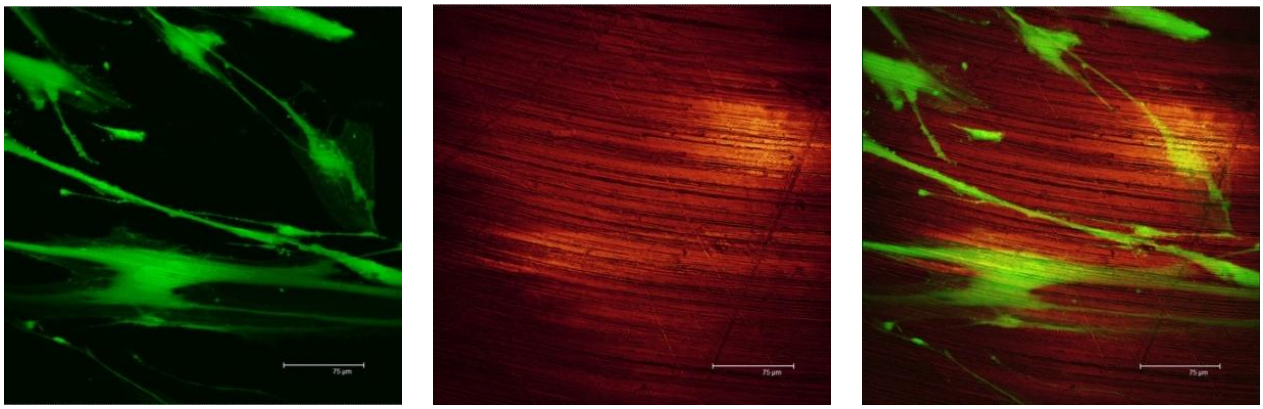

3.19-a) Mathines Ti surface

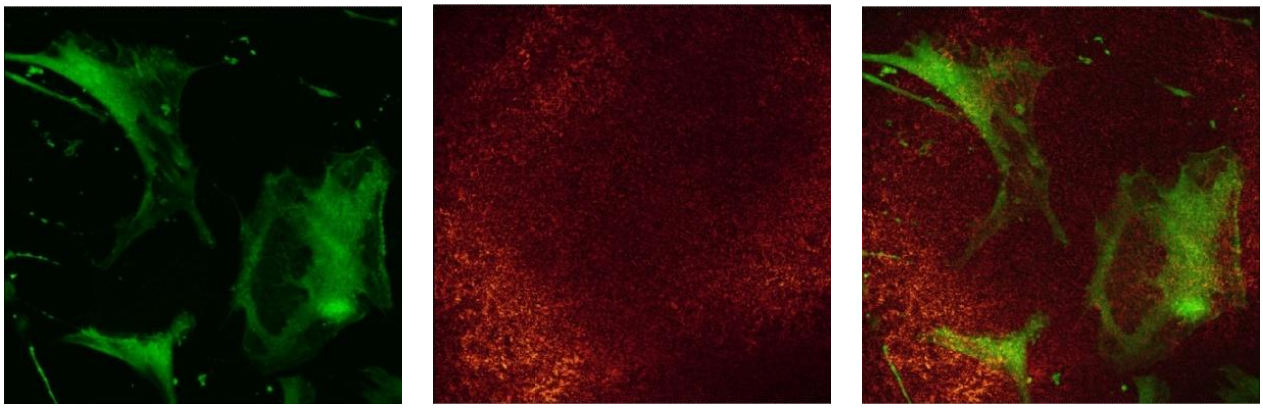

3.19-b) Osseotite Ti surface

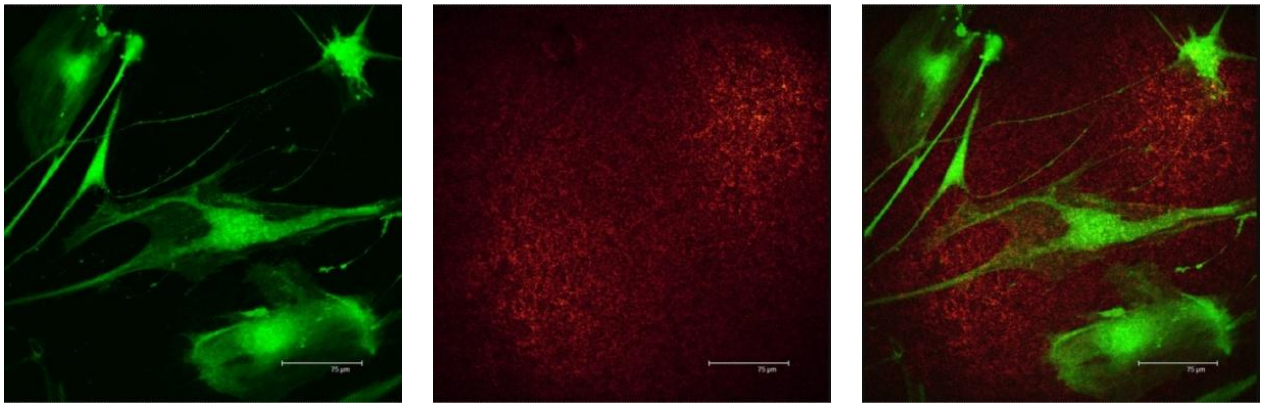

3.19-c) Nanotite Ti surface

Cell morphology of human gingival fibroblasts on Maschined (A), Osseotite (B) and Nanotite (C) titanium surfaces after 18-day incubation period. (magnification 40X,) The scale bar corresponds to a length of 300 μm.

Figure 3.19: Cell morphology of gingival fibroblasts after 18 days incubation B

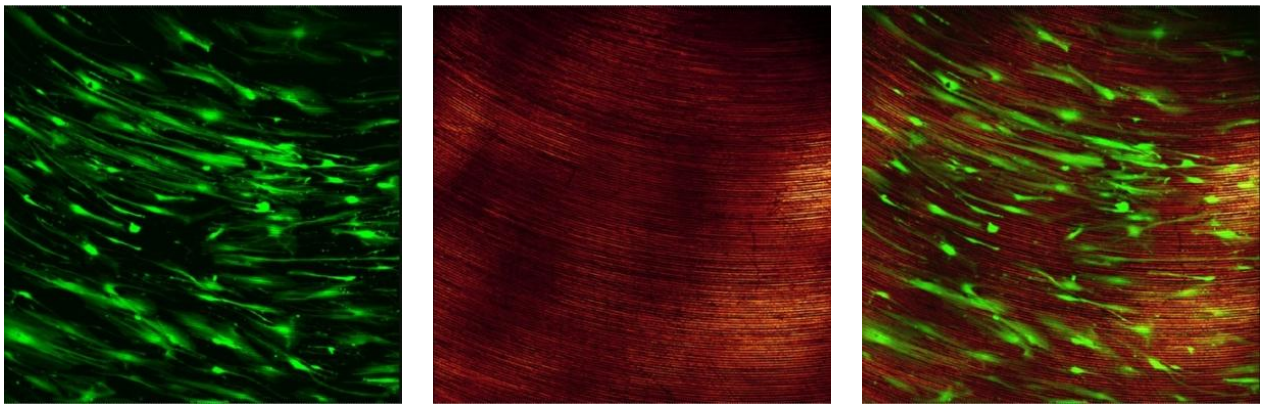

3.20-a) Mathines Ti surface

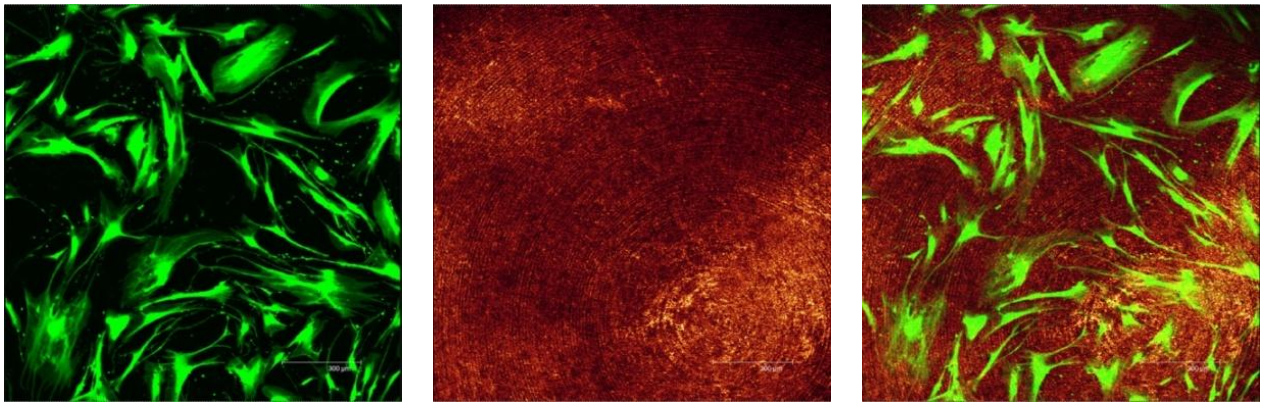

3.20-b) Osseotite Ti surface

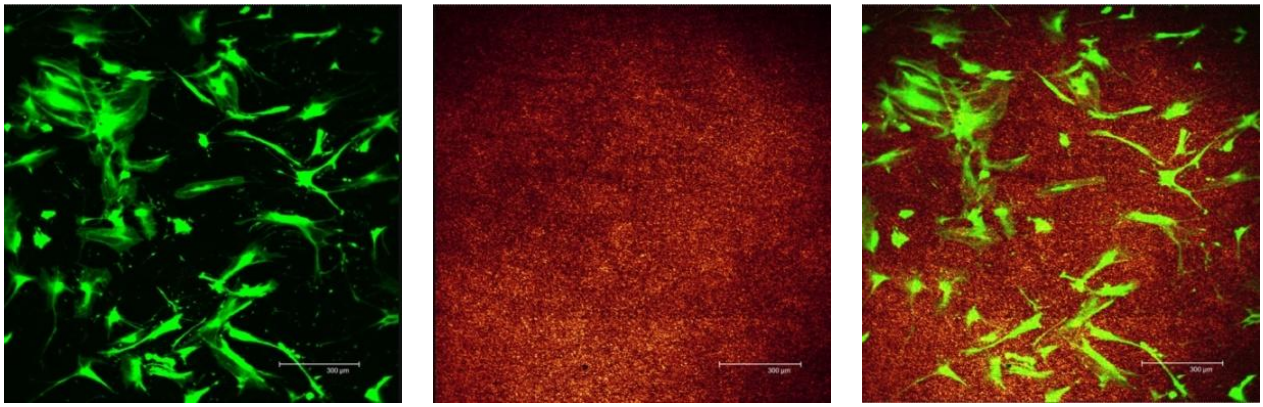

3.20-c) Nanotite Ti surface

Cell morphology of human gingival fibroblasts on Maschined (A), Osseotite (B) and Nanotite (C) titanium surfaces after 24-day incubation period. (magnification 10X,) The scale bar corresponds to a length of 300 μm.

Figure 3.20: Cell morphology of gingival fibroblasts after 24 days incubation A

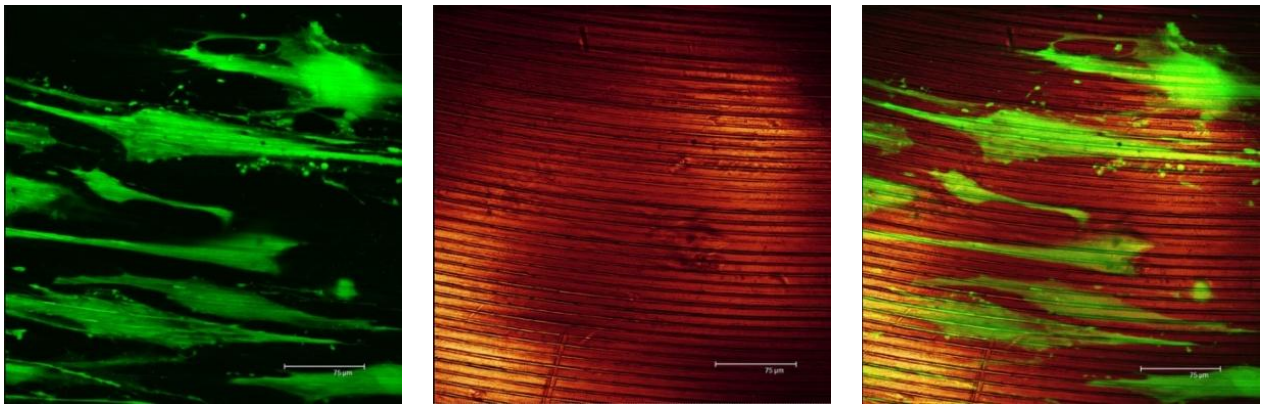

3.21-a) Mathines Ti surface

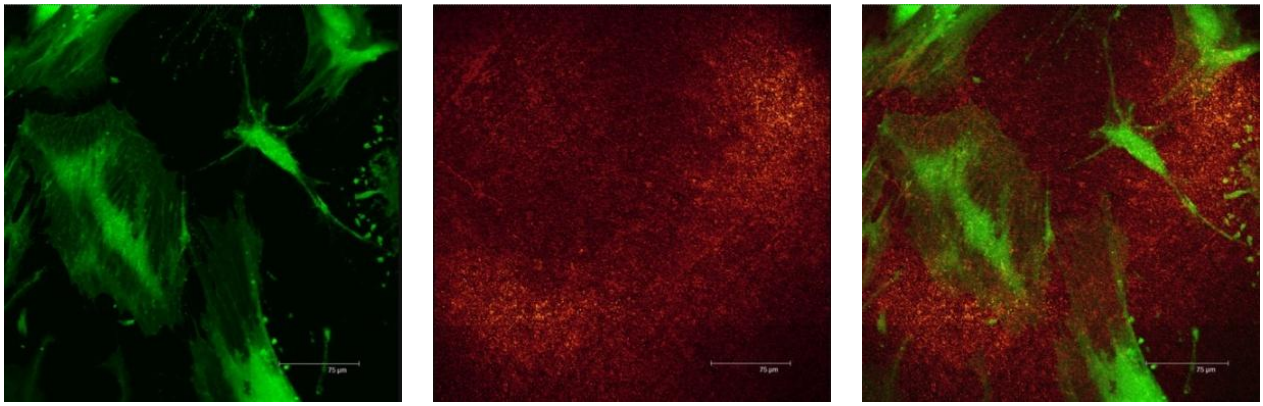

3.21-b) Osseotite Ti surface

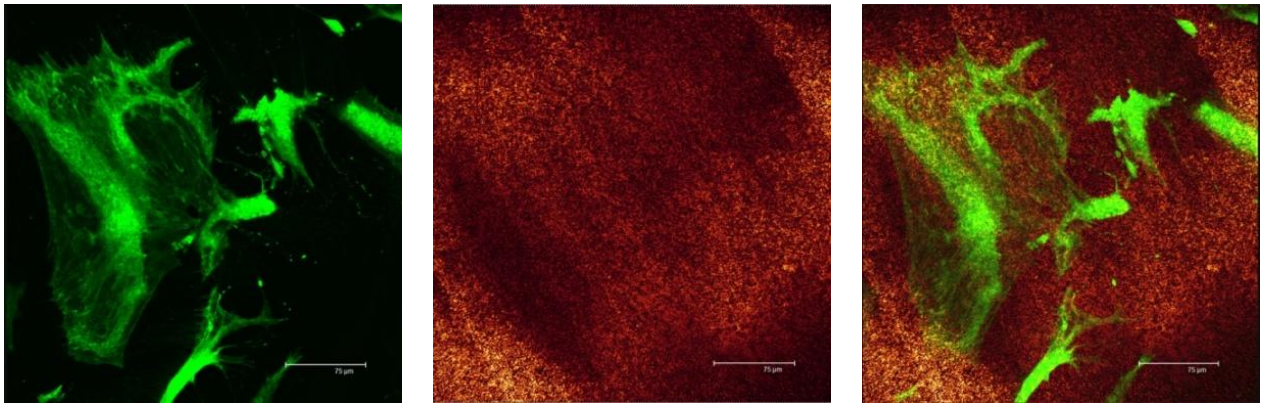

3.21-c) Nanotite Ti surface

Cell morphology of human gingival fibroblasts on Maschined (A), Osseotite (B) and Nanotite (C) titanium surfaces after 24-day incubation period. (magnification 40X,) The scale bar corresponds to a length of 300 μm.

Figure 3.21: Cell morphology of gingival fibroblasts after 24 days incubation B

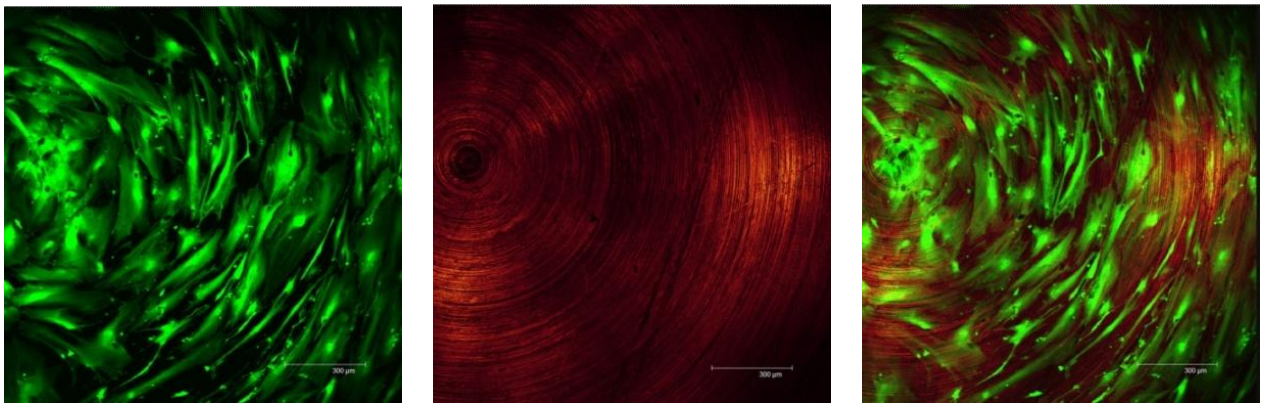

3.22-a) Mathines Ti surface

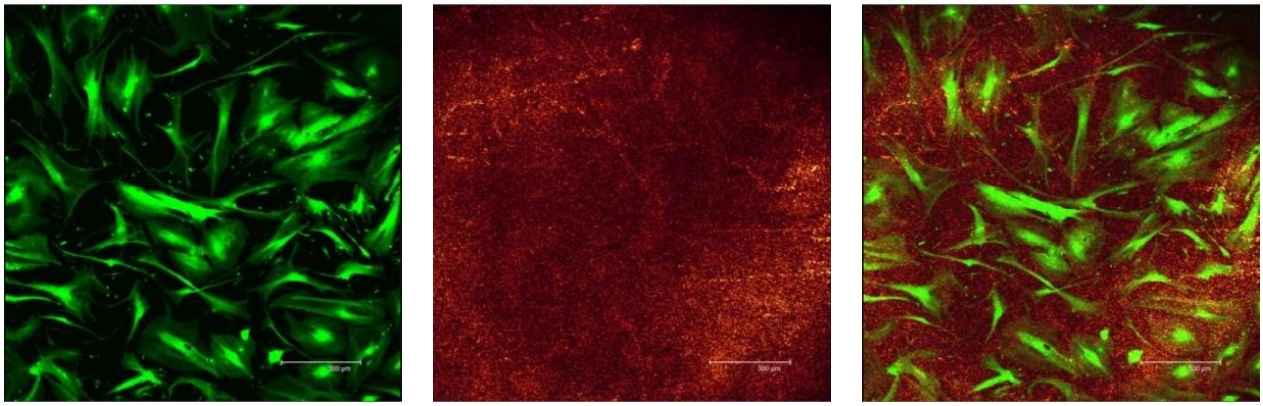

3.22-b) Osseotite Ti surface

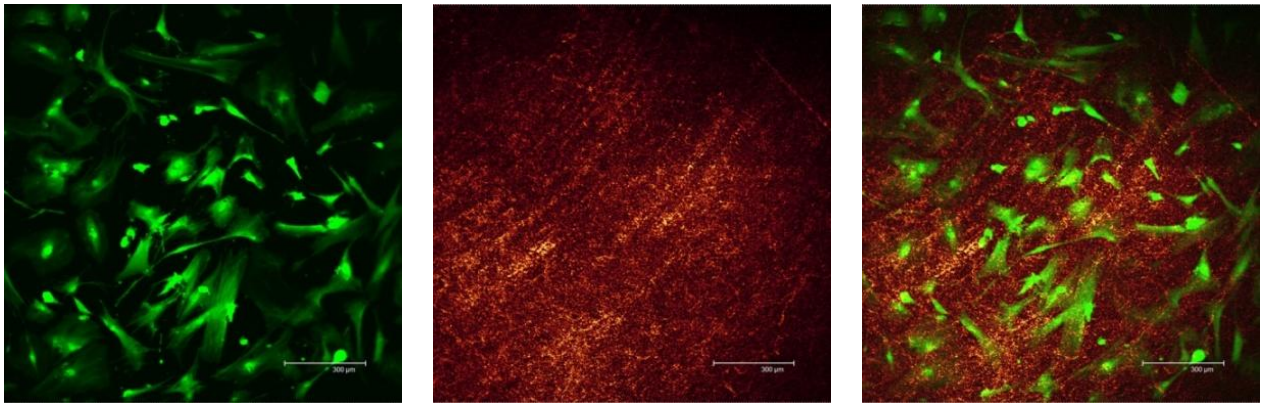

3.22-c) Nanotite Ti surface

Cell morphology of human gingival fibroblasts on Maschined (A), Osseotite (B) and Nanotite (C) titanium surfaces after 30-day incubation period. (magnification 10X,) The scale bar corresponds to a length of 300 μm.

Figure 3.22: Cell morphology of gingival fibroblasts after one month incubation A

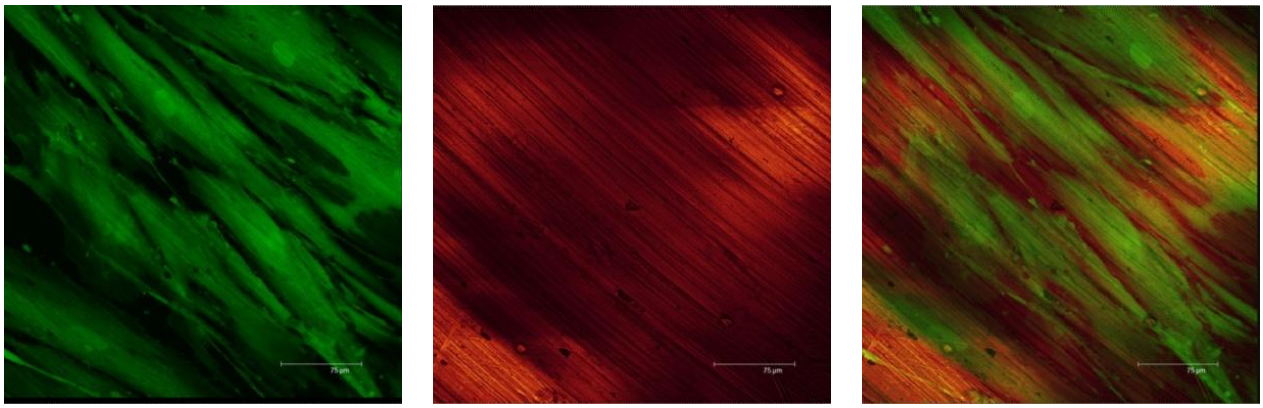

3.23-a) Mathines Ti surface

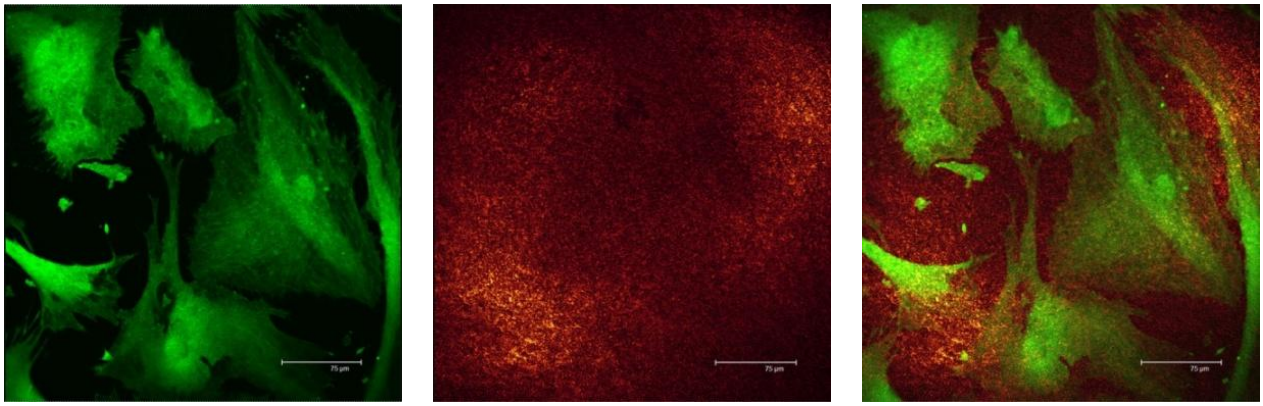

3.23-b) Osseotite Ti surface

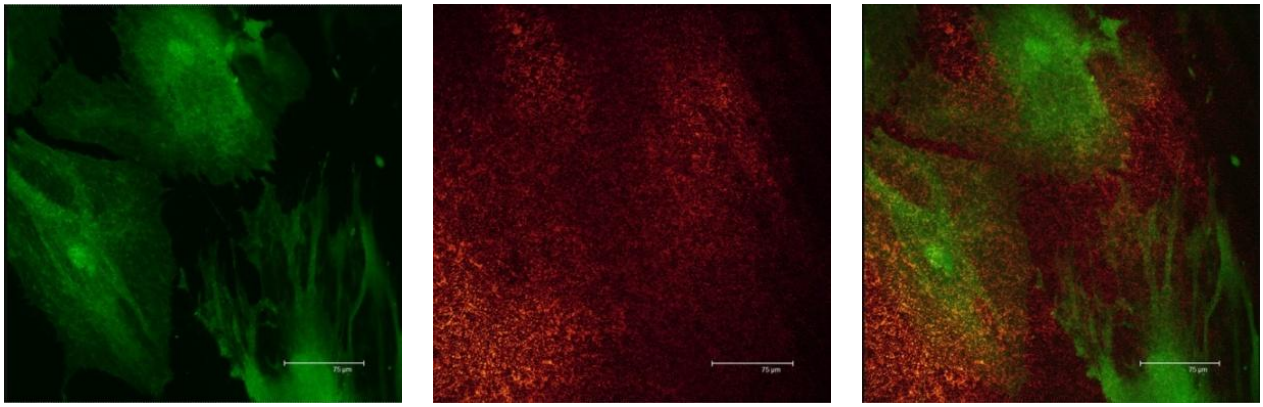

3.23-c) Nanotite Ti surface

Cell morphology of human gingival fibroblasts on Maschined (A), Osseotite (B) and Nanotite (C) titanium surfaces after 30-day incubation period. (magnification 40X,) The scale bar corresponds to a length of 300 μm.

Figure 3.23: Cell morphology of gingival fibroblasts after one month incubation B

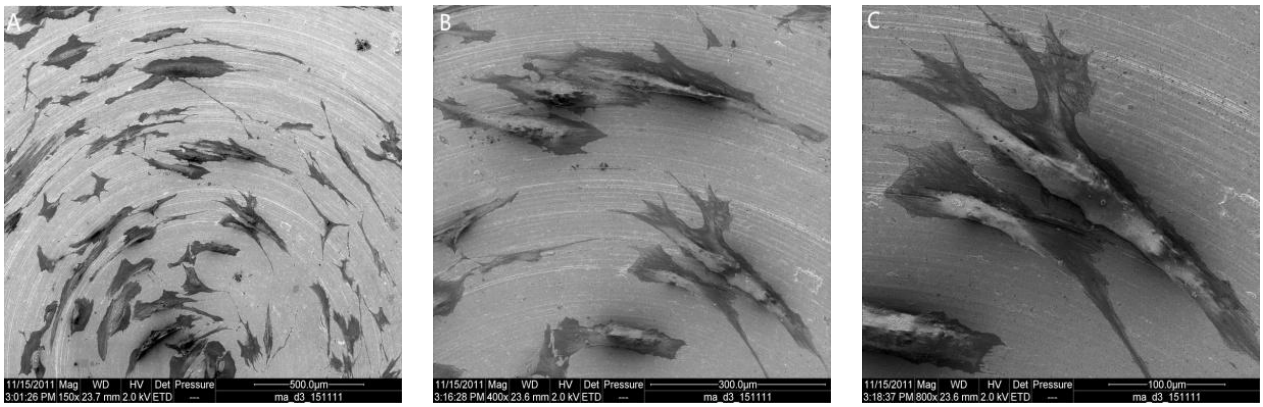

Cell morphology of human gingival fibroblasts on Machined titanium surfaces after 3-day incubation period. SEM was used to visualize HGF on the surface at an original magnification 150x (A), bar scale= 500μm; at an original magnification 400x (B), bar scale= 300μm and at an original magnification 800x (A), bar scale= 100μm.

Figure 3.24: Cell morphology of gingival fibroblasts after three days incubation (SEM)

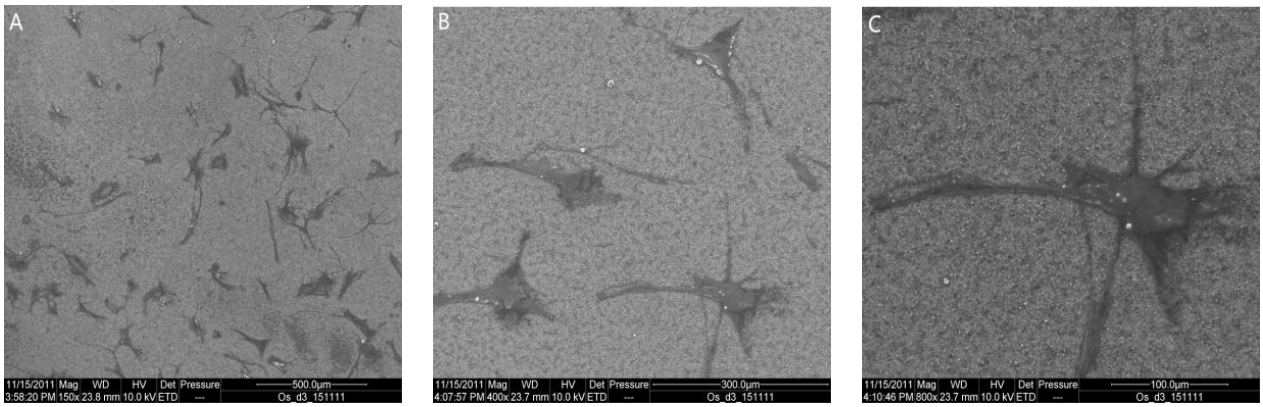

Cell morphology of human gingival fibroblasts on Osseotite titanium surfaces after 3-day incubation period. SEM was used to visualize HGF on the surface at an original magnification 150x (A), bar scale= 500μm; at an original magnification 400x (B), bar scale= 300μm and at an original magnification 800x (A), bar scale= 100μm.

Figure 3.25: Cell morphology of gingival fibroblasts after three days incubation (SEM)

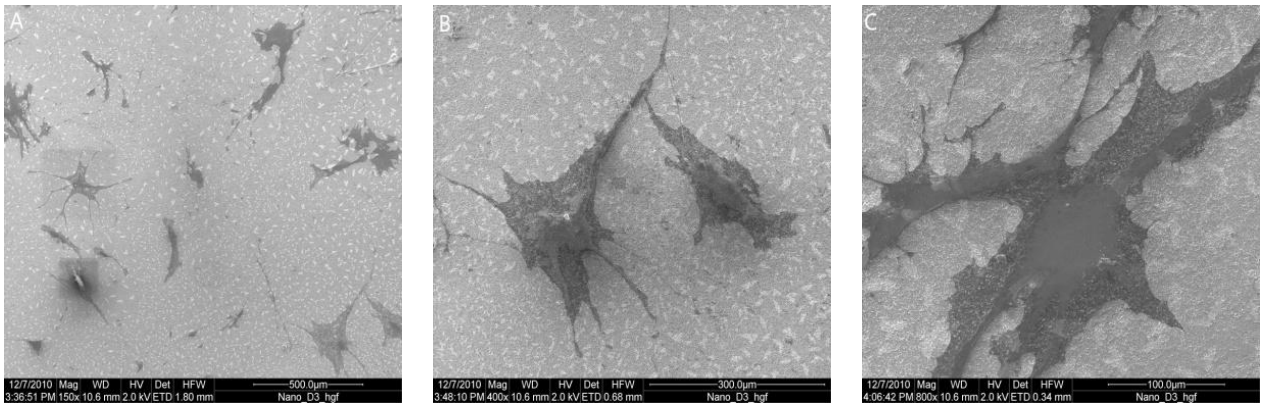

Cell morphology of human gingival fibroblasts on Nanotite titanium surfaces after 3-day incubation period. SEM was used to visualize HGF on the surface at an original magnification 150x (A), bar scale= 500μm; at an original magnification 400x (B), bar scale= 300μm and at an original magnification 800x (A), bar scale= 100μm.

Figure 3.26: Cell morphology of gingival fibroblasts after three days incubation (SEM)

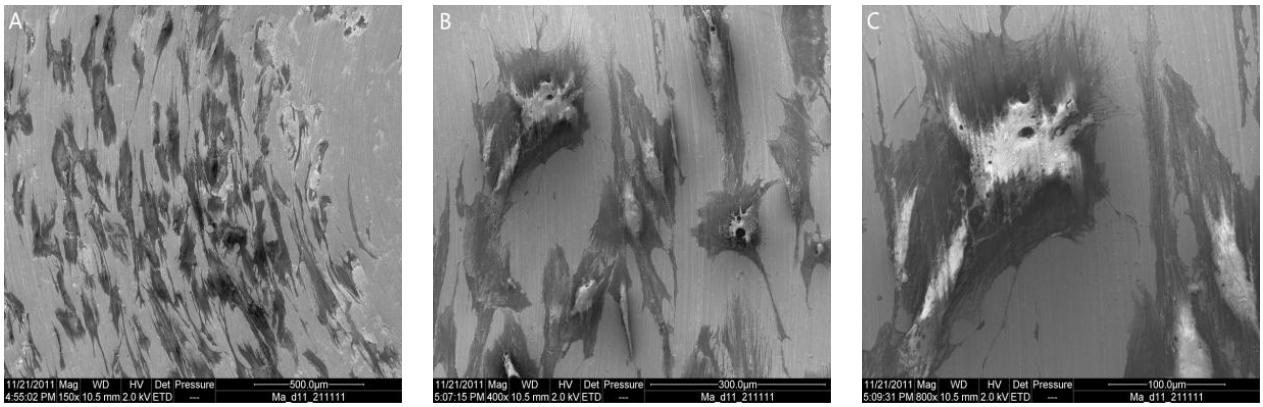

Cell morphology of human gingival fibroblasts on Machined titanium surfaces after 11-day incubation period. SEM was used to visualize HGF on the surface at an original magnification 150x (A), bar scale= 500μm; at an original magnification 400x (B), bar scale= 300μm and at an original magnification 800x (A), bar scale= 100μm.

Figure 3.27: Cell morphology of gingival fibroblasts after 11 days incubation (SEM)

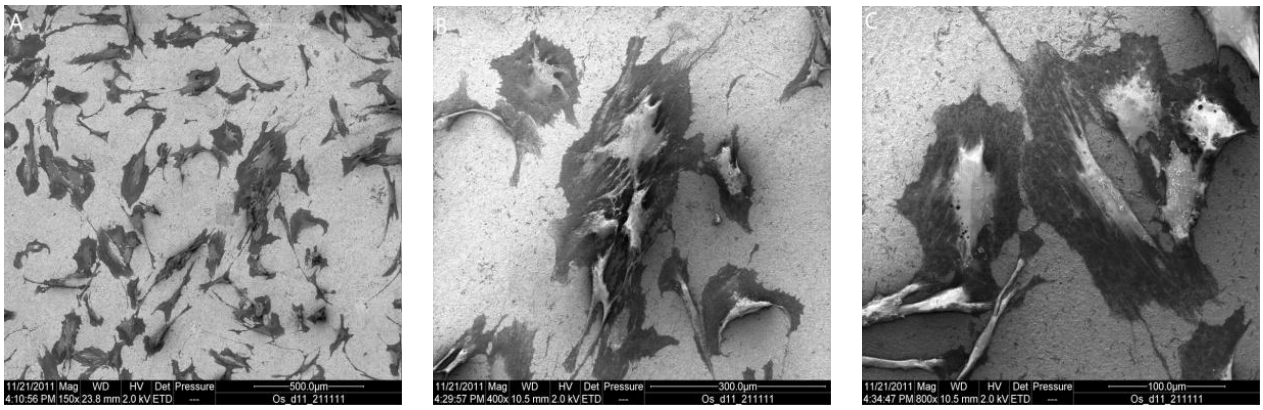

Cell morphology of human gingival fibroblasts on Osseotite titanium surfaces after 11-day incubation period. SEM was used to visualize HGF on the surface at an original magnification 150x (A), bar scale= 500μm; at an original magnification 400x (B), bar scale= 300μm and at an original magnification 800x (A), bar scale= 100μm.

Figure 3.28: Cell morphology of gingival fibroblasts after 11 days incubation (SEM)

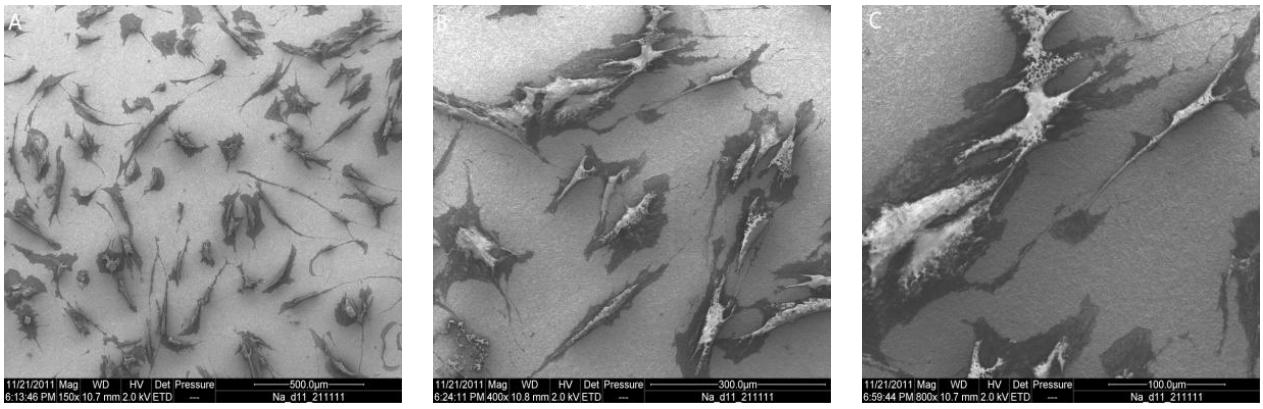

Cell morphology of human gingival fibroblasts on Nanotite titanium surfaces after 11-day incubation period. SEM was used to visualize HGF on the surface at an original magnification 150x (A), bar scale= 500μm; at an original magnification 400x (B), bar scale= 300μm and at an original magnification 800x (A), bar scale= 100μm.

Figure 3.29: Cell morphology of gingival fibroblasts after 11 days incubation (SEM)

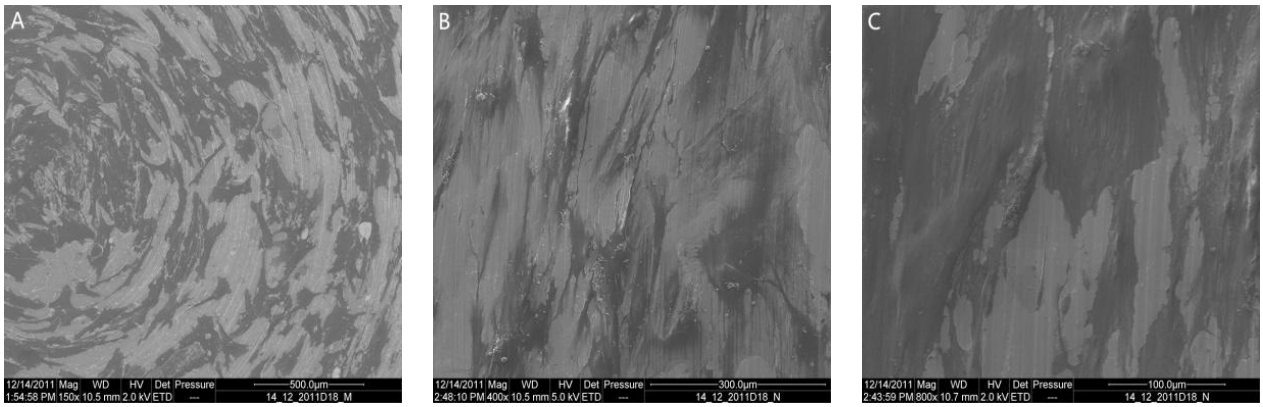

Cell morphology of human gingival fibroblasts on Machined titanium surfaces after 18-day incubation period. SEM was used to visualize HGF on the surface at an original magnification 150x (A), bar scale= 500μm; at an original magnification 400x (B), bar scale= 300μm and at an original magnification 800x (A), bar scale= 100μm.

Figure 3.30: Cell morphology of gingival fibroblasts after 18 days incubation (SEM)

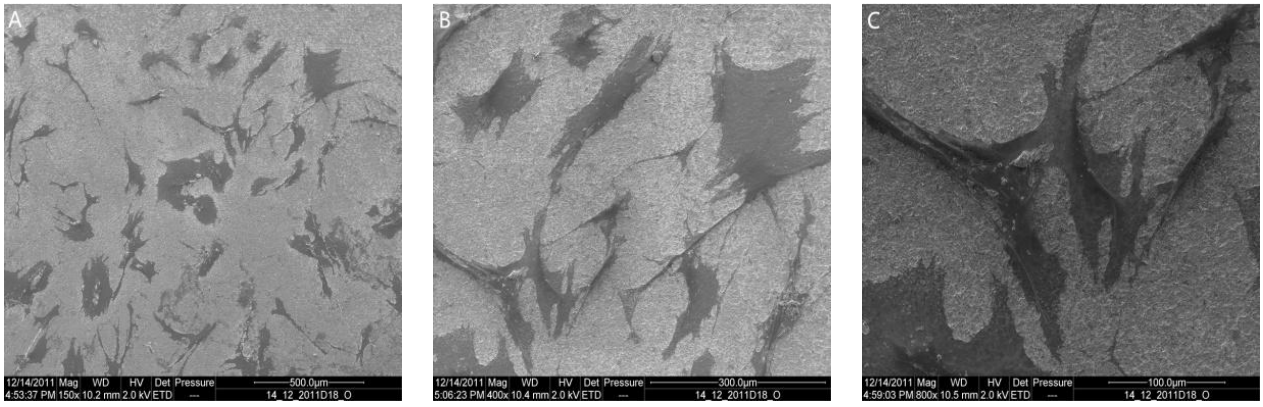

Cell morphology of human gingival fibroblasts on Osseotite titanium surfaces after 18-day incubation period. SEM was used to visualize HGF on the surface at an original magnification 150x (A), bar scale= 500μm; at an original magnification 400x (B), bar scale= 300μm and at an original magnification 800x (A), bar scale= 100μm.

Figure 3.31: Cell morphology of gingival fibroblasts after 18 days incubation (SEM)

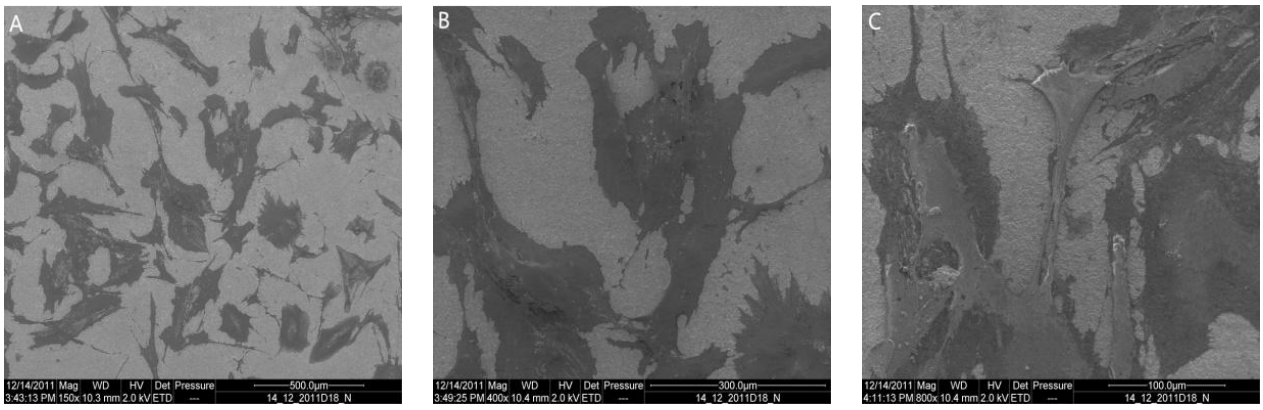

Cell morphology of human gingival fibroblasts on Nanotite titanium surfaces after 18-day incubation period. SEM was used to visualize HGF on the surface at an original magnification 150x (A), bar scale= 500μm; at an original magnification 400x (B), bar scale= 300μm and at an original magnification 800x (A), bar scale= 100μm.

Figure 3.32: Cell morphology of gingival fibroblasts after 18 days incubation (SEM)

3.3 Cell proliferation

In order to measure the cell proliferation, the AlamarBlue assay was performed by determining the cellular metabolism activity indirectly. AlamarBlue is a non-cytotoxic assay; the oxidised form of the AlamarBlue reagent is incubated with the cells and then converted to its reduced form resorufin by mitochondrial enzymes (Nociari *et al.* 1998). The extent of Alamar Blue reduction is directly proportional to metabolic activity of the cells. Each titanium substrate was seeded with 5,000 cells (human gingival fibroblasts), the proliferation was investigated at 3, 7 and 14 days. To make the results more reproducible, a total of three independent experiments were performed and averaged. An online alamarBlue® colorimetric calculator (provided by the AbD Serotec, USA) was used for measuring percent reduction and the result was shown in the table

From Figure 3.33, the Almar Blue assay confirmed the metabolic activity of fibroblasts on all surfaces tested. Enhanced cell attachment and cell metabolism were observed up to

Time	Machied	Osseotite	Nanotite
Day 3	18.1	16.3	12.2
Day 7	48.2	45.4	42.3
Day 14	60.3	64.2	65.1

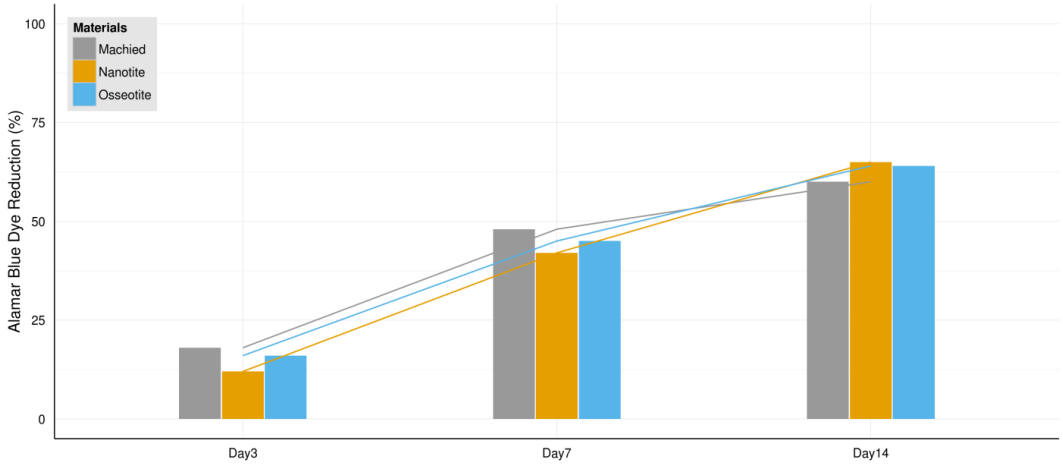

Cell proliferation assay by Alamar Blue measurement. The amount of Alamar Blue reduction is proportional to metabolic activity of the cells.

Figure 3.33: Cell proliferation assay by Alamar Blue measurement

14 days from the initial day of seeding on three group substrates. On first day, the results indicated similar levels of proliferation for the cells on both the Machined and Osseotite Ti surfaces, while lower cell number was detected on the Nanotite surfaces. At day 7, the metabolic activity of fibroblasts on Machined and Ossotite surfaces was significantly higher than that on the Nanotite surfaces. The maximal AlamarBlue reduction was indicated on machined surfaces. At day 14, the gingival fibroblasts grown on Osseotite and Nanotite surfaces showed a notable higher proliferation compared to the Machined surfaces; however, there is no considerable difference on cell proliferation between these two groups.

3.4 FACS analysis for integrin

Flow cytometry was performed to compare the expression of integrins subunit $\alpha 5$ (CD49e), $\beta 1$ (CD29) on human gingival fibroblasts on three tested groups at day 14 after culture.

Figure 3.34 and 3.35 showed the fluorescence intensities of $\alpha 5$ and $\beta 1$ integrins expressed on human gingival fibroblasts on three tested groups at day 14 after incubation. We found that human gingival fibroblasts expressed $\alpha 5\beta 1$ integrins on all disks. Because the fluorescence intensity increases logarithmically, the median was chosen here for the analysis of flow cytometry data as it is the mid-point of the population and less influenced by skew and outliers. On Osseotite specimens, the greatest increase in fluorescence intensities of $\alpha 5$ and $\beta 1$ integrins expression was observed. In comparison with Machined surfaces, we found a significant enhancement in fluorescence intensities of $\alpha 5$ and $\beta 1$ integrins expression on Nanotite surfaces.

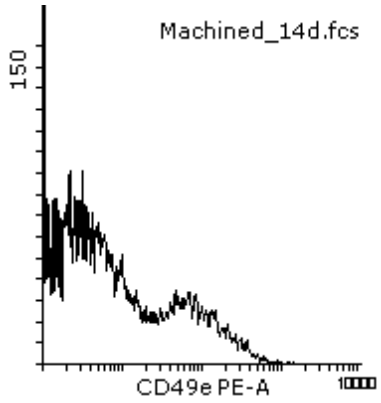

	Events	% of Vis	Mean	GeoMean	Median	CV
All events	15.244	100,00	30,18	5,67	3,59	259,73

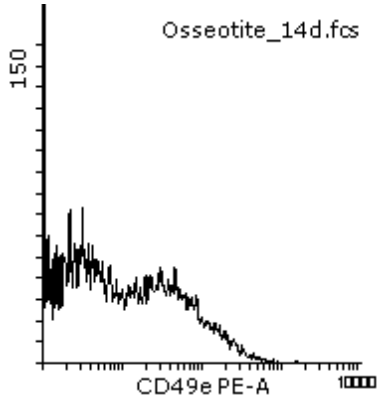

	Events	% of Vis	Mean	GeoMean	Median	CV
All events	12.728	100,00	30,40	7,29	5,28	232,34

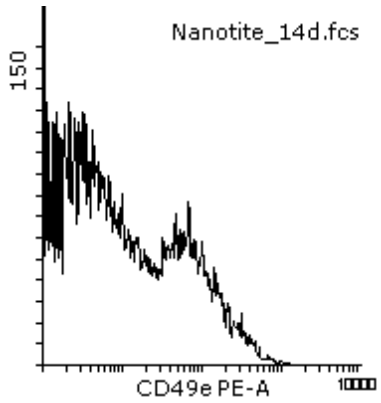

	Events	% of Vis	Mean	GeoMean	Median	CV
All events	24.420	100,00	33,71	6,99	4,66	236,29

Histogram and statistic data of flow cytometric analysis for the $\alpha 5$ integrin subunits on human gingival fibroblasts on Machined, Osseotite and Nanotite titanium surfaces after 14-day incubation period.

Figure 3.34: Flow cytometric analysis for the $\alpha 5$ integrin subunits

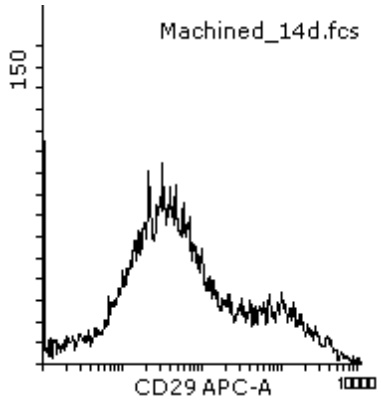

	Events	% of Vis	Mean	GeoMean	Median	CV
All events	15.244	100,00	354,70	55,66	44,91	260,64

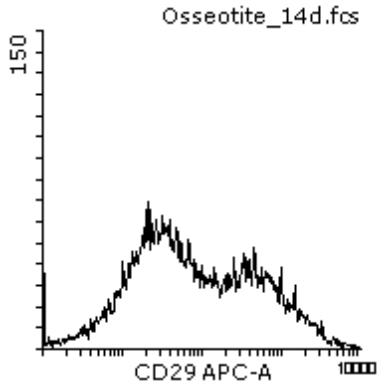

	Events	% of Vis	Mean	GeoMean	Median	CV
All events	12.728	100,00	357,98	77,40	62,08	222,82

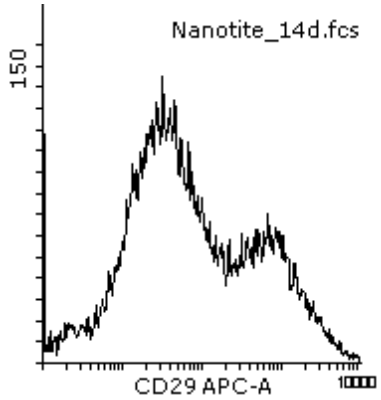

	Events	% of Vis	Mean	GeoMean	Median	CV
All events	24.420	100,00	381,78	69,96	53,76	233,32

Histogram and statistic data of flow cytometric analysis for the $\beta 1$ integrin subunits on human gingival fibroblasts on Machined, Osseotite and Nanotite titanium surfaces after 14-day incubation period.

Figure 3.35: Flow cytometric analysis for the $\beta 1$ integrin subunits

3.5 Analysis of actin cytoskeleton and vinculin

Immunofluorescence images (Fig 3.36-3.41) showed the actin cytoskeleton and vinculin distribution after 24 and 30 days of culture on three different titanium surfaces. The expressions of focal adhesion related proteins (actin and vinculin) confirmed the favorable effect of all tested surfaces.

After a 24-day incubation, the cells spread well on all surfaces. On the Machined surface, the cells are very flat and big, they form long and straight actin stress fibers parallel to the grooves; more extended actin stress fibers without a preferential direction and higher vinculin expression were reported on Osseotite compared to Nanotite samples. On the Machined and the Osseotite surfaces, vinculin expression was found commonly within central areas of the cell; On the Nanotite surface, distinct focal contacts localizations were evident at the cell edges. At day 30, high vinculin expression and a dense network of actin stress fibers on the human gingival fibroblasts were observed on all tested substrates. The F-actin distribution was similar on Osseotite and Nanotite surfaces.

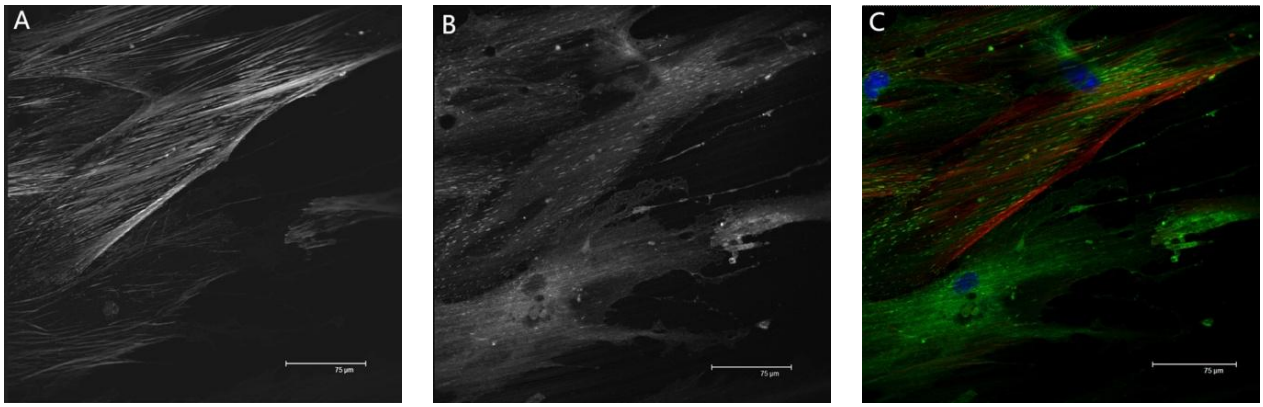

Fluorescence micrographs of actin stress fibers (A), vinculin focal contacts (B) and overlay (C) of HGF on Machined titanium surfaces after 24 days of culture.

Figure 3.36: Fluorescence micrographs on Machined Ti surface after 24 days incubation

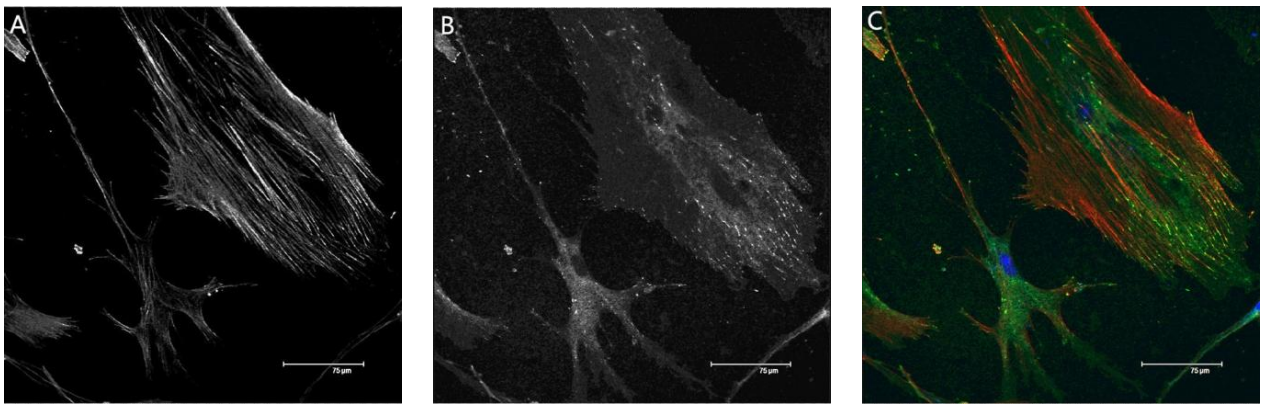

Fluorescence micrographs of actin stress fibers (A), vinculin focal contacts (B) and overlay (C) of HGF on Osseotite titanium surfaces after 24 days of culture.

Figure 3.37: Fluorescence micrographs on Osseotite Ti surface after 24 days incubation

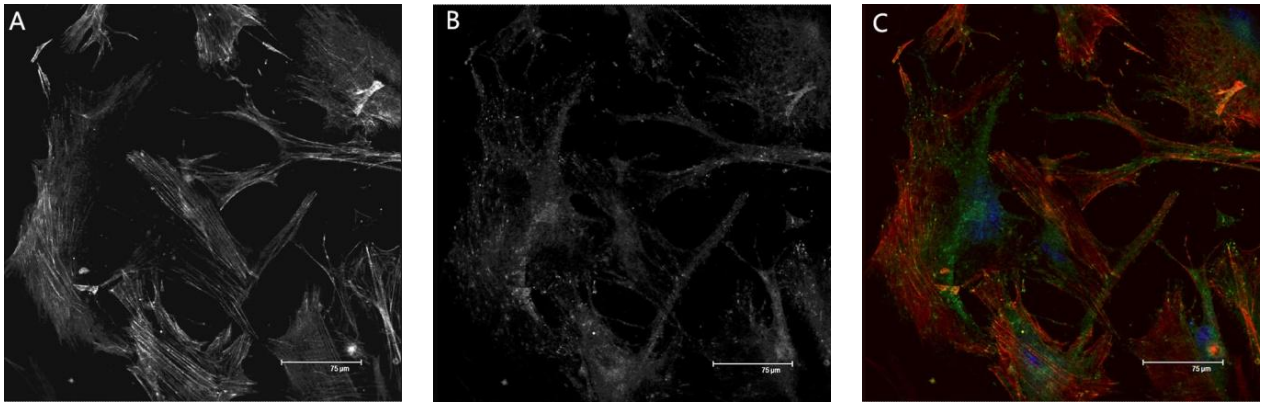

Fluorescence micrographs of actin stress fibers (A), vinculin focal contacts (B) and overlay (C) of HGF on Nanotite titanium surfaces after 24 days of culture.

Figure 3.38: Fluorescence micrographs on Nanotite Ti surface after 24 days incubation

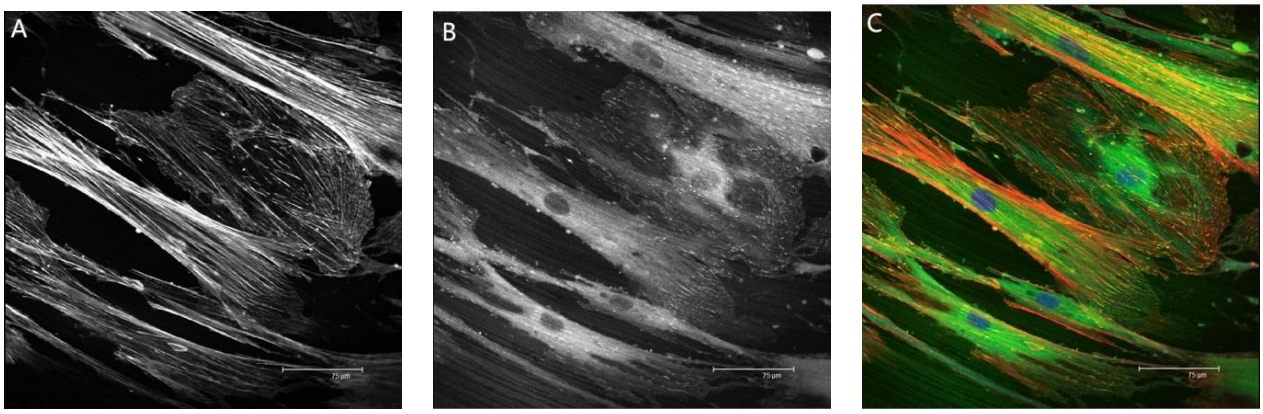

Fluorescence micrographs of actin stress fibers (A), vinculin focal contacts (B) and overlay (C) of HGF on Machined titanium surfaces after 30 days of culture.

Figure 3.39: Fluorescence micrographs on Machined Ti surface after 30 days incubation

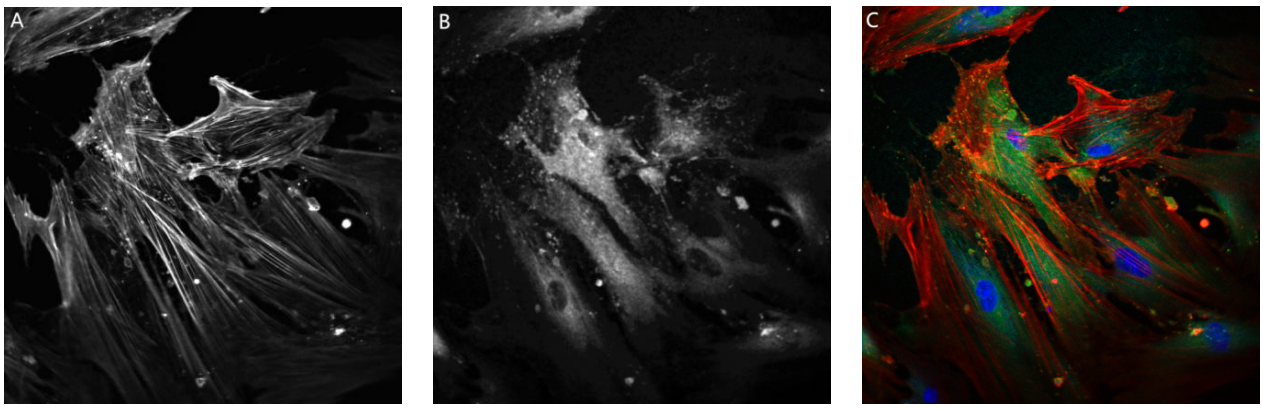

Fluorescence micrographs of actin stress fibers (A), vinculin focal contacts (B) and overlay (C) of HGF on Osseotite titanium surfaces after 30 days of culture.

Figure 3.40: Fluorescence micrographs on Osseotite Ti surface after 30 days incubation

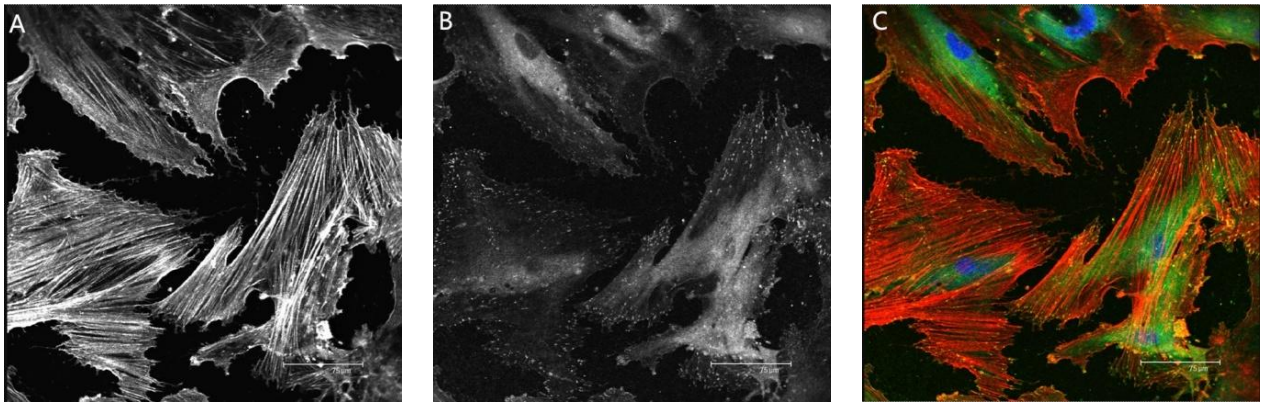

Fluorescence micrographs of actin stress fibers (A), vinculin focal contacts (B) and overlay (C) of HGF on Nanotite titanium surfaces after 30 days of culture.

Figure 3.41: Fluorescence micrographs on Nanotite Ti surface after 30 days incubation

Chapter 4

Discussion

The surface properties of dental implant play a critical role in the tissue responses and can predict its ultimate longevity. Since rapid progress was made in the field of nanotechnology, new materials were developed aim to enhance the overall performance in dental implant treatment. Even though some dental implants have been in use in clinics for some time, the biological responses to these implant materials are inadequately documented. The aim of this study was to provide some information in the reaction between a nanostructured implant surface and soft tissue interface, which provides better understanding for improving next generation of dental implants.

The basic goal of this work, to show how human gingival fibroblasts interact with three different titanium surfaces and to depict the cell morphology and the distribution of focal adhesions on titanium disks through electron microscopic methods. Three types of titanium surfaces were presented to an in vitro cell culture and compared. Further, the surface topographic features of three different titanium disks were compared by using techniques including SEM and CLSM. However, in cell focal adhesion investigation, due to the small labeling density of fluorescence-labeled vinculin molecules, it was difficult to make a quantitative analysis and comparision between different groups. But it was possible to represent the localization of focal adhesions with the utilization of immunofluorescence. Furthermore, the expression of $\alpha 5 \beta 1$ integrins on human gingival fibroblasts on three tested groups was compared at 14 day after incubation.

4.1 Characterization of Osseotite and Nanotite surfaces

In this study, the dual acid-etching and nanometer scale CaP coated titanium surfaces: Osseotite and Nanotite were investigated. Both of them are manufactured by 3i (Palm Beach Gardens, FL) and used as implant & abutment materials. Osseotite implant is desirable as a dental implant material since it was proved to have the capacity to speed up the bone healing process and form a tight bone contact (Lazzara *et al.* 1999). A number of clinical studies have been made to confirm the long-term performance of Osseotite implant (Gaucher *et al.* 2001, Sullivan *et al.* 2001, Testori *et al.* 2002). In order to improve the bone/implant interface and get rapid osseointegration, many efforts have been made in biomedical applications. Coating the titanium surface with hydroxyapatite (HA) is a technique in this field. There are various coating methods for calcium phosphate; among them, Plasma spraying and sputtering are two major techniques. Recently, a patented coating technique (Berckmans *et al.* n.d.), named Discrete Crystalline Deposition (DCD^{TM}), which used nanometer-scale, ultra small particles of Crystalline Calcium Phosphate (CaP) to suspend in the solution, these particles are then results in discrete crystal deposits of 20-100 nanometers on the Osseotite implant surface (Nanotite implant brochure BioMET 3i). Many reports indicate that the shear strength of CaP coatings obtained by current coating methods is not enough for their attachment to titanium alloys (Whitehead *et al.* 1993, Yang *et al.* 2008) and implant failures have been reported. While the DCD method can get better attachment to implant surfaces than traditional HA coatings, thus lead an improvement on the rate and extent of osseointegration.

According to the manufacture, a dual thermo-etching is performed to produce the Osseotite surfaces (Beaty 1997); that is, the titanium surface was successively immersed in a 15% HF bath to remove the native titanium oxide layer and then etched in a mixture

of H_2SO_4/HCl acids (ratio of 6:1), and heated at 60–80°C for 3–10 min to create the surface texture. We can find from the SEM images that the Osseotite surfaces were mainly characterized by micro sharp pits, which were obtained by dual acid etching process and these strucures are noticeable when they are viewed at high magnification (20000 x). Etching with strong acids such as HCl, H_2SO_4, HF and HNO_3 is a common method to produce a rough titanium surface. The concentration of the acid, the etching temperature condition and the treatment time may decide the shape of pits; the surface roughness increased as the etching time is prolonged (Zareidoost *et al.* 2012). For example: pickling with HF/H_2SO_4 results in wide and rounded pits on titanium surfaces, while etching with HCl or HCl/H_2SO_4 obtained relatively sharp pits (Szmukler-Moncler *et al.* 2004). The results showed that such treatment removes the grooves produced by the polishing process and created a new surface texture with randomly distributed micro sharp pits, making the surface area enlarged. The Nanotite surface was produced by adding a thin layer of calcium phosphate crystals between 20-100 nm in length over the textured surface, SEM pictures showed that small nano particles were mostly evenly covered on the surface, the treatment results in a topographic surface alteration on a nano scale, the roughness of the surface was prominently reduced compared to Osseotite.

4.2 Cell morphology, attachment and proliferation

The cellular reaction is influenced by the surface properties. They include the surface roughness, surface chemical composition, surface wettability and surface topography. Initial cell attachment to the dental implant surface is one of the most important steps determining the biocompatibility of biomaterials. In this study, we have chosen human gingival fibroblast as a model to investigate the in vitro cellular response to the three different titanium surfaces, because they are the major celluar constituent of of the peri-

implant fibrous connective tissue. After biomaterials are inserted into the host bone, human gingival fibroblasts contact the surface of implants in a relatively short time. In vitro cell culture experiment, the cell morphology varied according to the titanium surface topography and seeding time. As we observed from the CLSM images: on the first day after seeding, on the polished surfaces with lowest roughness, fibroblasts were flat, evenly spread and start to contact with each other; they appeared to grow following the orientation parallel to the grinding lines; on the Osseotite surfaces, the roughest surface among the three groups, the shape of fibroblasts were irregular, the cells started to form bridges with the adjacent cells and the filopodia could also be seen; on the Nanotite surfaces with intermediate surface roughness, the shape of cells are round or dendritic, they did not spread well and are relative isolated. Significant increase in cell number and attchment were detected in all tested surfaces over the incubation time. On each titanium surfaces, the shape and the size of the gingival fibroblasts varied during the different culture time, it is postulated that the cells were at the different stages of their cell cycle. At the end of culture (day 30), the cell number increased on all the implant materials, moreover, the cells grow on Osseotite surfaces formed a higher surface coverage than on Nanotite samples. It was demonstrated that the human gingival fibroblasts attached, spread and proliferated on all these three titanium surfaces with the greatest extension on Machined surfaces and smallest extension on Nanotite surfaces. These results indicated that surface characteristics can influence the cell grow behavior, such as attachment, spread and proliferation, especially in the early phase of cell-material interaction.

With regard to surface roughness, several studies have reported that the gingival fibroblasts attached and spread more readily on smooth Ti surfaces compared on rough Ti surfaces Furuhashi *et al.* (2012), Mustafa *et al.* (1998). An in vitro investigation performed by Köunönen *et al.* (1992) on titanium implants have also demonstrated that the fibroblasts attach better on electropolished surfaces than on the sandblasted and acid-etched surfaces. Our finding is in part in agreement with their reported results; Fur-

thermore, we suggest that Osseotite surface is more favorable to the initial attachment of gingival fibroblasts than Nanotite surface with greater adhesion cell numbers; it is shown that a surface with a certain roughness can facilitate the cell adhesion since the Nanotite surface has a smaller roughness than Osseotite surfaces. This is consistent with a recent study, which suggests that fibrosis at the dental implant surface may be prevented by using abutment materials with an appropriate surface roughness (Kim *et al.* 2015). The interaction of cells with the titanium substratum is a very complex process which is determined by many factors. Based on our findings, the surface wettability and surface chemistry may also be considered contributing factors in the cell-material interaction in the current cases. In a previous study, the static contact angle of the three different titanium surfaces were measured using Sessile Drop method, the authors found that the machined surface and Osseotite surface were hydrophilic whereas the surface with nano-CaP (Nanotite) were hydrophobic (Prabhu 2007). Several studies have revealed that implant surfaces with higher wettability have positive influences on the connective tissue healing with better cell attachment and decreased inflammatory responses (An *et al.* 2012, Kloss *et al.* 2011). The data on growth behavior of HGFs cultured on experimental surfaces showed a significant difference at early culture stage, and this observation seems to indicate that reduced hydrophilicity may have a negative effect on gingival fibroblasts response to the Nanotite surfaces. Moreover, the Nanotite surface is designed to alter the chemical composition by coating nano particles of calcium phosphate, which also play a possible role in cell attachment and spreading. In fact, an in vitro investigation by Guy *et al.* (1993) suggested that fibroblast attachment was greater to titanium than non-porous or porous hydroxyapatite.

The electron microscopic images revealed the initial cell attchment and behavior as well. The cells attached quickly on all surfaces after three days of seeding, the cells on Machined surfaces were more flat, spread well and adapt to the underlying substrate; a reduced amount of cell-cell contacts were detected on Nanotite surfaces compared to the other

surfaces, this result is in agreement with the results from CLSM investigations. However, during the dehydration procedure, the morphology of cells could be altered, which made the resluts are not completely alike to those from CLSM images. Furthermore, may be due to the limitation of culture time (18 days), no significant difference on cell shape was seen between Osseotite and Nanotite surfaces.

Cell proliferation is also an important factor in biocompatibility of dental implants as it is necessary to provide enough cells to interact with the titanium surface. The results of the Alamar Blue assay presented a feature of weakest cell proliferation on Nanotite surfaces after a culture period of 3 and 7 days, the same relationship can be obtained from the results of CLSM images. However, at day 14, there were more fibroblasts grown on Osseotite and Nanotite surfaces compared to the Machined surfaces. This result may reflect the tendency of the fibroblasts grow on Machined surfaces to form flattened monolayers and reached the confluence thus stop growing, with less cells grown on them. Recently, A study conducted by Ramaglia *et al.* (2015) also confirmed that the etched surface promoted a higher cell proliferation and improved the biological behavior of HGFs.

4.3 FACS and Immunofluorescence analysis

In the present study, the fluoresence intensity was measured using flow cytometry to evaluate the expression levels of integrin $\alpha5\beta1$. The flow cytometry data analysis showed that, after two weeks of incubation, the expression of integrins subunit $\alpha5\beta1$ in human gingival fibroblasts on Osseotite surfaces was significantly enhanced compared to Machined and Nanotite surfaces. An integrin $\alpha5\beta1$ is the fibronectin receptor and mediate cell adhesion thus stronger adhesion strength was shown on Osseotite surfaces. From the data presented here, we propose that gingival fibroblasts have the capacity to adhere to

Osseotite surfaces with increased expression of focal adhesion protein integrin $\alpha 5\beta 1$, while nanotopographic structure on titanium material failed to show obvious improvement on fibroblast cellular attachment. Moreover, the in vitro investigation by Ramaglia *et al.* (2015) suggested that HGF attachment and differentiation was promoted on Osseotite surfaces than on Machined ones. Their data is partly in consistent with our results.

The cytoskeletal protein vinculin is associated with the interaction between cell-cell and cell-matrix. It frequently links the integrin receptors to the contractile actin cytoskeleton. As shown by immunofluorescence staining results, although it is merely by visual observation, after 24 days of incubation, fibroblasts clearly showed strong adhesion on all titanium surfaces. It appeared that vinculin expression was higher on Machined and Osseotite surfaces, when compared with Nanotite groups. At day 30, this difference became smaller, the vinculin and the F-actin distribution was similar on Osseotite and Nanotite surfaces.

However, the up-regulation of the integrin was not fully consistent with the distribution of actin and vinculin on three different surfaces. The possible reasons might be: the complexity of signal transduction to the actin cytoskeleton, involving cell-cell contact and integrin-mediated matrix production and could not fully explained by the current investigation. A study conducted by Abrahamsson et al. (2013) also suggested Nanotite dental implants does not improve the early soft tissue integration, which corroborate the data presented in our current experiment.

Chapter 5

Conclusions

In conclusion, the present in vitro study for long-term cellular responses on three different titanium surfaces demonstrated that topographic structures can influence the morphology, proliferation and adhesion of human gingival fibroblasts. The results of current study suggested that :

1. In general, after extended culture periods (30 days), the human gingival fibroblasts responded to Osseotite surfaces in a manner similar to or even better than their behavior on Nanotite surfaces. The morphology of the fibroblasts on Osseotite and Nanotite surfaces demonstrated that they are cuboidal in shape and have the dendritic branching pattern characteristic.The cells on Osseotite surfaces were more spread and formed even a higher surface coverage than on Nanotite surfaces. In contrast, the cells on the Machined surfaces appear more flattened.

2. After two weeks of culture, the gingival fibroblasts grown on Osseotite and Nanotite surfaces showed a notable higher proliferation compared to the Machined surfaces; however, there is no considerable difference on cell proliferation between these two groups.

3. After a 14-day incubation, the flow cytometry data analysis suggested that the cells grown on the Osseotite implant material produce a better initial attachment with a higher $\alpha 5$ and $\beta 1$ integrins expression than on machined and Nanotite materials.

4. After 24 days of cell incubation, immunofluorescence labelling analysis showed that more extended actin stress fibers and higher vinculin expression were on Osseotite compared to Nanotite samples. Vinculin expression localized mainly within central areas of the cell grown on the Machined and the Osseotite surfaces; distinct focal contacts localizations were evident at the cell edges on the Nanotite surface. At day 30, high vinculin expression and a dense network of actin stress fibers on the human gingival fibroblasts were observed on all tested substrates; a similar F-actin distribution was found on Osseotite and Nanotite surfaces.

In conclusion, the data of our present study indicate that in vitro all the three different experimental surfaces show significant interactions with HGFs; however, there is not enough evidence to show that the Nanotite implants is more benificial to the growth behavior of human gingival fibroblasts, compared with Osseotite surfaces; especially at the early stage of incubation.

These celluar effects play a key role in maintaining a biological barrier at the interface between the implant material surface and surrounding connective tissue, our findings may contribute to a better understanding of the processes involved in the soft tissue integration surrounding dental implants.

Bibliography

A Gupta, M Dhanraj, G Sivagami. 2008. Implant surface modification: review of literature. *The Internet Journal of Dental Science.*, **7**(1). 00006.

Abercrombie, M., & Dunn, G. A. 1975. Adhesions of fibroblasts to substratum during contact inhibition observed by interference reflection microscopy. *Experimental Cell Research*, **92**(1), 57–62. 00295.

Abrahamsson, I., Berglundh, T., Wennström, J., & Lindhe, J. 1996. The peri-implant hard and soft tissues at different implant systems. A comparative study in the dog. *Clinical Oral Implants Research*, **7**(3), 212–219. 00403.

Abrahamsson, I., Zitzmann, N. U., Berglundh, T., Linder, E., Wennerberg, A., & Lindhe, J. 2002. The mucosal attachment to titanium implants with different surface characteristics: an experimental study in dogs. *Journal of Clinical Periodontology*, **29**(5), 448–455. 00135.

Aguet, François, Van De Ville, Dimitri, & Unser, Michael. 2008. Model-based 2.5-d deconvolution for extended depth of field in brightfield microscopy. *IEEE transactions on image processing: a publication of the IEEE Signal Processing Society*, **17**(7), 1144–1153.

Ahmed, S. A., Gogal, R. M., & Walsh, J. E. 1994. A new rapid and simple non-radioactive assay to monitor and determine the proliferation of lymphocytes: an alternative to [3H]thymidine incorporation assay. *Journal of Immunological Methods*, **170**(2), 211–224. 00000.

An, Na, Rausch-fan, Xiaohui, Wieland, Marco, Matejka, Michael, Andrukhov, Oleh, & Schedle, Andreas. 2012. Initial attachment, subsequent cell proliferation/viability and gene expression of epithelial cells related to attachment and wound healing in response to different titanium surfaces. *Dental Materials: Official Publication of the Academy of Dental Materials*, **28**(12), 1207–1214.

Atsuta, Ikiru, Yamaza, Takayoshi, Yoshinari, Masao, Goto, Tetsuya, Kido, Mizuho A., Kagiya, Tadayoshi, Mino, Satoya, Shimono, Masaki, & Tanaka, Teruo. 2005. Ultrastructural localization of laminin-5 (gamma2 chain) in the rat peri-implant oral mucosa around a titanium-dental implant by immuno-electron microscopy. *Biomaterials*, **26**(32), 6280–6287. 00000.

Bao Hong Zhao, Inho Han, Hai Lan Feng, Wei Bai, Cui, Fu-Zhai, & Lee, In-Seop. 2007. Histological and histomorphometrical study of connective tissue around calcium phosphate coated titanium dental implants in a canine model. *Surface and Coatings Technology*, **201**(9-11), 5696–5700. 00003.

Bauman, G. R., Rapley, J. W., Hallmon, W. W., & Mills, M. 1993. The peri-implant sulcus. *The International Journal of Oral & Maxillofacial Implants*, **8**(3), 273–280. 00035.

Beaty, Keith D. 1997 (Feb.). *Implant surface preparation utilizing acid treatment.* 00000 U.S. Classification 128/898, 623/920, 427/2.24, 623/901, 427/2.27, 433/201.1; International Classification A61L27/28, A61F2/30, B24C11/00, A61L27/30, A61L27/32, A61C8/00, A61F2/02, A61F2/00, A61L27/06, A61L27/50; Cooperative Classification Y10S623/92, Y10S623/901, A61L27/306, A61F2002/30838, A61F2002/30925, A61C8/0015, A61F2310/00796, C23F1/26, A61L27/50, A61F2/3094, A61F2310/0097, A61C2008/0046, A61L2400/18, A61L2430/02, A61F2002/30904, A61F2310/00023, A61L2430/12, A61L27/06, A61C8/0013, B24C11/00, A61C8/0012, A61C8/00, C23F1/02, A61F2310/00616, A61F2/30771, A61F2310/00976, A61F2/30767,

B24C1/08, C23G1/106, A61F2002/30906; European Classification A61C8/00E1C, B24C11/00, A61F2/30L2, A61C8/00E, A61L27/30R, A61C8/00, A61L27/06, A61L27/50, A61F2/30L, C23G1/10C, C23F1/02, C23F1/26, B24C1/08.

Berckmans, Bruce, Towse, Ross, & Mayfield, Robert. *Deposition of discrete nanoparticles on an implant surface*. 00000.

Berglundh, T., Lindhe, J., Ericsson, I., Marinello, C. P., Liljenberg, B., & Thornsen, P. 1991. The soft tissue barrier at implants and teeth. *Clinical Oral Implants Research*, **2**(2), 81–90. 00610.

Berglundh, T., Lindhe, J., Jonsson, K., & Ericsson, I. 1994. The topography of the vascular systems in the periodontal and peri-implant tissues in the dog. *Journal of Clinical Periodontology*, **21**(3), 189–193. 00229.

Bozzola, John J. 2001. Electron Microscopy. *In:* John Wiley & Sons, Ltd (ed), *Encyclopedia of Life Sciences*. Chichester, UK: John Wiley & Sons, Ltd. 00000.

Brånemark, P. I., Adell, R., Breine, U., Hansson, B. O., Lindström, J., & Ohlsson, A. 1969. Intra-osseous anchorage of dental prostheses. I. Experimental studies. *Scandinavian Journal of Plastic and Reconstructive Surgery*, **3**(2), 81–100. 01781.

Buser, D., Weber, H. P., Donath, K., Fiorellini, J. P., Paquette, D. W., & Williams, R. C. 1992. Soft tissue reactions to non-submerged unloaded titanium implants in beagle dogs. *Journal of Periodontology*, **63**(3), 225–235. 00339.

Chinga, Gary, Johnsen, Per Olav, Dougherty, Robert, Berli, Elisabeth Lunden, & Walter, Joachim. 2007. Quantification of the 3D microstructure of SC surfaces. *Journal of Microscopy*, **227**(3), 254–265.

Cohen, Ariel, Liu-Synder, Peishan, Storey, Dan, & Webster, Thomas J. 2007. Decreased Fibroblast and Increased Osteoblast Functions on Ionic Plasma Deposited Nanostructured Ti Coatings. *Nanoscale Research Letters*, **2**(8), 385–390. 00020.

Cooper, J. A. 1987. Effects of cytochalasin and phalloidin on actin. *The Journal of Cell Biology*, **105**(4), 1473–1478. 01646.

Dean, J. W., Culbertson, K. C., & D'Angelo, A. M. 1995. Fibronectin and laminin enhance gingival cell attachment to dental implant surfaces in vitro. *The International Journal of Oral & Maxillofacial Implants*, **10**(6), 721–728. 00078.

Eisenbarth, E., Meyle, J., Nachtigall, W., & Breme, J. 1996. Influence of the surface structure of titanium materials on the adhesion of fibroblasts. *Biomaterials*, **17**(14), 1399–1403. 00172.

Fields, R. D., & Lancaster, M. V. 1993. Dual-attribute continuous monitoring of cell proliferation/cytotoxicity. *American Biotechnology Laboratory*, **11**(4), 48–50. 00214.

Furuhashi, Akihiro, Ayukawa, Yasunori, Atsuta, Ikiru, Okawachi, Hideyuki, & Koyano, Kiyoshi. 2012. The difference of fibroblast behavior on titanium substrata with different surface characteristics. *Odontology / the Society of the Nippon Dental University*, **100**(2), 199–205. 00018.

Gallant, Nathan D., Michael, Kristin E., & García, Andrés J. 2005. Cell adhesion strengthening: contributions of adhesive area, integrin binding, and focal adhesion assembly. *Molecular Biology of the Cell*, **16**(9), 4329–4340. 00252.

Gaucher, H., Bentley, K., Roy, S., Head, T., Blomfield, J., Blondeau, F., Nicholson, L., Chehade, A., Tardif, N., & Emery, R. 2001. A multicentre study of Osseotite implants supporting mandibular restorations: a 3-year report. *Journal (Canadian Dental Association)*, **67**(9), 528–533. 00022.

Glauser, Roland, Schüpbach, Peter, Gottlow, Jan, & Hämmerle, Christoph H. F. 2005. Periimplant soft tissue barrier at experimental one-piece mini-implants with different surface topography in humans: A light-microscopic overview and histometric analysis. *Clinical Implant Dentistry and Related Research*, **7 Suppl 1**, S44–51. 00099.

Goegan, P., Johnson, G., & Vincent, R. 1995. Effects of serum protein and colloid on the alamarBlue assay in cell cultures. *Toxicology in vitro: an international journal published in association with BIBRA*, **9**(3), 257–266. 00094.

Golji, Javad, & Mofrad, Mohammad R. K. 2013. The interaction of vinculin with actin. *PLoS computational biology*, **9**(4), e1002995. 00010.

Gould, T. R., Westbury, L., & Brunette, D. M. 1984. Ultrastructural study of the attachment of human gingiva to titanium in vivo. *The Journal of Prosthetic Dentistry*, **52**(3), 418–420. 00153.

Guida, Luigi, Oliva, Adriana, Basile, Maria Assunta, Giordano, Michele, Nastri, Livia, & Annunziata, Marco. 2013. Human gingival fibroblast functions are stimulated by oxidized nano-structured titanium surfaces. *Journal of Dentistry*, **41**(10), 900–907. 00013.

Guy, S.c., McQuade, M.j., Scheidt, M.j., McPherson, J.c., Rossmann, J.a., & Van Dyke, T.e. 1993. In Vitro Attachment of Human Gingival Fibroblasts to Endosseous Implant Materials. *Journal of Periodontology*, **64**(6), 542–546.

Hormia, M., Ylänne, J., & Virtanen, I. 1990. Expression of integrins in human gingiva. *Journal of Dental Research*, **69**(12), 1817–1823. 00043.

Humphries, Jonathan D., Wang, Pengbo, Streuli, Charles, Geiger, Benny, Humphries, Martin J., & Ballestrem, Christoph. 2007. Vinculin controls focal

adhesion formation by direct interactions with talin and actin. *The Journal of Cell Biology*, **179**(5), 1043–1057. 00353.

Karthik, Kaneesh, Sivakumar, Sivaraj, & Thangaswamy, Vinod. 2013. Evaluation of implant success: A review of past and present concepts. *Journal of Pharmacy & Bioallied Sciences*, **5**(Suppl 1), S117–S119. 00005.

Kim, Shawna S., Wen, Weiyan, Prowse, Paul, & Hamilton, Douglas W. 2015. Regulation of matrix remodelling phenotype in gingival fibroblasts by substratum topography. *Journal of Cellular and Molecular Medicine*, **19**(6), 1183–1196.

Kioka, N. 1999. Vinexin: A Novel Vinculin-binding Protein with Multiple SH3 Domains Enhances Actin Cytoskeletal Organization. *The Journal of Cell Biology*, **144**(1), 59–69. 00152.

Kloss, Frank R., Steinmüller-Nethl, Doris, Stigler, Robert G., Ennemoser, Thomas, Rasse, Michael, & Hächl, Oliver. 2011. In vivo investigation on connective tissue healing to polished surfaces with different surface wettability. *Clinical Oral Implants Research*, **22**(7), 699–705.

Köunönen, M., Hormia, M., Kivilahti, J., Hautaniemi, J., & Thesleff, I. 1992. Effect of surface processing on the attachment, orientation, and proliferation of human gingival fibroblasts on titanium. *Journal of Biomedical Materials Research*, **26**(10), 1325–1341. 00231.

Lazzara, R. J., Testori, T., Trisi, P., Porter, S. S., & Weinstein, R. L. 1999. A human histologic analysis of osseotite and machined surfaces using implants with 2 opposing surfaces. *The International Journal of Periodontics & Restorative Dentistry*, **19**(2), 117–129. 00245.

Lengsfeld, A. M., Löw, I., Wieland, T., Dancker, P., & Hasselbach, W. 1974. Interaction of phalloidin with actin. *Proceedings of the National Academy of Sciences of the United States of America*, **71**(7), 2803–2807. 00184.

Liu, Dan, Abdullah, Che Azurahanim Che, Sear, Richard P., & Keddie, Joseph L. 2010. Cell adhesion on nanopatterned fibronectin substrates. *Soft Matter*, **6**(21), 5408–5416. 00013.

Liñares, Antonio, Domken, Olivier, Dard, Michel, & Blanco, Juan. 2013. Peri-implant soft tissues around implants with a modified neck surface. Part 1. Clinical and histometric outcomes: a pilot study in minipigs. *Journal of Clinical Periodontology*, **40**(4), 412–420. 00002.

McKinney, Ralph V., Steflik, David E., & Koth, David L. 1985. Evidence for a Junctional Epithelial Attachment to Ceramic Dental Implants. *Journal of Periodontology*, **56**(10), 579–591. 00114.

Miller, D.C., Vance, R.J., Thapa, A., Webster, T.J., & Haberstroh, K.M. 2005. Comparison of fibroblast and vascular cell adhesion to nano-structured poly(lactic-co-glycolic acid) films. *Applied Bionics and Biomechanics*, **2**(1), 1–7. 00011.

Miura, Shingo, & Takebe, Jun. 2012. Biological behavior of fibroblast-like cells cultured on anodized-hydrothermally treated titanium with a nanotopographic surface structure. *Journal of Prosthodontic Research*, **56**(3), 178–186. 00009.

Moon, I. S., Berglundh, T., Abrahamsson, I., Linder, E., & Lindhe, J. 1999. The barrier between the keratinized mucosa and the dental implant. An experimental study in the dog. *Journal of Clinical Periodontology*, **26**(10), 658–663. 00000.

Mullins, R. D., Heuser, J. A., & Pollard, T. D. 1998. The interaction of Arp2/3 complex with actin: nucleation, high affinity pointed end capping, and formation of

branching networks of filaments. *Proceedings of the National Academy of Sciences of the United States of America*, **95**(11), 6181–6186. 00986.

Mustafa, Kamal, Lopez, Blanca Silva, Hultenby, Kjeil, Wennerberg, Ann, & Arvidson, Kristina. 1998. Attachment and proliferation of human oral fibroblasts to titanium surfaces blasted with TiO2 particles. A scanning electron microscopic and histomorphometric analysis. *Clinical Oral Implants Research*, **9**(3), 195–207. 00099.

Nociari, M. M., Shalev, A., Benias, P., & Russo, C. 1998. A novel one-step, highly sensitive fluorometric assay to evaluate cell-mediated cytotoxicity. *Journal of Immunological Methods*, **213**(2), 157–167. 00305.

Oates, Thomas W., Maller, Steven C., West, Jason, & Steffensen, Bjorn. 2005. Human gingival fibroblast integrin subunit expression on titanium implant surfaces. *Journal of Periodontology*, **76**(10), 1743–1750. 00022.

Ojaniemi, M., Martin, S. S., Dolfi, F., Olefsky, J. M., & Vuori, K. 1997. The proto-oncogene product p120(cbl) links c-Src and phosphatidylinositol 3'-kinase to the integrin signaling pathway. *The Journal of Biological Chemistry*, **272**(6), 3780–3787. 00000.

Ostman, Pär-Olov, Hupalo, Markijan, del Castillo, Robert, Emery, Robert W., Cocchetto, Roberto, Vincenzi, Giampaolo, Wagenberg, Barry, Vanassche, Bruno, Valentin, Andreas, Clausen, Gerard, Hogan, Paul, Goené, Ronnie, Evans, Christopher, & Testori, Tiziano. 2010. Immediate provisionalization of NanoTite implants in support of single-tooth and unilateral restorations: one-year interim report of a prospective, multicenter study. *Clinical Implant Dentistry and Related Research*, **12 Suppl 1**(May), e47–55.

Palumbo, Anthony. 2011. The Anatomy and Physiology of the Healthy Periodontium. *In:* Panagakos, Fotinos (ed), *Gingival Diseases - Their Aetiology, Prevention and Treatment*. InTech. 00000.

Petit, Valérie, & Thiery, Jean-Paul. 2000. Focal adhesions: Structure and dynamics. *Biology of the Cell*, **92**(7), 477–494. 00306.

Pivodova, Veronika, Frankova, Jana, & Ulrichova, Jitka. 2011. Osteoblast and gingival fibroblast markers in dental implant studies. *Biomedical Papers of the Medical Faculty of the University Palacký, Olomouc, Czechoslovakia*, **155**(2), 109–116.

Prabhu, Gubbi. 2007. *Hydrophobic/Hydrophilic Characteristic of titanium surfaces: Machined, Dual Acid Etched (OSSEOTITE) And Dual Acid Etched With Nanometer-Scale Cap (NanoTite).*

Ramaglia, Luca, Di Spigna, Gaetano, Capece, Gabriele, Sbordone, Carolina, Salzano, Salvatore, & Postiglione, Loredana. 2015. Differentiation, apoptosis, and GM-CSF receptor expression of human gingival fibroblasts on a titanium surface treated by a dual acid-etched procedure. *Clinical Oral Investigations*, Apr.

Reinhard, M., Halbrügge, M., Scheer, U., Wiegand, C., Jockusch, B. M., & Walter, U. 1992. The 46/50 kDa phosphoprotein VASP purified from human platelets is a novel protein associated with actin filaments and focal contacts. *The EMBO journal*, **11**(6), 2063–2070. 00340.

Rompen, Eric, Domken, Olivier, Degidi, Marco, Pontes, Ana Emilia Farias, & Piattelli, Adriano. 2006. The effect of material characteristics, of surface topography and of implant components and connections on soft tissue integration: a literature review. *Clinical Oral Implants Research*, **17 Suppl 2**(Oct.), 55–67. 00145.

Schindelin, Johannes, Arganda-Carreras, Ignacio, Frise, Erwin, Kaynig, Verena, Longair, Mark, Pietzsch, Tobias, Preibisch, Stephan, Rueden, Curtis, Saalfeld, Stephan, Schmid, Benjamin, Tinevez, Jean-Yves, White, Daniel James, Hartenstein, Volker, Eliceiri, Kevin, Tomancak, Pavel, & Cardona, Albert. 2012. Fiji: an open-source platform for biological-image analysis. *Nature Methods*, **9**(7), 676–682.

Schwarz, Frank, Mihatovic, Ilja, Becker, Jürgen, Bormann, Kai Hendrik, Keeve, Philip L., & Friedmann, Anton. 2013. Histological evaluation of different abutments in the posterior maxilla and mandible: an experimental study in humans. *Journal of Clinical Periodontology*, **40**(8), 807–815. 00009.

Sullivan, D. Y., Sherwood, R. L., & Porter, S. S. 2001. Long-term performance of Osseotite implants: a 6-year clinical follow-up. *Compendium of Continuing Education in Dentistry (Jamesburg, N.J.: 1995)*, **22**(4), 326–328, 330, 332–334. 00049.

Szmukler-Moncler, S., Perrin, D., Ahossi, V., Magnin, G., & Bernard, J. P. 2004. Biological properties of acid etched titanium implants: effect of sandblasting on bone anchorage. *Journal of Biomedical Materials Research. Part B, Applied Biomaterials*, **68**(2), 149–159. 00083.

Testori, Tiziano, Szmukler-Moncler, Serge, Francetti, Luca, Del Fabbro, Massimo, Trisi, Paolo, & Weinstein, Roberto L. 2002. Healing of Osseotite implants under submerged and immediate loading conditions in a single patient: a case report and interface analysis after 2 months. *The International Journal of Periodontics & Restorative Dentistry*, **22**(4), 345–353. 00081.

Vega-Avila, Elisa, & Pugsley, Michael K. 2011. An overview of colorimetric assay methods used to assess survival or proliferation of mammalian cells. *Proceedings of the Western Pharmacology Society*, **54**, 10–14. 00076.

Veronika I. Zarnitsyna, & Zhu, Cheng. 2011. Adhesion frequency assay for in situ kinetics analysis of cross-junctional molecular interactions at the cell-cell interface. *Journal of Visualized Experiments: JoVE*, e3519. 00008.

Watzak, Georg, Zechner, Werner, Tangl, Stefan, Vasak, Christoph, Donath, Karl, & Watzek, Georg. 2006. Soft tissue around three different implant types after 1.5 years of functional loading without oral hygiene: a preliminary study in baboons. *Clinical Oral Implants Research*, **17**(2), 229–236. 00000.

Wen, Kuo-Kuang, Rubenstein, Peter A., & DeMali, Kris A. 2009. Vinculin nucleates actin polymerization and modifies actin filament structure. *Journal of Biological Chemistry*, Sept., jbc.M109.021295. 00040.

Whitehead, R. Y., Lacefield, W. R., & Lucas, L. C. 1993. Structure and integrity of a plasma sprayed hydroxylapatite coating on titanium. *Journal of Biomedical Materials Research*, **27**(12), 1501–1507. 00087.

Wozniak, Michele A, Modzelewska, Katarzyna, Kwong, Lina, & Keely, Patricia J. 2004. Focal adhesion regulation of cell behavior. *Biochimica et Biophysica Acta (BBA) - Molecular Cell Research*, **1692**(2-3), 103–119. 00570.

Yang, Yang, Wang, Xiaohui, & Li, Longtu. 2008. Crystallization and Phase Transition of Titanium Oxide Nanotube Arrays. *Journal of the American Ceramic Society*, **91**(2), 632–635. 00045.

Zareidoost, Amir, Yousefpour, Mardali, Ghaseme, Behrooz, & Amanzadeh, Amir. 2012. The relationship of surface roughness and cell response of chemical surface modification of titanium. *Journal of Materials Science. Materials in Medicine*, **23**(6), 1479–1488. 00017.

Ziegler, Wolfgang H., Liddington, Robert C., & Critchley, David R. 2006. The structure and regulation of vinculin. *Trends in Cell Biology*, **16**(9), 453–460. 00337.

Zitzmann, N. U., Abrahamsson, I., Berglundh, T., & Lindhe, J. 2002. Soft tissue reactions to plaque formation at implant abutments with different surface topography. *Journal of Clinical Periodontology*, **29**(5), 456–461. 00086.

Acknowledgement

I would like to express my sincerest thanks to all the people who helped me and made this thesis possible, who contributed to it with both their experience and suggestions and who supported me constantly throughout my work.

Foremost, I would like to acknowledge and thank my supervisors, Professor Dr. Karl-Heinz Kunzelmann and Professor Dr. Heinz Duschner for giving me the unique chance to work in his laboratory on this interesting scientific topic and for their constructive support, guidance, encouragement. I am also very grateful to Professor Dr. Karl-Heinz Kunzelmann for his patience, enthusiasm, and immense knowledge. His guidance helped me in all the time of research and writing of this thesis.

Many thanks to Frau E. Köbele, Frau G. Dachs and Dr. Indra Nyamaa for their valuable support and advices on my work. I am also gratitude to Herr Dipl.-Phys. Hermann Götz and Herr Dipl.-Ing. T. Obermeier, for their help and constant support during my study. I am very thankful to Dr. yvonne scheller, for her encouragement and insightful comments.

Furthermore, I would like to specially thank Prof. Dr. Reinhard Hickel, Dean of the Dental School at the Ludwig Maximilians University in Munich, Germany, for his generous support and providing me the opportunity to conduct scientific work at the Department of Operative/Restorative of dentistry, in Germany.

Finally, and above all, I would like to thank my loving parents, my brothers and my husband Jian Jin, for their unending support, care, love and for continuously supporting me spiritually.